AD-A078 091 SRI INTERNATIONAL MENLO PARK CA F/G 7/4
PHOTODISSOCIATION AND PHOTODETACHMENT OF ATMOSPHERIC NEGATIVE I--ETC(U)
AUG 79 J T MOSELEY , L C LEE , R V HODGES F49620-78-C-0119
UNCLASSIFIED SRI-MP-79-66 AFOSR-TR-79-1262 NL

1 OF 2
ADA 078091

PHOTODISSOCIATION AND PHOTODETACHMENT OF ATMOSPHERIC NEGATIVE IONS

12

LEVEL II

Final Report
Covering the Period 15 August 1978 to 14 August 1979

August 1979

By: J. T. Moseley, L. C. Lee, R. V. Hodges, and G. P. Smith

Prepared for:

U.S. Air Force Office of Scientific Research
Bolling Air Force Base
Washington, D.C. 20322

Attention: Captain Russell Armstrong
Directorate of Chemistry

AFOSR Contract No. F49620-78-C-0119

SRI Project 7736

MP 79-66

SRI International
333 Ravenswood Avenue
Menlo Park, California 94025
(415) 326-6200
Cable: SRI INTL MPK
TWX: 910-373-1246

UNCLASSIFIED

SECURITY CLASSIFICATION OF THIS PAGE (When Data Entered)

REPORT DOCUMENTATION PAGE	READ INSTRUCTIONS BEFORE COMPLETING FORM
1. REPORT NUMBER: AFOSR-TR-79-1262	2. GOVT ACCESSION NO. / 3. RECIPIENT'S CATALOG NUMBER
4. TITLE (and Subtitle): PHOTODISSOCIATION AND PHOTODETACHMENT OF ATMOSPHERIC NEGATIVE IONS.	5. TYPE OF REPORT & PERIOD COVERED: Final rept. 15 Aug 78 - 14 Aug 79; 6. PERFORMING ORG. REPORT NUMBER
7. AUTHOR(s): J. T. Moseley, L. C. Lee, R. V. Hodges and G. P. Smith	8. CONTRACT OR GRANT NUMBER(s): F49620-78-C-0119, DAAG29-76-C-0023
9. PERFORMING ORGANIZATION NAME AND ADDRESS: SRI International, 333 Ravenswood Avenue, Menlo Park, CA 94025	10. PROGRAM ELEMENT, PROJECT, TASK AREA & WORK UNIT NUMBERS: 61102F, 2303/B1
11. CONTROLLING OFFICE NAME AND ADDRESS: U. S. Air Force Office of Scientific Research/NC, Bolling Air Force Base, Washington, D. C. 20322	12. REPORT DATE: August 1979; 13. NUMBER OF PAGES: 110
14. MONITORING AGENCY NAME & ADDRESS(if different from Controlling Office): 2303	15. SECURITY CLASS. (of this report): Unclassified; 15a. DECLASSIFICATION/DOWNGRADING SCHEDULE

16. DISTRIBUTION STATEMENT (of this Report)

Approved for public release; distribution unlimited. B1

11 Aug 79

17. DISTRIBUTION STATEMENT (of the abstract entered in Block 20, if different from Report)

14 SRI-MP-79-66

18. SUPPLEMENTARY NOTES

12 114

19. KEY WORDS (Continue on reverse side if necessary and identify by block number)

photodestruction; negative ions; atmospheric ions; drift tube mass spectrometer; rare gas halogen laser; ion lasers; excited ions.

Angstroms

20. ABSTRACT (Continue on reverse side if necessary and identify by block number)

Photodetachment and photodissociation cross section measurements have been made for a wide variety of negative ions considered to be of atmospheric importance at wavelengths of 2484, 3500, (3507 and 3569 combined), 4067, and 4131 Å. The ions for which cross sections were measured included O^-, OH^-, O_2^-, O_3^-, O_4^-, CO_3^-, HCO_3^-, CO_4^-, NO_2^-, NO_3^-, Cl_2^-, ClO_2^-, Cl_3^-, and

410281

DD FORM 1 JAN 73 1473

UNCLASSIFIED

SECURITY CLASSIFICATION OF THIS PAGE (When Data Entered)

UNCLASSIFIED

SECURITY CLASSIFICATION OF THIS PAGE(When Data Entered)

$BrCl_2^-$, as well as hydrates of many of these ions. The photodissociation of CO_3^- in the region of the threshold near 6550 Å was reinvestigated in detail, because of the present controversy concerning the bond energy of this ion. These measurements more strongly confirmed our previous conclusion that the bond energy of this ion is less than 1.9 eV. All measurements were made using a drift tube mass spectrometer photodestruction apparatus and with a krypton ion laser or a rare gas halogen laser.

Unclassified

CONTENTS

I. INTRODUCTION

Any process that affects the electron and ion densities in the atmosphere is very important for defense purposes because these densities directly affect radio and radar transmission. Ion and electron charge densities routinely vary as a result of natural phenomena, such as sunrise and auroral events, and can be markedly changed by a nuclear burst or a chemical release. Complex models of the atmospheric reactions that control the electron and ion densities have been developed to predict the effectiveness of communications and missile detection following these events. These models require laboratory determinations of the ion-molecule reaction rates and of the photodetachment and photodissociation cross sections[1,2] that control the ion and electron populations.

It was in recognition of this need that we began research in April 1973 to study the ion-molecule reaction rates and photodetachment and photodissociation cross sections for negative ions of atmospheric importance, using a unique drift tube mass spectrometer and laser facility[3] of our design and construction. This research was sponsored by the Ballistics Research Laboratories (BRL) through the Army Research Office (ARO) under Contract No. DAHC04-73-C-0016. The work was continued through ARO Contract No. DAAG29-76-C-0023, also supported by BRL, and Contract No. DAEA18-71-A-0204, supported by the Army Atmospheric Sciences Laboratory.

In 1978, responsibility for research related to the upper atmosphere was removed from the Army. Therefore, it was unable to support what was to be the final year of the above-described research program, that would extend the cross section measurements into the ultraviolet. This final

year of support was provided by the Air Force Office of Scientific Research (AFOSR) and the Air Force Geophysics Laboratory (AFGL), under AFOSR Contract Number F49620-78-C-0019. This last year of research, from August 15, 1978 to August 14, 1979, is the subject of this report.

Before our research began, it was only possible to account for the photodetachment of O^- in the atmospheric models; photodissociation was not considered at all. At the end of the current contract, we have enough information to account for photodestruction of nearly all of the ions considered to be important, covering the wavelength range from 2484 to 8600 Å. In addition, we have learned about the structure and excited states of these ions. Many of the photodestruction processes we have studied appear to be important[1,2,4] in determining the ion and electron densities in the atmosphere.

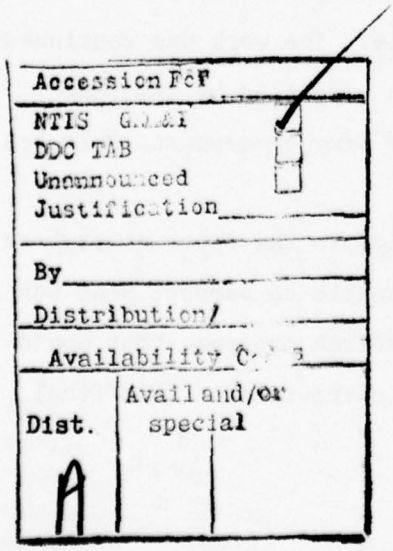

II. RESEARCH ACCOMPLISHMENTS

A. Photodissociation and Photodetachment of Oxygen-Based Ions

Under the present contract, photodestruction cross sections for the ions O_2^-, $O_2^- \cdot H_2O$, O_3^-, $O_3^- \cdot H_2O$, O_4^-, and OH^- were measured using the combined 3507 and 3564 Å lines of a Kr^+ ion laser and using the 4067 and 4131 Å lines individually. Those measurements were combined with measurements that covered the wavelength range from 4300 to 5400 Å and from 6300 to 8600 Å made under a previous contract. This work is reported in detail in Appendix A titled "Photodissociation and Photodetachment of Molecular Negative Ions. VI. Ions in $O_2/CH_4/H_2O$ Mixtures from 3500 to 8600 Å."

B. Photodissociation and Photodetachment of Carbon-Dioxide-Based Ions

Photodestruction of CO_3^-, $CO_3^- \cdot H_2O$, CO_4^-, $CO_4^- \cdot H_2O$, HCO_3^-, and $HCO_3^- \cdot H_2O$ was investigated at (3507 + 3564), 4067, and 4131 Å. In addition, the possible excitation of CO_3^- was investigated in detail, and no evidence was found for any excitation. To the contrary, strong evidence was found supporting our earlier conclusion that the bond energy $D(CO_2 - O^-)$ *is less than or equal to* 1.9 eV. Thus, the existing uncertainty[5,6] in the bond energies and electron attachment energies of O_3^- and CO_3^- remains unresolved. The detailed results of this research are given in Appendix B, a preprint of a paper which also contains the measurements between 4300 and 5300 Å that were made under a previous contract.

C. Photodissociation and Photodetachment of Nitrogen Dioxide-Based Ions

Photodestruction of NO_2^-, $NO_2^- \cdot H_2O$, NO_3^-, and $NO_3^- \cdot H_2O$, as well

as of the peroxy isomers of NO_3^- and its hydrate, $O_2^- \cdot NO$ and $O_2^- \cdot NO \cdot H_2O$, were investigated at (3507 and 3564), 4067, and 4131 Å. An interesting aspect of this work was the study of the isomeric NO_3^- ions. These ions, which are likely to be formed in the ionosphere in approximately equal numbers as the ground state, are very stable against further reaction. However, the ions are easily destroyed by photodissociation and possibly by photodetachment. Further study of the formation and reaction destruction mechanisms of these ions is clearly indicated. This work is described in detail in Appendix C, which also includes results of measurements covering the wavelength range of 4300 to 8250 Å obtained under a previous contract.

D. Photodissociation and Photodetachment of Chlorine-Based Ions

It has been recently suggested[7] that the ion ClO^- might be important in the ion chemistry of the D-region. In addition, ions such as Cl_2^- and Cl_3^- are believed[8] to be important constituents of rare gas-chlorine laser media. Thus, photodestruction cross sections were measured for these ions, as well as $BrCl_2^-$, at the previously mentioned wavelengths used in this contract and out to 7600 Å under a previous contract. The results of this work are given in Appendix D.

E. Photodestruction Cross Sections at 3511 and 2484 Å

Even though the solar flux in the D-region is decreasing rapidly for wavelengths shorter than 3500 Å, many of the photodestruction cross sections are rising rapidly as they approach this wavelength. Furthermore, it is of interest to be able to model the ionosphere under disturbed conditions, where increased short-wavelength radiation may be present. Thus, it is important to extend the photodestruction measurements beyond 3500 Å. Unfortunately, no intense CW laser is presently available in this

region. However, the newly developed rare gas-halogen laser provides intense pulsed radiation at 3510, 3080, 2484, and 1930 Å. We have successfully applied this laser to the present experiment and extended the wavelength range of the measurements to 2484 Å. Measurements at 1930 Å were not successful because of the substantial electron production from scattered light striking surfaces and multiphoton ionization of the background gas, leading to negative ion production when the laser was on. This production masked the negative ion destruction that we were trying to measure.

The details of the use of a pulsed laser with the present apparatus are described in a preprint given in Appendix E.

The results of this work along with the other photodestruction cross sections measured under the present contract, are also given in Table 1.

TABLE 1.

PHOTODISSOCIATION AND PHOTODETACHMENT CROSS-SECTION* MEASUREMENTS FROM 2484 to 4131 Å

	WAVELENGTH (Å)					
ION	2484	3511	(3507 + 3564)	4067	4131	6200
O^-	11.3	8.2	8.2	6.3	6.3	6.3
O_2^-	9.5	3.4	3.7	2.6	2.6	1.3
$O_2^- \cdot H_2O$	8.5	-	2.6	1.6	1.5	0.3
O_3^-	10.2	2.3	2.1	5.0	3.7	0.1
$O_3^- \cdot H_2O$	-	-	1.0	4.3	3.8	0.56
O_4^-	13.1	8.4	8.6	2.9	3.2	1.1
OH^-	-	-	7.7	7.1	5.8	-
CO_3^-	2.7	-	0.07	0.4	0.4	1.5
$CO_3^- \cdot H_2O$	1.6	-	0.1	0.5	0.5	7.0
CO_4^-	10.1	-	0.45	-	<0.06	<0.02
$CO_4^- \cdot H_2O$	-	-	<0.2	-	<0.13	-
HCO_3^-	4.0	-	<0.08	-	<0.08	<0.03
$HCO_3^- \cdot H_2O$	2.9	-	<0.07	-	<0.06	-
NO_2^-	10.2	-	3.2	1.5	1.3	<0.01
$NO_2^- \cdot H_2O$	9.8	-	1.2	-	0.16	<0.02
NO_3^-	10.2	-	0.1	-	<0.07	-
$NO_3^- \cdot H_2O$	-	-	0.4	-	<0.1	-

* Cross Section in units of $10^{-18} cm^2$.

ION	2484	3511	(3507 + 3564)	4067	4131	6200
$O_2^- \cdot NO$	9.8	9.1	7.0	6.2	6.1	0.1
$O_2^- \cdot NO \cdot H_2O$	-	-	3.5	4.6	4.0	0.08
Cl_2^-	-	-	35.1	14.9	10.8	0.2
ClO^-	-	-	3.1	3.5	3.6	0.1
Cl_3^-	-	-	6.7	-	0.79	< 0.02
$BrCl_2^-$	-	-	3.3		0.94	< 0.03

* Other cross section measurements are measured relative to O^-, using the cross section listed. The total uncertainty in these measurements is typically $\pm$ 20%. The values of the cross sections at 6200 Å are shown for comparison. The pulsed laser results at 3511 Å are in good agreement with the CW laser measurements at (3507 and 3564) Å. It is clear that most cross sections are rising rapidly in the ultraviolet.

III. CUMULATIVE LIST OF PUBLICATIONS

1. L. C. Lee and G. P. Smith, "Photodissociation and Photodetachment of Molecular Negative Ions. VI. Ions in $O_2/CH_4/H_2O$ Mixtures from 3500 to 8600 Å", J. Chem. Phys. 70, 1727 (1979).
2. G. P. Smith, L. C. Lee, and J. T. Moseley, "Photodissociation and Photodetachment of Molecular Negative Ions. VII. Ions Formed in $CO_2/O_2/H_2O$ Mixtures, 3500-5300 Å", J. Chem Phys. (in press).
3. G. P. Smith, L. C. Lee, and P. C. Cosby, "Photodissociation and Photodetachment of Molecular Negative Ions. VIII. Nitrogen Oxides and Hydrates, 3500 - 8250 Å", J. Chem. Phys. (in press).
4. L. C. Lee, G. P. Smith, J. T. Moseley, P. C. Cosby, and J. A. Guest, "Photodissociation and Photodetachment of Cl_2^-, ClO^-, Cl_3^-, and $BrCl_2^-$", J. Chem. Phys. 70, 3237 (1979).
5. R. V. Hodges, L. C. Lee, and J. T. Moseley, "Photodissociation and Photodetachment of Molecular Negative Ions. IX. Atmospheric Ions at 2484 and 3511 Å", Submitted to J. Chem. Phys.
6. G. P. Smith and L. C. Lee, "Photodissociation Spectroscopy of O_3^- and $O_3^- \cdot H_2O$. 4170-4700 Å", J. Chem. Phys. 71, 2323 (1979).

IV. PROFESSIONAL PERSONNEL ASSOCIATED WITH THIS RESEARCH

1. Principal Investigator and Project Supervisor:

   Dr. J. T. Moseley, Program Manager, Photochemistry

2. Project Leader:

   Dr. L. C. Lee, Senior Physicist

3. Other SRI Personnel:

   Dr. G. P. Smith, Chemist

   Dr. R. V. Hodges, Chemical Physicist

   Dr. P. C. Cosby, Chemical Physicist

   Dr. J. R. Peterson, Associate Director

REFERENCES

1. L. Thomas, J. Atmos. Terr. Phys. 35, 397 (1973).
2. F. E. Niles and M. G. Heaps, Abstract J163 IAGA/IAMAP Joint Assembly, Seattle (1977).
3. J. T. Moseley, P. C. Cosby, R. A. Bennett, and J. R. Peterson, J. Chem. Phys. 62, 4826 (1975).
4. J. R. Peterson, J. Geophys. Res. 81, 1433 (1976).
5. I. Dotan, J. A. Davidson, G. E. Streit, D. L. Albritton, and F. C. Fehsenfeld, J. Chem. Phys. 67, 2874 (1977).
6. S. E. Novick, P. C. Egelking, P. L. Jones, J. H. Futrell, and W. C. Lineberger, J. Chem. Phys. 70, 2652 (1979).
7. R. P. Turco, J. Geophys. Res. 82, 3585 (1977).
8. J. J. Ewing and C. A. Brau, Appl. Phys. Lett. 27, 350 (1975); J. R. Murray, and H. T. Powell, Appl. Phys. Lett. 29, 252 (1976); J. I. Levatter, J. H. Morris, and S. C. Lin, Appl. Phys. Lett. 32, 630 (1978).

Appendix A

PHOTODISSOCIATION AND PHOTODETACHMENT OF MOLECULAR NEGATIVE IONS. VI. IONS IN $O_2/CH_4/H_2O$ MIXTURES FROM 3500 to 8600 Å

Photodissociation and photodetachment of molecular negative ions. VI. Ions in $O_2/CH_4/H_2O$ mixtures from 3500 to 8600 Å

L. C. Lee and G. P. Smith

Molecular Physics Laboratory, SRI International, Menlo Park, California 94025
(Received 8 September 1978)

The photodestruction cross sections for O^-, O_2^-, $O_2^-\cdot H_2O$, O_3^-, $O_3^-\cdot H_2O$, O_4^-, OH^-, and OD^- have been measured in the 3500–5400 Å and 6300–8600 Å wavelength regions. The ions were produced in a drift tube mass spectrometer and interacted with a dye laser or ion laser inside the laser cavity. The photodetachment cross sections for O^- and $OH^-(OD^-)$ have sharp onsets at wavelengths near 8480 and 6795 Å, respectively, and at shorter wavelengths their values are nearly constant. The photodestruction cross sections for O_2^-, O_4^-, and $O_2^-\cdot H_2O$ increase monotonically with increasing photon energy. In contrast, in the photodestruction cross section for O_3^-, structure is observed over this wavelength region. The processes for creation and photodestruction of the various negative ions are discussed. Comparison is made with other measurements.

I. INTRODUCTION

Within the last few years the photodissociation and photodetachment cross sections for many negative[1–5] and positive[6,7] ions have been measured in our laboratory. These cross sections are important for modeling the charge density in the *D* region of the ionosphere.[8] As an example, the photodestruction cross sections for CO_3^-, $CO_3^-\cdot H_2O$, and O_3^- have been used to explain the rapid increase of electron density in the *D* region of the ionosphere at sunrise.[9]

The photodestruction cross sections of ions are of fundamental interest for several reasons. The vibrational frequencies of negative ions have been determined[10–12] from the structure observed in the photodestruction spectra;[2,3,12] the electron affinities of neutral parent molecules have been obtained from the thresholds of photodetachment cross sections[13–15]; and the repulsive states of ions have been established from the dissociation continua.[7,16]

In this paper, we report the photodestruction cross sections for various ions formed in mixtures of O_2, CH_4, D_2, and H_2O over the wavelength regions 3500–5400 and 6300–8600 Å. These cross sections have been previously examined at various wavelengths by several investigators.[1–5,13,14,17–21] However, few measurements are available for the wavelength regions of interest here. The results of our measurements are compared with others.

II. EXPERIMENTAL

The experimental apparatus used for our measurements has been described in some detail in several previous publications.[1–3] Briefly, a drift tube mass spectrometer apparatus was used as the ion source, drift region, mass analyzer, and ion detector. The source and drift regions were filled with the gas of interest at a pressure of 0.05–0.5 Torr. The negative ions were formed in the gas phase by electron attachment processes and by subsequent ion–molecule reactions. Under the influence of a weak uniform electric field, the ions drifted toward a 1 mm-diameter exit aperture. The ratio of the applied electric field to the neutral gas density, E/N, was limited to 10 or 20 Td (1 Td = 10^{-17} V-cm^2); thus, the ion drift velocity was only about one-tenth the mean thermal speed of the ions and neutral molecules at room temperature. The drift distance, which could be varied over a range of 2.5–50.8 cm, was chosen so that the ions experience many thermalizing collisions after their production and are essentially in thermal equilibrium[16] with the neutral molecules at 300 K.

The drifting ions intersect a laser beam of ~1.5 mm diameter in front of the exit aperture. The light source in the near infrared region was a dye laser pumped by the 6471 and 6764 Å lines of nominal 4 W krypton ion laser. The dyes[22] used were rhodamine 640 perchlorate for the 6200–6950 Å region, oxazine 1 perchlorate for 6950–7900 Å, and 3-3′-diethyloxatricarbocyanine iodide (DEOTC) for 7700–8600 Å. In the short wavelength region, various lines of the Ar^+ and Kr^+ ion lasers were used. The laser lines were tuned by a prism, except the ultraviolet line from the Kr^+ ion laser. The UV line consists of 66% 3507 Å and 34% 3569 Å. The interaction region of the laser with the ions was inside the dye laser cavity, and the laser polarization was perpendicular to the ion drift velocity. The intracavity laser power varied from 5 to 100 W for the various wavelengths. The ions of interest were selected by a quadrupole mass spectrometer and detected by an electron multiplier. The laser was mechanically chopped at 100 Hz. The ions were counted for equal periods during which the laser was on and off. The cross sections were placed on an absolute scale by normalization to negative ions for which the photodestruction cross sections are known. The mobilities, K_0, and the ions chosen for normalization are listed in Table I. The mobilities are adopted from published values[23] or are scaled[20,23] from masses of the ion and gas molecules.

The distance and the gas pressure were chosen to optimize the concentration of ions of interest and to minimize the interference from other species in the drift tube. The gas mixtures and the gas pressures are listed in Table I. The density of ions in the drift tube was kept low so that the cross section measurements were not significantly affected by secondary processes such as mutual repul-

TABLE I. Experimental conditions of the mobilities K_0, and the ions chosen for normalization.

Ion	Gas	Pressure (Torr)	Normalized to	K_0 (cm^2/V sec)
D^-	D_2	0.1, 0.2		30.0
O^-	O_2	0.1	D^- in D_2, O_2^- in O_2	3.20
O_2^-	O_2	0.2	O^- in O_2, D^- in D_2	2.16
$O_2^- \cdot H_2O$	O_2/trace H_2O	0.4	O_2^- in O_2	2.58
O_3^-	O_2	0.4	O_2^- in O_2	2.56
$O_3^- \cdot H_2O$	O_2/trace H_2O	0.4	O_2^- in O_2	2.20
O_4^-	O_2	0.4	O_2^- in O_2	2.08
OH^-	O_2, 2% CH_4	0.2	O^- in O_2	3.18
OH^-	He, 2% O_2, 1% CH_4	0.2	O^- in He	20.2
OD^-	O_2, 2% D_2, 2% CH_4	0.2	O^- in O_2	3.16

sion. The percentage of ions photodissociated was limited to less than 15% of the ions of interest by adjusting the dye laser power. This low destruction rate minimizes the effect of the ion diffusion (from the noninteraction region into the photon interaction region) on the measured cross section. This effect has been discussed in detail in a previous paper.[6]

At each wavelength the number of ion counts was accumulated until the statistical uncertainty in the photodestruction signal was less than 10%. The statistical uncertainties are indicated by error bars along with the data shown later. The laser power and the ion mobility are known to within 5% of their true values. Including the uncertainty in the normalization procedure, the experimental uncertainty for the absolute photodissociation cross sections is estimated to be ±20%.

III. RESULTS AND DISCUSSION

A. O^-

All previous measurements of photodestruction cross sections for ions made in drift tubes have been normalized[1-7,20,21] to the photodetachment cross section of the O^- ion. However, the absolute cross section for this ion has been measured only in a beam apparatus using broad-band wavelength selection[14,19] of the photons. Detailed measurements on the photodetachment cross section of O^- at high resolution are of great interest, especially at the threshold where the cross section has a sharp onset.

The photodetachment cross section of the H^- ion is an attractive candidate for the normalization standard. This cross section has been extensively investigated both theoretically[24-28] and experimentally.[29,30] Representative results are plotted in Fig. 1. As indicated in this figure, the data given by various investigators are in good agreement, with a variation at each wavelength of less than 10%. The relative H^- cross section measured by Smith and Burch[29] was put on an absolute scale by normalization to the theoretical calculations of Geltman.[24] The experimental uncertainties are estimated to be 10% for the measurements of Smith and Burch[29] and 8% for Popp and Kruse.[30] The mean values of all the experimental and theoretical data shown in Fig. 1 are adopted for the normalization standard.

In the current measurement, the photodetachment cross section for O^- was normalized to D^-, instead of H^-. This is because (i) H^- has higher mobility[31] than D^- so that the percentage of the H^- ions destroyed by the laser is smaller than that of D^- at the same laser power, and (ii) H^- is harder to form and detect in the drift tube than D^-. Both isotopes are expected to have the same photodetachment cross section at each wavelength, because they have the same electronic structure and their wave functions differ only by the electron reduced mass ($\frac{1}{1840}$). The photodetachment cross section of O^- normalized to D^- is shown in Fig. 2 for the wavelength region from 6300 to 8600 Å. The error bar indicates the statistical uncertainty. The

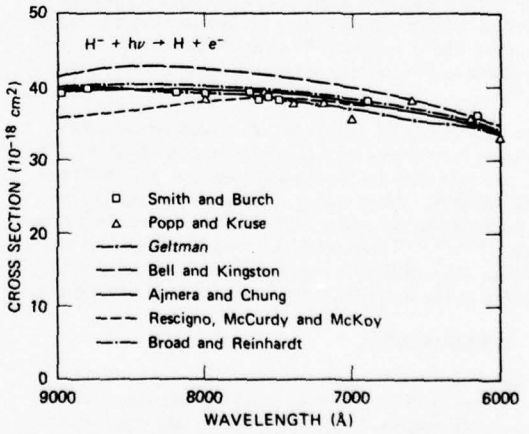

FIG. 1. The photodetachment cross section for H^- in the wavelength region 6000–9000 Å. Calculations were done by Geltman (Ref. 24), Bell and Kingston (Ref. 25), Ajmera and Chung (Ref. 26), Rescigno *et al.* (Ref. 27), and Broad and Reinhardt (Ref. 28). Measurements were made by Smith and Burch (Ref. 29) and Popp and Kruse (Ref. 30). The relative measurements of Smith and Burch were placed on an absolute scale by Geltman.

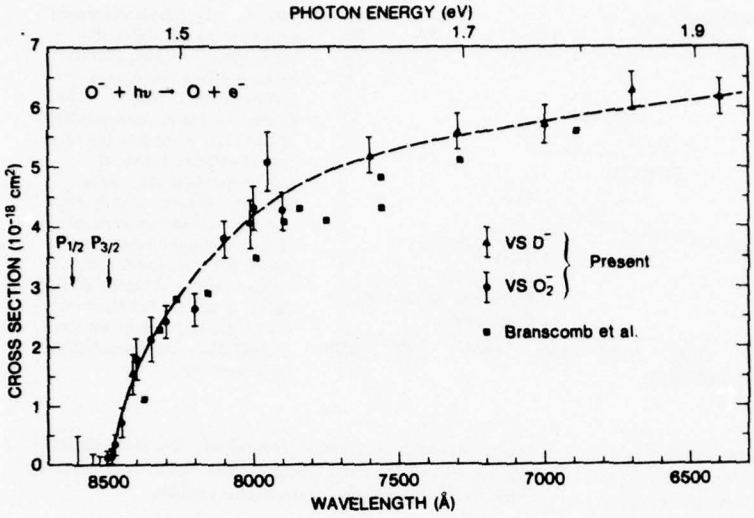

FIG. 2. The photodetachment cross section for O^- in the wavelength region 6300–8600 Å, placed on an absolute scale by normalization to D^- and O_2^-. The measurements of Branscomb *et al.* (Ref. 14) are included for comparison. The cross section near the second threshold (8480 Å) is fit by a a threshold law, which is indicated by the solid line. The thresholds for photodetachment of $O^-(^2P_{3/2})$ and $O^-(^2P_{1/2})$ are indicated. The dashed lines *only serve to join the data*. The error bars indicate experimental uncertainty.

D^- reduced mobility of $K_0 = (30.0 \pm 0.9)$ cm^2/V-sec is adopted from Graham *et al.*[31]

To better define the rapid increase of the cross section in the threshold region, we measured the O^- cross section relative to O_2^-. In this wavelength region the O_2^- cross section, which is obtained by normalization to D^-, shows a slow variation with wavelength (see next section). It is advantageous to normalize the O^- photodetachment cross section against O_2^- instead of D^-, because O^- and O_2^- can be alternatively observed in the same parent gas, which minimizes experimental uncertainties such as variations in the laser–ion interaction region. The O^- cross section obtained by normalization to O_2^- is also shown in Fig. 2. These values are consistent with the data obtained by normalization to D^-.

The earlier absolute cross sections of Branscomb *et al.*[14] measured with a bandwidth of 100 Å are also shown in Fig. 2. The experimental uncertainties are not given in Ref. 14, but from a previous paper[17] they may be estimated to be about 10%. The present measurements give values slightly higher than the data of Branscomb *et al.*,[14] but both measurements agree within their experimental uncertainties. Therefore, all the previous measurements in the visible region,[1-7,10,11,20] which have used the O^- photodetachment cross section of Branscomb *et al.*[14] as a normalization standard, are not substantially affected by the present results.

The data in Fig. 2 are joined together by the solid and dashed lines, which indicate the values to be used as a normalization standard for other ions. The dashed lines only serve to join the data points, but the solid line is fit by a threshold law, which is described as follows.

The dependence of the O^- photodetachment cross section on the wavelength near threshold has been discussed by Branscomb *et al.*[17] The ground state of O^- is ^2P, which has the configuration $(1s)^2(2s)^2(2p)^5$. In the photodetachment process one of the $2p$ electrons makes an electric dipole transition to a continuum orbital, s or d. As indicated in Fig. 2, the O^- ion has two thresholds, depending on whether the ion is initially in the $^2P_{3/2}$ or $^2P_{1/2}$ state. The $O^-(^2P_{1/2})$ state has an energy[32] of 181 cm^{-1} higher than $O^-(^2P_{3/2})$, so that its threshold energy is lower. As shown in Fig. 2, the apparent photodetachment cross section for the wavelengths between these two thresholds is very small. This is because in this wavelength region only the $O^-(^2P_{1/2})$ ions are photodetached. The concentration of O^- in the $^2P_{1/2}$ state is only about 20% of O^- in the $^2P_{3/2}$ state when estimated from a Boltzmann distribution at 300 K. At the $^2P_{3/2}$ threshold, λ_0, the photodetachment cross section has a sharp onset. The photodetachment cross section for wavelengths slightly shorter than this threshold is given[17] by

$$\sigma(\lambda) = \frac{\gamma}{\lambda}\left(\frac{1}{\lambda} - \frac{1}{\lambda_0}\right)^{1/2} + \frac{\gamma A_1}{\lambda}\left(\frac{1}{\lambda} - \frac{1}{\lambda_0}\right)^{3/2}, \quad (1)$$

where γ and A_1 are parameters to be determined from the experimental data.

For wavelengths in the 8300–8500 Å region, the experimental data are fit by $\gamma = 1.275 \times 10^{-23}$ cm$^{7/2}$ and $A_1 = 6.87 \times 10^{-5}$ cm, with $\lambda_0 = 8480$ Å as shown by the solid curve in Fig. 2. The first term in Eq. (1), which results from the transition to the s continuum orbital, is dominant. The uncertainty for λ_0 is ±10 Å. The electron affinity of $O(^3P)$ determined from λ_0 is 1.462 ± 0.002 eV, which is identical to the value of 1.462 ± 0.003 eV recently recommended by Hotop and Lineberger.[32]

B. O_2^-

The photodetachment cross section of O_2^- has been previously measured by several authors.[2,3,13,19,20,33] In this paper, extended measurements at 3500–5000 and 7000–8400 Å are reported. The O_2^- cross section is obtained by normalization to O^- in O_2, except at 8400 Å where it is normalized to D^- in D_2. The results are plotted in Fig. 3, in which the measurements given by Cosby *et*

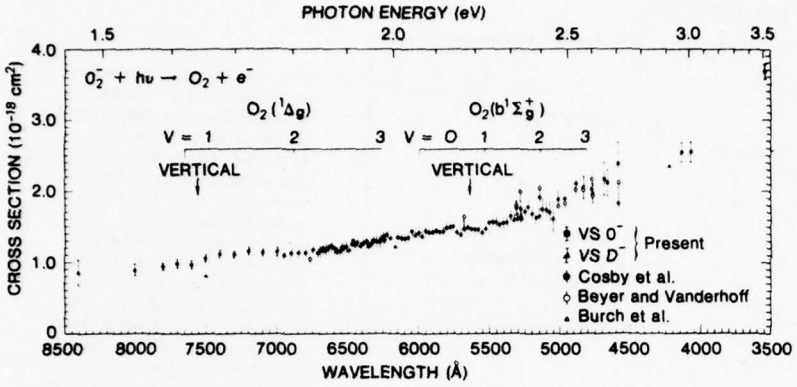

FIG. 3. The photodetachment cross section for O_2^- in the 3500–8500 Å region, placed on an absolute scale by normalization to D^- and O^-. The thresholds for photodetachment of O_2^- ($X\,^2\Pi$, $v=0$) into the various vibrational levels of $O_2(^1\Delta_g)$ and $O_2(b\,^1\Sigma_g^+)$ are indicated. The vertical thresholds for photodetachment of O_2^- into these two electronic states are also shown. The measurements of Cosby *et al.* (Refs. 2 and 3), Burch *et al.* (Ref. 13), and Beyer and Vanderhoff (Ref. 20) are indicated for comparison.

al.,[2,3] Burch *et al.*,[13] and Beyer and Vanderhoff[20] are also shown. The present results agree very well with other measurements in the shorter wavelength region, but are slightly higher than those of Burch *et al.*[13] in the longer wavelength region. The data given by Warneck[19] in the 3000–6200 Å region and by Burt[33] at 4000–20 000 Å are not included in Fig. 3. Warneck's data are consistent with those of Burch *et al.*,[13] but Burt's data[33] are much higher than the present values. Burt's data are possibly affected by the improper normalization of the O_2^- cross section to O^- at high pressure, as discussed by Cosby *et al.*[2]

The photodestruction process in the present wavelength region can be definitely attributed to photodetachment. By combining the measured electron affinity for $O(^3P)$ of 1.462 ± 0.002 eV with the electron affinity for $O_2(X\,^3\Sigma_g^-)$ of 0.440 ± 0.008 eV[34] and the dissociation energy for $O_2(X\,^3\Sigma_g^-)$ of 5.1159 ± 0.0012 ev,[35] we obtain a dissociation energy for $O_2^-(X\,^2\Pi_g)$ of 4.094 ± 0.011 eV. Because the photon energy in the present region is less than 3.5 eV, only photodetachment is energetically possible.

In this wavelength region the photodetachment cross section of O_2^- does not depend on the drift distance, gas pressure, and laser power, but it does depend slightly on E/N, as shown in Fig. 4. Such E/N dependence has been reported previously.[2] At 5208 Å, the cross section decreases with higher E/N, but at 4131 Å, the cross section increases slightly with higher E/N. This is because O_2^- is effectively vibrationally excited by the applied electric field. The vibrationally excited states of O_2^- will have different transition probabilities from the ground state, so that the photodetachment cross section for O_2^- depends on the applied electric field. (Details of such effects are discussed elsewhere.)[36]

No prominent discrete structure is observed in the photodetachment cross section for O_2^-. This indicates that the photodetachment of O_2^- does not result from a preionization process. This result is consistent with the potential curves of O_2^- recently calculated by Das *et al.*[37] There is only one bound electronic excited state, $O_2^-(a\,^4\Sigma_u^-)$, energetically accessible at the present photon energies. However, the transition from the ground state, $O_2^-(X\,^2\Pi_g)$, to this excited state is optically forbidden, so that its oscillator strength is small. Therefore, the photodetachment cross section for O_2^- is not expected to have discrete structure in the present wavelength region.

The O_2^- cross section increases as the photon energy increases, as shown in Fig. 3. Burch *et al.*[13] have fit this increase over a wide range of photon energies by a threshold law

$$\sigma = A_0 \frac{1}{\lambda}\left(\frac{1}{\lambda} - \frac{1}{\lambda_0}\right)^{3/2} . \tag{2}$$

In fact, the threshold law is valid only in a small wavelength region (~200 Å for O^-). To justify their fitting, Burch *et al.*[13] have suggested that electron detachment is being observed from many vibrational levels of the $^4\Sigma_u^-$ state. According to the potential curves of Das *et al.*,[37] the $O_2^-(a\,^4\Sigma_u^-)$ state has an energy about 2 eV above $O_2(X\,^3\Sigma_g^-)$, and it is expected to have a short lifetime in the drift tube at a pressure of 0.4 Torr because it may undergo a collision-induced preionization to $O_2(X\,^3\Sigma_g^-)$. The preionization lifetime is expected to be short. For example, the preionization lifetime of $O_2^-(X\,^2\Pi_g, v=4)$ has

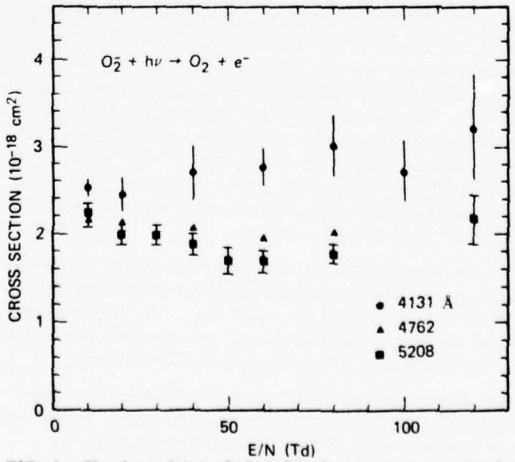

FIG. 4. The dependence of photodetachment cross section for O_2^- on E/N at the photon wavelengths 4131, 4762, and 5208 Å.

been estimated[38] to be $(1.0 \pm 0.3) \times 10^{-10}$ sec; the lifetime of higher levels is expected to be comparably short. Consequently, $O_2^-(a\,^4\Sigma_u^-)$ is not expected to exist in the drift tube. This is in accord with the inability to observe this state in the photoelectron spectrum[34] of O_2^-. The wavelength dependence of the O_2^- photodetachment cross section thus requires a new interpretation.

The 4880 Å photoelectron spectrum of O_2^-[34] indicates that the O_2^- ions are photodetached into every state in O_2 that is energetically accessible. The cross section for photodetachment of O_2^- into each state of O_2 may have a photon energy dependence similar to that for atomic photodetachment. That is, the photodetachment cross section[32] is nearly constant at photon energies more than ~0.1 eV above the photodetachment threshold, as is demonstrated by the O^- photodetachment cross section shown in Fig. 2. Each state of O_2 that is available for O_2^- to photodetach into will contribute to the photodetachment cross section. The photodetachment cross section for O_2^- will increase as the number of available states of O_2 increases. Thus, the photodetachment cross section for O_2^- will increase as the photon energy increases. This assertion is further supported by the fact that the rate of increase of the O_2^- photodetachment cross section changes at the thresholds for photodetachment of $O_2^-(X\,^2\Pi_g, v=0)$ into the various vibrational levels of $O_2(a\,^1\Delta_g, b\,^1\Sigma_g^+)$. The thresholds are calculated from the electron affinity[34] and the energies of electronic states[39] of O_2 and are indicated in Fig. 3. The vertical thresholds obtained from *the* $O_2^-(X\,^2\Pi_g)$ *potential curve of Das et al.*[37] *are also* indicated in Fig. 3. The rate of increase in the cross section changes only at photon energies higher than the vertical threshold. The changes are prominent at the vibrational thresholds.

C. $O_2^- \cdot H_2O$

The photodestruction cross section of $O_2^- \cdot H_2O$ has been measured by Cosby *et al.*[3] in the wavelength region 5200–6700 Å, by Smith *et al.*[5] in 7100–8250 Å, and by Vanderhoff[40] at 4100 Å. Extended measurements in the 3500–5400 Å region are reported in this paper and are shown in Fig. 5.

The $O_2^- \cdot H_2O$ ions were formed in the drift region by the reaction

$$O_4^- + H_2O \rightarrow O_2^- \cdot H_2O + O_2 \qquad (3)$$

with a rate constant[41] of 1.4×10^{-9} cm^3/sec. The O_4^- is formed by a three-body reaction[41] (see Sec. F).

The other process that forms $O_2^- \cdot H_2O$ is

$$O_2^- + H_2O + O_2 \rightarrow O_2^- \cdot H_2O + O_2 \ , \qquad (4)$$

with a rate constant[41,42] of 3×10^{-28} cm^6/sec.

The bonding between a negative ion and a H_2O molecule is through a hydrogen bond.[43,44] The clusters of negative ions that have been studied theoretically, such as $F^- \cdot H_2O$,[43] $Cl^- \cdot H_2O$,[43] and $CN^- \cdot H_2O$,[44] are found to have the most stable structure when the negative ions and the hydrogen and oxygen atoms are collinear. Accordingly, the most stable structure for $O_2^- \cdot H_2O$ is likely to be

$$O_2^- \text{—H—} \overset{\displaystyle H}{\underset{\displaystyle |}{O}} \ .$$

The $O_2^- \cdot H_2O$ ion may be photodissociated by breaking the O_2^-–HOH bond with a dissociation energy of 0.8 eV.[45] It may also undergo dissociative photodetachment

$$O_2^- \cdot H_2O + h\nu \rightarrow O_2 + e + H_2O \ . \qquad (5)$$

The photodestruction cross section of $O_2^- \cdot H_2O$ shown in Fig. 5 has a wavelength dependence qualitatively similar to the photodetachment cross section of O_2^- shown in Fig. 3, except for a shift to the blue. The photodestruction process of $O_2^- \cdot H_2O$ is therefore most likely dominated by the dissociative photodetachment process (5). The threshold energy for process (5) will exceed the electron affinity of O_2 (0.44 eV)[34] by approximately the $O_2^- \cdot H_2O$ bond energy (0.8 eV).[45] The threshold energy for dissociative photodetachment $O_2^- \cdot H_2O$ into $O_2(X\,^3\Sigma_g^-, v=0) + e + H_2O$ is thus estimated to be 1.24 eV. The apparent threshold for photodestruction of $O_2^- \cdot H_2O$ obtained by extrapolation of the cross section to zero is 1.8 ± 0.1 eV.[5] Additional energy is carried away by the photofragments.

Photodestruction of $O_2^- \cdot H_2O$ by the photodissociation process is energetically possible in the wavelength

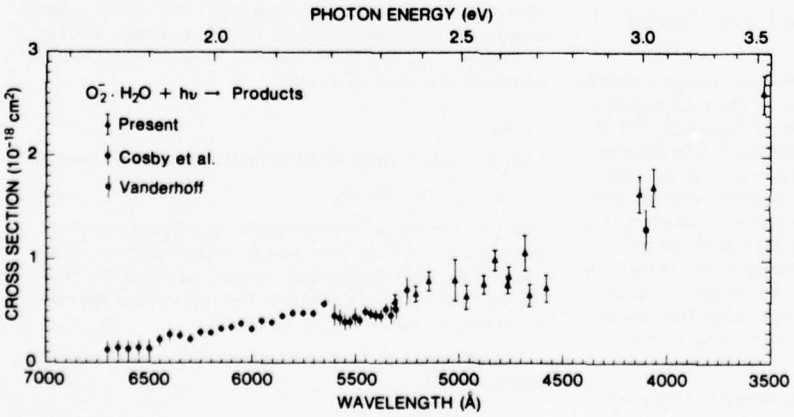

FIG. 5. The photodestruction cross section for $O_2^- \cdot H_2O$ in the 3500–6800 Å region. The measurements of Cosby *et al.* (Ref. 3) and Vanderhoff (Ref. 40) are indicated.

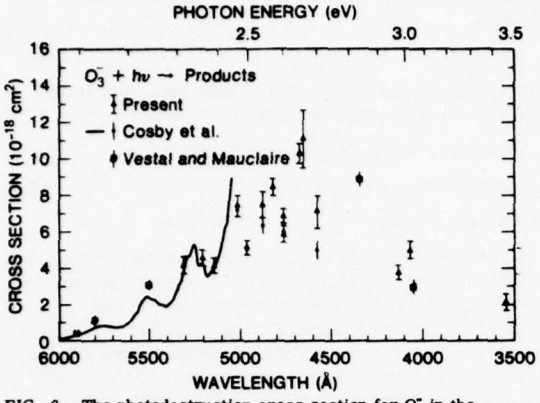

FIG. 6. The photodestruction cross section for O_3^- in the 3500–6000 Å region. The measurements of Cosby *et al.* (Refs. 2 and 3) and Vestal and Mauclaire (Ref. 47) are indicated.

region of interest. However, it is difficult to identify this process in the present experimental arrangement because any possible O_2^- photofragment signal is obscured by the large amount of O_2^- in the drift tube.

D. O_3^-

The photodestruction processes of O_3^- in the gas phase have been previously investigated by several authors.[2,3,11,12,46,47] O_3^- is formed by a three-body reaction[41,48]

$$O^- + 2O_2 \rightarrow O_3^- + O_2 \tag{6}$$

with a rate constant[41] of 1×10^{-30} cm^6/sec^{-1}.

The O_3^- ions can undergo photodetachment

$$O_3^- + h\nu \rightarrow O_3 + e^- \tag{7}$$

with a threshold at 2.1028 eV,[12,46] and can also undergo photodissociation

$$O_3^- + h\nu \rightarrow O^- + O_2 \tag{8}$$

or

$$O_3^- + h\nu \rightarrow O + O_2^- \tag{9}$$

with thermodynamic thresholds[2] at 1.7 ± 0.2 and 2.7 ± 0.2 eV, respectively.

In the photon energy range of interest, the photodissociation (8) is the dominant process.[3] The photodetachment process (7) has a cross section[46] less than 10% of the total photodestruction cross section.[2] The photodestruction cross section of O_3^- is shown in Fig. 6. The present measurements are shown together with the previous measurements[2,3] made at longer wavelengths. The cross sections for both processes (8) and (9) given by Vestal and Mauclaire[47] are also shown in Fig. 6 for comparison. In their measurements, the initial vibrational distribution of O_3^- is not known, and a large fraction of the O_3^- ions is expected to be in vibrationally excited states.

As shown in Fig. 6, the photodestruction cross section has discrete structure with maxima at about 5760, 5510, 5270, 5050, 4850, and 4660 Å. The structure at wavelengths longer than 5000 Å has been analyzed in detail by Cosby *et al.*[11] This structure is attributed to the transitions from the ground O_3^- state to the vibrational levels of a quasibound excited electronic state, which predissociate. The structure observed in this study at shorter wavelengths is a result of the same progression, because the separations between the primary maxima are about the same, ~820 cm^{-1}. The structure will be examined in detail in the near future using a tunable dye laser in this wavelength region.

E. $O_3^- \cdot H_2O$

The $O_3^- \cdot H_2O$ ions are formed by a three-body reaction,[42]

$$O_3^- + H_2O + O_2 \rightarrow O_3^- \cdot H_2O + O_2 \tag{10}$$

with a rate constant of 2.7×10^{-28} cm^6 sec^{-1}.

Similar to $O_2^- \cdot H_2O$, it is likely that O_3^- will be clustered through hydrogen bonding (~0.5 eV).[43–45] The photodestruction of $O_3^- \cdot H_2O$ in the present wavelength region is mainly attributable to the photodissociation processes,[4]

$$O_3^- \cdot H_2O + h\nu \rightarrow O_3^- + H_2O \tag{11}$$

and

$$O_3^- \cdot H_2O + h\nu \rightarrow O^- + O_2 + H_2O \ . \tag{12}$$

The cross section for the dissociative photodetachment process

$$O_3^- \cdot H_2O + h\nu \rightarrow O_3 + e + H_2O \tag{13}$$

is expected to be small, because the photodetachment of O_3^- is small compared to photodissociation (see Sec. D). In addition, $O_3^- \cdot H_2O$ photodetachment will take place only at wavelengths shorter than 4700 Å, because the threshold for photodetachment of $O_3^- \cdot H_2O$ is higher than the threshold for O_3^- (2.1028 eV)[12] by the bond energy of $O_3^- \cdot H_2O$ (~0.5 eV).

The photodestruction cross section of $O_3^- \cdot H_2O$ is shown in Fig. 7, along with the previous measurements[4] at longer wavelengths. In the previous measurements, discrete structure similar to that shown in O_3^- has been observed.[4] However, extension of this structure is not apparent in the present measurements. The laser wavelengths currently used may be too few to illustrate this structure. Further investigation of the structure using a tunable dye laser is planned.

F. O_4^-

O_4^- ions are formed from O_2^- by the three-body reaction

$$O_2^- + O_2 + O_2 \rightleftharpoons O_4^- + O_2 \ . \tag{14}$$

The rate constants[41] for the forward and reverse reactions are 4×10^{-31} cm^6/sec and 2.7×10^{-14} cm^3/sec, respectively. The O_4^- ions are created all along the drift region, and the ions created in the region near the laser beam may be vibrationally excited.[5]

The O_4^- ions may be photodestroyed by dissociative photodetachment

$$O_4^- + h\nu \rightarrow O_2 + e + O_2 \tag{15}$$

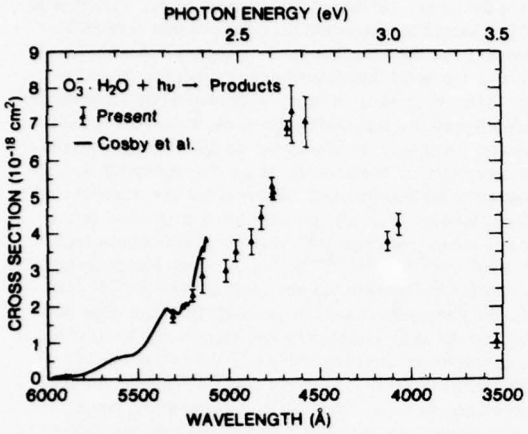

FIG. 7. The photodestruction cross section for $O_3^- \cdot H_2O$ in the 3500–6000 Å region. The measurements of Cosby *et al.* (Ref. 4) are indicated.

or by photodissociation

$$O_4^- + h\nu \rightarrow O_2^- + O_2 \ . \tag{16}$$

The photodestruction cross sections of O_4^- are shown in Fig. 8. The cross section at the UV line (66% 3507 Å and 34% 3569 Å) is $(8.64 \pm 0.80) \times 10^{-18}$ cm^2, which is not included in Fig. 8. The previous measurements given by Cosby *et al.*[2,3] and Smith *et al.*[5] are also shown. The photodestruction cross sections increase with increasing photon energy. The dependence of the O_4^- photodestruction cross section on wavelength is very similar to that of the O_2^- photodetachment cross section. This may suggest that the photodetachment process (15) is the dominant process for the photodestruction of O_4^-. The threshold for (15) is higher than the electron affinity for O_2 (0.440 eV)[34] by the O_4^- dissociation energy of 0.6 eV.[49] This threshold of 1.04 eV is consistent with the observed threshold at ~9000 Å obtained by extrapolation of the cross section to zero. The rate of increase of the cross section changes at wavelengths of ~7500 and 5500 Å. This may be attributable to dissociative photodetachment of O_4^- into the excited states of O_2, in a manner similar to that observed in O_2^- photodetachment.

Burt[50] has reported that the average photodetachment cross section of O_4^- in the 4500 Å region is 9×10^{-18} cm^2. This value is larger than the present measurements by a factor of about four. However, Burt's measurements[50] contained a large experimental uncertainty.

G. OH^- and OD^-

The OH^- ions are produced in a gas mixture of 2% CH_4 in O_2 by the reaction[51]

$$O^- + CH_4 \rightarrow OH^- + CH_3 \tag{17}$$

with a rate constant of 8×10^{-11} cm^3 sec^{-1}. With such a fast reaction rate, the O^- ions produced in the source region will be converted into OH^- within 1 cm when the CH_4 pressure is 4 mTorr and $E/N = 10$ Td. For a drift distance of 20 cm and an O_2 pressure of 0.2 Torr, the OH^- ions will experience about 1000 collisions before interacting with the laser; hence, the OH^- ions should be well relaxed and equilibrated with the surrounding gas at 300 K.

The OD^- ions are produced in a gas mixture of 2% CH_4 and 2% D_2 in O_2. The reaction of O^- and D_2 has two product channels,[52]

$$O^- + D_2 \rightarrow D_2O + e \tag{18}$$

$$\rightarrow OD^- + D \tag{19}$$

with rate constants of 4×10^{-10} and 1.5×10^{-11} cm^3 sec^{-1}, respectively. The rate for reaction (19) is very slow when compared with reactions (17) and (18). Therefore, OD^- is not primarily produced by reaction (19), but probably by the exchange process,

$$OH^- + D_2 \rightarrow OD^- + HD \ , \tag{20}$$

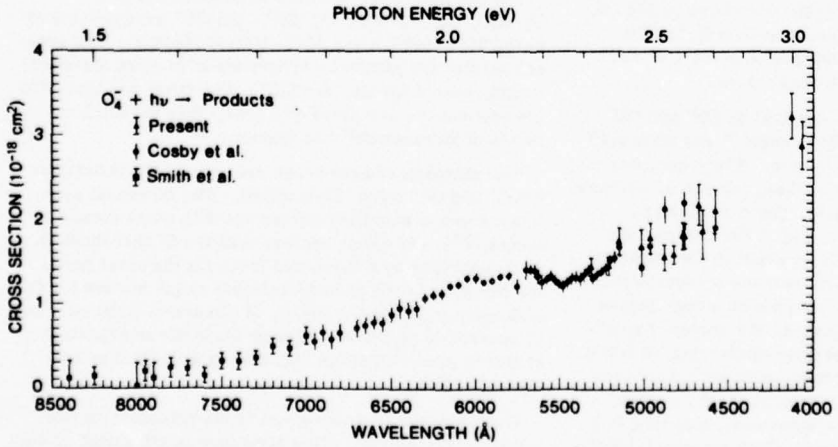

FIG. 8. The photodestruction cross section for O_4^- in the 4000–8500 Å region. The measurements of Cosby *et al.* (Refs. 2 and 3) and Smith *et al.* (Ref. 5) are shown.

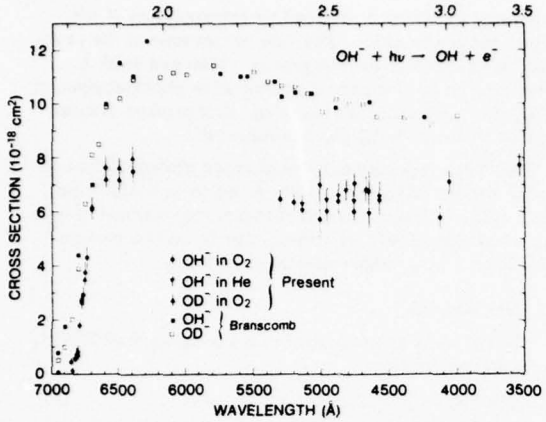

FIG. 9. The photodetachment cross sections for OH^- and OD^- in the 3500–700 Å region, measured in O_2 and He. The results of Branscomb (Ref. 18) are indicated for comparison.

where OH^- is initially produced by reaction (17).

The photodestruction of OH^- in the present photon energy region (< 3.5 eV) occurs only through photodetachment,

$$OH^- + h\nu \rightarrow OH + e \quad . \tag{21}$$

With electron affinities of 1.825 and 1.462 eV for OH[15] and O,[32] respectively, and a dissociation energy of 4.35 eV for OH,[53] the dissociation energy of OH^- is 4.71 eV, which is higher than the photon energy region investigated here.

The mobilities of OH^- and OD^- in O_2 have not been measured. However, if mass scaling is used, their mobilities should be nearly equal to that of O^- in O_2. This assumption was verified by measuring the cross sections of OH^- in a gas mixture of 1% CH_4 and 2% O_2 in He. The mobilities of OH^- and O^- in He are known and are nearly equal.[23] The photodetachment cross sections of OH^- and OD^- measured both in O_2 and in He are shown in Fig. 9. Since the cross sections measured in both O_2 and He gases are consistent, the mobilities used for OH^- and OD^- in O_2 must be close to the real values.

The photodetachment cross sections of OH^- and OD^- have also been measured by Branscomb[18] and Warneck[19] using crossed ion and photon beams. Their measurements are consistent with each other, but are 40% higher than the present measurements. The data given by Branscomb[18] are also shown in Fig. 9 for comparison. The discrepancy may be partly inherent in the different experimental techniques. In Branscomb's experiment, the ions were produced in discharge with a high degree of internal excitation, in contrast to the present experiment where the ions are in thermal equilibrium at 300 K. Also, Branscomb's data represent average values over a photon bandwidth of 50 Å, in contrast to the narrow laser bandwidth (0.5 Å for dye lasers and less than 0.1 Å for the Ar^+ and Kr^+ ion lasers). Such technical differences may explain the discrepancy at the threshold, where the cross section of Branscomb *et al.*[18] extends to slightly longer wavelengths than the present threshold. However, for wavelengths shorter than the threshold, both experimental techniques should give the same result. The cross section is not expected to be significantly affected by the bandwidth, because the cross section is nearly constant. It should not be affected by the rotational excitation, because the transition moments are not expected to be significantly different for the different rotational levels. Vibrational excitation may exist in the fast ion beam, although the vibrational spacing is high [$\omega_e = 3735$ cm^{-1} for $OH^-(^1\Sigma^+)$].[18] However, considering the similarity between the potential curves for OH and OH^-, the photodetachment cross section is not expected to be significantly affected by the vibrational excitation. The discrepancy between these OH^- measurements is large, when compared with the good agreement for the measurements of O^-[14] and O_2^-.[13] The possible experimental errors in the present measurements have been examined by measuring the cross section using various gas mixtures, gas pressures, and applied electric fields, but the results do not vary. At present, the discrepancy is not understood.

At the threshold, the present measurements agree quite well with the relative cross section measurements of Hotop *et al.*[15] The cross section shown in Fig. 9 has a sharp onset at 6795 ± 5 Å (14713 ± 11 cm^{-1}), in good agreement with the onset at 14 700 cm^{-1} observed by Hotop *et al.*[15] The sharp onset corresponds to the opening of the Q branches in the $OH(X\,^2\Pi_{3/2}) - OH^-(X\,^1\Sigma^+)$ transition[15] and should have the same wavelength in both measurements. The OH^- rotational temperature in the measurements of Hotop *et al.*[15] is about 1200 K, which is much higher than the temperature in the present measurements at 300 K. This results in the measurements of Hotop *et al.*[15] having a significant cross section at the wavelengths longer than the sharp onset, in contrast to the present measurements where the cross section at the longer wavelengths is small.

IV. CONCLUDING REMARKS

The photodestruction cross sections for O^-, O_2^-, $O_2^- \cdot H_2O$, O_3^-, $O_3^- \cdot H_2O$, O_4^-, OH^-, and OD^- were measured in the 3500–5400 Å and 6300–8600 Å regions. The present results are generally consistent with other measurements, except for OH^- and OD^-. For these two ions, the present results are about 40% lower than the measurements of Branscomb[18] and Warneck.[19]

The photodetachment cross sections at the thresholds for O^- and OH^- were investigated. The threshold wavelengths are in excellent agreement with other measurements.[15,32] The cross section near the O^- threshold is well described by a threshold law. On the other hand, the increase in the photodetachment cross section for O_2^- with increasing photon energy is attributed to the increase in accessible O_2 states, in contrast to the interpretation of Burch *et al.*[13] that the increase is explained by the threshold law.

Structure has been observed in the photodestruction cross section for O_3^-. This structure is attributed to the same progression previously observed at longer wave-

Appendix B

PHOTODISSOCIATION AND PHOTODETACHMENT OF MOLECULAR NEGATIVE IONS. VII. IONS FORMED IN $CO_2/O_2/H_2O$ MIXTURES, 3500-5300 Å

PHOTODISSOCIATION AND PHOTODETACHMENT OF MOLECULAR NEGATIVE IONS. VII. IONS FORMED IN $CO_2/O_2/H_2O$ MIXTURES, 3500-5300 Å*

G. P. Smith, L. C. Lee, and J. T. Moseley

Molecular Physics Laboratory

SRI International, Menlo Park, California 94025

ABSTRACT

Photodestruction cross sections have been measured for CO_3^-, $CO_3^- \cdot H_2O$, CO_4^-, $CO_4^- \cdot H_2O$, HCO_3^-, and $HCO_3^- \cdot H_2O$ at various ion laser and dye laser wavelengths between 5300 and 3500 Å using a drift tube mass spectrometer as the source of the ions. CO_3^- shows a structureless peak centered about 4500 Å, which is attributed to photodissociation. The possible excitation of CO_3^- in these studies was investigated in detail and no evidence was found for any excitation. Additional evidence is presented which indicates that the bond energy $D(CO_2\text{-}O^-)$ is less than or equal to 1.9 eV. The $CO_3^- \cdot H_2O$ cross section decreases smoothly with decreasing wavelength over this wavelength range. CO_4^- photodestruction was observed at 3500 Å, but the other ions listed above have cross sections below 10^{-19} cm^2, and possibly zero, throughout this spectral region.

* Submitted to the Journal of Chemical Physics (in press).

I. INTRODUCTION

The photodissociation and photodetachment of negative ions are important ionospheric processes, affecting both ion composition and the electron density. Thus, cross section measurements for these processes are needed to understand the D-region ion chemistry[1]. Previous work[2-5] has examined photodestruction processes of atmospheric negative ions at wavelengths between 4579 and 8400 Å. We have recently extended these measurements to 3500 Å, and report here the photodestruction cross sections for the following carbon-containing ions from 3500 to 5300 Å : CO_3^-, $CO_3^- \cdot H_2O$, CO_4^-, $CO_4^- \cdot H_2O$, HCO_3^-, and $HCO_3^- \cdot H_2O$. Results for oxygen and nitrogen containing atmospheric negative ions (O_3^-, NO_3^-, $O_2^- \cdot H_2O$, etc.) at these wavelengths will be reported elsewhere.[6,7]

These measurements also provide information on the electronic structure of the negative ions. Previous work has measured and interpreted the structure in the CO_3^- photodissociation cross section.[8] We have now examined the CO_3^- photodestruction cross section at higher photon energies, where photodetachment is also reported to occur.[9] Possible excitation of the CO_3^- was investigated, and it is concluded that the CO_3^- in this and previous studies in this laboratory is either thermally relaxed, or has an unusually stable excited state. The implications of these experiments on the CO_3^- and O_3^- thermochemistry are discussed.

II. EXPERIMENTAL TECHNIQUE

The basic apparatus consists of a drift tube mass spectrometer and an ion or tunable dye laser, and has been described in detail previously.[2,3] Briefly, the negative ions are formed by electron attachment in the source region, and by subsequent ion-molecule reactions. They drift to the end of the tube under the influence of a weak electric field, at a fraction of their thermal velocity. Approximately 0.2 cm in front of the exit aperture in the end plate of the drift tube, the ions intersect the cavity of a chopped tunable dye laser or prism-tuned Ar or Kr ion laser. The ions then pass through the exit aperture into a high vacuum region containing a quadrupole mass spectrometer which selects the ion to be studied. A two-channel counter accumulates the data, laser on (I) and off (I_o).

The present measurements were all made with an intracavity laser beam intersecting the ion swarm. A prism was used to select the 4579, 4658, 4765, 4880, 4965, 5017, and 5145 Å Ar laser lines and the 4067, 4131, 4680, 4762, 4825, 5208, 5309 Å Kr laser lines. Ultraviolet measurements were made with a Kr laser using only UV mirrors. The intracavity beam was measured to be 25% 3564 Å and 75% 3507 Å by focusing the reflection off a Brewster window into a monochromator.

Dye laser measurements from 4250 to 4600 Å were made using the dye Stilbene 420 (Exciton Chemical Co.), pumped by the 4W UV output of an Ar laser. Measurements directed toward the study of excited CO_3^- were

made at 6550 Å, using the dye Rhodamine 640 pumped by an Ar laser.

All cross sections were measured relative to the O_2^- photodetachment cross section, and normalized to our previously reported values.[3,4,6] The cross section for an ion A^- is given by:

$$\sigma_{A^-}(\lambda) = \sigma_{O_2^-}(\lambda) \frac{\ell n(I_o/I)_{A^-} P_{O_2^-} K_{A^-}}{\ell n(I_o/I)_{O_2^-} P_{A^-} K_{O_2^-}} , \qquad (1)$$

where P is the measured laser output power and K is the reduced ion mobility. Values[5,10] used for K are 2.51 $cm^2/V \cdot sec$ for CO_3^- in O_2, 2.4 for CO_4^- and 2.3 for $CO_4^- \cdot H_2O$ in O_2, and 1.34 for HCO_3^- and 1.3 for $HCO_3^- \cdot H_2O$ in CO_2.

Measurements were made at 0.4 torr pressure, with a ratio of the drift field to the gas number density (E/N) of 10 Td (1 Td = 10^{-17} $V \cdot cm^2$), where the ion drift velocity is approximately one-tenth its thermal velocity, and a drift distance of 20 cm. The CO_3^- ions were produced in various mixtures of 0.01% to 10% CO_2 in O_2. The CO_4^- ions were made using 2% CO_2 in O_2, and HCO_3^- was made using 4% CH_4 in CO_2. These conditions insure that O^- photofragment recombination with CO_2 to form CO_3^- is negligible.[2] Hydrates were formed by adding a trace of H_2O. Sufficient mass spectrometer resolution was maintained to prevent contamination of the $CO_3^- \cdot H_2O$ signal by $HCO_3^- \cdot H_2O$.

III. CO_3^- PHOTODESTRUCTION FROM 3500 TO 5300 Å

Detailed dye laser measurements of the structured CO_3^- cross section have previously been made between 5200 and 6900 Å, and the spectrum has been analyzed.[8] Argon laser wavelength measurements were also made.[4] We have repeated these Ar laser measurements, determined the cross sections at the Kr laser wavelengths between 3500 and 5309 Å, and made dye laser measurements of the cross section for the 4250 to 4600 Å region. The results are shown in Figure 1. The Ar laser data disagree slightly beyond statistical uncertainties with the previous results at 4765, 4880 and 5145 Å. The slight disagreement between ion and dye laser results may be attributable in part to the much narrower bandwidth of the ion laser. The current measurements also agree well with the Ar laser measurements made by Beyer and Vanderhoff,[11] using a similar apparatus. The previous Ar laser measurements were made in CO_2, while the current measurements were made in O_2 with only trace amounts of CO_2 present.

The new results are consistent with a lack of sharp detailed structure below 5000 Å, but do show a broad peak in the cross section near 4550 Å. No obvious relationship is apparent between this peak and the structure at longer wavelength, suggesting the existence of a dissociative transition to a repulsive electronic state. Increased O^- photofragment detection between 4765 and 4579 Å, observed previously,[2] supports the conclusion that the photodissociation in this wavelength range is due to

a different transition than that at longer wavelength. The 4000 to 5000 Å measurements are consistent with the photodissociation cross sections measured by Vestal and Mauclaire[12] using a tandem mass spectrometer ion beam technique.

Hong, Woo, and Helmy[9] report values for the CO_3^- photodetachment cross section, determined by measuring photoelectron currents from CO_3^- relative to O^- using a drift tube and various cutoff filters. They infer a very sharp peak in the photodetachment cross section near 4500 Å, with a magnitude of $\sim 1 \times 10^{-18}$ cm^2, and a second broader peak from 2900 to 3900 Å. The total photodestruction cross section at 3500 Å reported here is only about 25% of their photodetachment cross section alone. In the 4500 Å region, the good agreement between our total photodestruction cross section and the photodissociation measurements of Ref. 11 are not consistent with significant photodetachment here.

To investigate this problem further, the total O^- photofragment current from CO_3^- was measured between 4300 and 4880 Å. The ratios of O^- photofragment appearance to CO_3^- photoloss are given in Table I. No significant change in this ratio is detectable between 4300 and 4579 Å, where the ratio is essentially 1. No evidence is seen for a sharp photodetachment threshold at 4590 Å or rapidly declining photodetachment cross section at 4300 Å.[9] The nearly constant O^- photoproduction ratio throughout this region indicates no new photodestruction process, such

as photodetachment, occurs on a scale comparable to photodissociation to $O^- + CO_2$. The decrease in O^- photofragments between 4579 Å and 4880 Å is consistent with existing observations and interpretations[2,8] that the photodissociation at wavelengths between 5145 and 4880 Å (2.41 to 2.53 eV) is due primarily to the $2^2B_2 \leftarrow 1^2B_2$ transition, which is parallel, while at wavelengths shorter than 4880 Å the perpendicular $1^2A_2 \leftarrow 1^2B_2$ transition dominates. The structured cross section at wavelengths longer than 5145 Å has been assigned to a third transition $1^2A_1 \leftarrow 1^2B_2$.

We conclude that the CO_3^- studied here photodissociates, but does not significantly photodetach for wavelengths longer than 4300 Å. If it is assumed that O^- and CO_3^- are detected with equal efficiency, the data are consistent with 100% photodissociation. From the uncertainties in the relative O^- observed, the upper limits shown in Table I can be placed on the photodetachment cross section. Evidence presented below strongly indicates that the CO_3^- studied here is in its ground electronic state, and is essentially thermalized to 300K.

IV. THERMODYNAMICS AND EXCITED STATES OF CO_3^-

The picture of CO_3^- that results from this and our previous work[2,8] is consistent and reasonable. These conclusions are, in summary, as follows: (i) the ground state, 1^2B_2, has a bond dissociation energy of 1.8 ± 0.1 eV; (ii) the first observed excited state is 1^2A_1, which has its origin 1.520 eV above the ground vibrational level of the ground state, has three stretching vibrational modes with energies of 880 cm^{-1}, 990 cm^{-1} and 1470 cm^{-1}, and is predissociated above 1.8 eV; (iii) the second observed excited state is 2^2B_2 and leads to direct dissociation between 2.41 eV (5145 Å) and 2.53 eV (4880 Å); (iv) the third observed excited state, 1^2A_2 is mainly responsible for dissociation above 2.53 eV; and (v) the electron affinity of CO_3 is 2.9 ± 0.3 eV. However, our conclusion that the 1.8 eV dissociation energy refers to the ground state has been called into question by results from other laboratories.

The measurements made by Vestal and Mauclaire[12] on the photodissociation of CO_3^-, while they agree quite well with the measurements presented here between 4000 and 5000 Å, show significant differences at longer wavelengths. Near 6000 Å their measurements depended strongly on the ion source pressure. The cross section magnitude increased with decreasing source pressure, and agreed with the drift tube results only at low pressure. This pressure dependence was attributed to an excited state of CO_3^-, which is slowly

relaxed by collisions with CO_2. It was determined that a relaxation rate of 5×10^{-14} cm^3/sec would explain their results.

Wu and Tiernan[13] have studied the collisional dissociation of CO_3^- by measuring the translational energy threshold for the dissociation. They observed that when CO_3^- was formed from the reaction[14]

$$O_3^- + CO_2 \rightarrow CO_3^- + O_2, \tag{2}$$

it exhibited a collisional dissociation threshold of 2.5 eV, while a fraction of the CO_3^- formed from the reaction

$$O^- + CO_2 + M \rightarrow CO_3^- + M \tag{3}$$

exhibited a threshold at 1.8 eV, with a second threshold at 2.5 eV. This lower energy threshold was interpreted as being indicative of an excited state of CO_3^-, which is not effectively collisionally deactivated, even at relatively high source pressures. It was thus suggested that the photodissociation threshold observed near 1.8 eV refers to this excited state.

Dotan, Davidson, Streit, Albritton and Fehsenfeld[15] have pointed out that there is a significant discrepancy in the reported dissociation energies and electron affinities of O_3^-, O_3, CO_3^-, and CO_3. They determined that $D(CO_2\text{-}O^-) - D(O_2\text{-}O^-) \geq 0.58$ eV. The O_3^- dissociation energy can be determined from the recently measured O_3 electron affinity[16] of

2.1028 ± 0.0025 eV. These two numbers are related by

$$EA(O_3) = D(O_2\text{-}O^-) + EA(O) - D(O_2\text{-}O) \quad , \tag{4}$$

where the oxygen atom electron affinity[17] is 1.462 ± 0.003 eV and the ozone dissociation energy[18] is 1.05 ± 0.02 eV. This results in $D(O_2\text{-}O^-) = 1.69$ eV, and thus implies $D(CO_2\text{-}O^-) \geq 2.27$ eV.

A value near 2.5 eV for the bond energy of CO_3^- would be consistent with the observations from these three laboratories.[12,13,15] We therefore investigated the photodissociation of CO_3^- in the region of 1.9 eV in more detail.

First, in the drift tube apparatus it is possible to form CO_3^- either primarily by reaction (2), or primarily by reaction (3). Measurement of the photodissociation cross section near 1.9 eV as a function of the formation mechanism will then test for the presence of excited CO_3^- if it is formed, as reported, from reaction (3), and if it survives deexcitation to cross the laser cavity. The ion production mechanisms can be accurately modeled since the reaction rates and mobilities involved are reasonably well known. The rate for reaction (2) is 5.5×10^{-10} cm^3/sec,[14] and for (3) is 1×10^{-27} cm^6/sec[19] when CO_2 is the third body, 3.1×10^{-28} cm^6/sec[14] when O_2 is the third body. The third needed reaction, the formation of O_3^-,

$$O^- + O_2 + M \rightarrow O_3^- + M, \tag{5}$$

has a rate of 1×10^{-30} cm^6/sec[20] when O_2 is the third body. The drift velocities for O^-, O_3^- and CO_3^- in O_2 are[10] 0.860, 0.691, and 0.677×10^4 cm/sec, respectively, at the E/N of 10 Td used here.

Figure 2 shows the results of integrating the rate equations (2), (3), and (5) to predict ion intensities, as compared with experimental measurements. The effect of diffusion was removed from the measurements by comparison with Cl^-, an ion formed on the filament which does not react with O_2 or CO_2. Figure 2a shows the relative ion intensity and the model calculation for 0.003% CO_2 in O_2; Figure 2b for 0.1% CO_2 in O_2; and Figure 2c for 1.0% CO_2 in O_2. The difference between these situations is clear. In Figure 2a CO_3^- is being produced primarily from O_3^-, reaction (2), while in 2c most of it is being produced primarily from O^-, reaction (3). The model predicts that for a drift distance of 30 cm, 96% of the CO_3^- is produced by reaction (2) for 0.003% CO_2 in O_2, 62% for 0.1%, and only 15% for 1%. The model consistently accounts for the observed chemistry for CO_2 percentages ranging from 0.001% to 100%, and predicts that over this range the percentage of CO_3^- produced by reaction (2) varies from zero to 98%.

Since the reaction rates are not precisely known, these percentages are subject to some uncertainty. However, the conclusion that CO_3^- can be produced primarily by reaction (2), or by reaction (3), is inescapable. For example, to model the data of Figure 2a under the assumption that the

CO_3^- was produced primarily by reaction (3) would require increasing the rate of this reaction by an order of magnitude while decreasing the rate for reaction (2) by a similar amount. The uncertainties in these reaction rates are no more than a factor of two, and further, the data at higher CO_2 concentrations could not be fit using such rates.

It is therefore clear that the production mechanism for CO_3^- can be varied from primarily reaction (2) to primarily reaction (3). If either of these reactions produces a substantial amount of excited CO_3^-, and if the excitation survives to reach the interaction region, then the photodissociation cross section near 1.9 eV should reflect this excitation. Table II lists the CO_3^- photodissociation cross section at 6550 Å (1.89 eV), measured at 10 Td, 0.40 torr total pressure, and 30.5 cm drift distance, for various percentages of CO_2 in oxygen. Also listed is the percentage of CO_3^- produced by reaction (2), as predicted by the kinetic model. This wavelength corresponds to the lowest photon energy where there is a large peak in the photodissociation cross section.

Although these experiments clearly span the range of CO_2 partial pressures over which the CO_3^- production mechanism changes, no significant variation of the cross section is observed. Thus we conclude that the CO_3^- studied here, and consequently in previous research in this laboratory, has a dissociation energy $D(CO_2\text{-}O^-) \leq 1.9$ eV. If, as suggested by Wu and Tiernan,[13] reaction (3) produces some excited CO_3^-, this excitation is apparently substantially relaxed by the time the ions encounter the

laser photons. The question of whether or not both reactions produce equally excited CO_3^-, which is subsequently not easily relaxed, is unresolved. However, this seems unlikely due to the very different exothermicities of the two reactions.

As a further test for possible excitation common to both reaction (2) and (3), the CO_3^- photodissociation cross section was measured at 6550 Å (1.89 eV) as a function of drift distance, both in pure CO_2, and in O_2 with 1% CO_2. In both cases the primary formation mechanism for CO_3^- is reaction (3).

The results for 0.2 torr pure CO_2 are shown in Fig. 3a. At this pressure, virtually all O^- is converted to CO_3^- within 2 cm of the ion source. The error bars represent one standard deviation statistical uncertainty in the count rate. The solid line gives the most rapidly decreasing cross section consistent with these error limits, and yields a maximum deexcitation rate constant of 1×10^{-15} cm^3/sec. The data are certainly consistent with a constant cross section, i.e., no deexcitation. If an excited state of CO_3^- is responsible for the dissociative photoabsorption, its relaxation rate is very slow. This rate is a factor of 50 smaller than that assumed by Vestal and Mauclaire[12] to explain their results. The rate assumed by Vestal and Mauclaire would lead to relaxation of any excited CO_3^- within about 10 cm from the ion source, and thus would have led to a decrease of the photodissociation cross section to zero over the range of drift distance in Figure 3a, if absorption from an excited state were responsible.

Figure 3b shows similar data obtained for 1% CO_2 in 0.4 torr of O_2 at an E/N of 10 Td. The main differences between these data and those of Fig. 3a is that for the conditions of Fig. 3b the production of the CO_3^- is spread out over a much greater drift distance, and the deexcitation is by O_2 rather than CO_2. The photodissociation cross section is larger at drift distances shorter than 5 cm, indicating that the CO_3^- may be initially formed with significant excitation from reaction (3). Wu and Tiernan[13] also observe excited CO_3^- from reaction (3), although the interpretations of these two studies disagree. The excitation we observe is substantially relaxed after 15 cm of drift, and only a slight decrease in the cross section is observed for longer drift distances. From the data between 15 and 46 cm, an upper limit of 6.1×10^{-15} cm^3/sec can be placed on the deexcitation rate constant for CO_3^- in O_2. However, the data at shorter drift distances shows that the deexcitation rate for nascent CO_3^- formed from reaction (3) is faster. A deexcitation rate for drift distances between 5 and 15 cm is somewhat greater than 1.3×10^{-14} cm^3/sec. This faster deexcitation observed at shorter drift distances where there is significant CO_3^- formation may be that observed by Vestal and Mauclaire.[12]

V. CONCLUSIONS ON CO_3^-

A number of conclusions can thus be drawn from this study of the photodissociation of CO_3^- at 6550 Å. First, CO_3^- produced by either reaction (2) or (3) photodissociates at 6550 Å, and the cross section for photodissociation does not vary significantly with the production mechanism if the ions are allowed to undergo on the order of 5000 collisions after formation. Further, the cross section at this wavelength is substantial, and is the largest value observed from the threshold near 7000 Å to 3500 Å. Thus the dissociation here cannot reasonably be attributed to a small fraction of excited ions. It seems necessary to conclude that the CO_3^- studied here is reasonably well relaxed, and that the bond energy of the ground state of CO_3^- is less than or equal to 1.9 eV.

An alternate possibility is that both reactions (2) and (3) produce equally excited CO_3^-, and that this excited CO_3^- is very stable, with a relaxation rate in CO_2 of less than 10^{-15} cm^3/sec. This possibility seems very unlikely, and would not resolve the previously described thermodynamic dilemma. The flow-drift tube measurements of Dotan et al.[15] were made over similar time and pressure regimes as the measurements reported here, and the CO_3^- was formed primarily by reaction (2). Thus the bond energy difference determined between O_3^- and CO_3^- would refer to the presumed excited state of CO_3^-.

It does appear (see Fig. 3b) that CO_3^- produced from reaction (3) is excited, and that this excitation is relaxed by O_2 at a rate exceeding 1.3×10^{-14} cm^3/sec. All CO_3^- photodissociation cross sections reported from our laboratory have been obtained under conditions such that this initial excitation is substantially relaxed.

VI. OTHER OBSERVATIONS ON CO_3^-

In a further search for evidence of excitation of CO_3^-, the dependence of the photodissociation cross section at 6550 Å on total pressure and on E/N was investigated. These experiments were done at low CO_2 partial pressures, so the previously observed effects[2] of the fast three-body recombination reaction (3) of the photofragment O^- to reform CO_3^- are negligible for these measurements.

The pressure dependence of the CO_3^- photodestruction cross section at 6550 Å, measured at 10 Td and a drift distance of 10 cm, is shown in Fig. 4. The observed decline with increased pressure is independent of the method of CO_3^- production. The measured values are the same for a 0.025% CO_2 in O_2 gas mixture, in which most of the CO_3^- is formed via reaction (2), and for a 1% CO_2 in N_2 mixture in which CO_3^- is produced entirely by reaction (3). Furthermore, the position dependence measurements discussed in the previous section rule out relaxation of vibrationally excited CO_3^- at higher pressures as a possible explanation. The fact that increasing the number of collisions by increasing the drift distance does not cause a decrease in the cross section, while increasing collisions by increasing the pressure does cause such a decrease, indicates the pressure dependence is due to a variation in the number of collisions following laser irradiation, just in front of the drift tube exit aperture. It is thus that a likely mechanism for the observed pressure dependence involves collisional quenching of laser excited CO_3^{-*}.

The predictions of such a model are given by the dashed line in Figure 4, and are developed in the following discussion.

The proposed mechanism for CO_3^- photodissociation is fully discussed in Ref. 2. The CO_3^- photodestruction cross section is smaller and more structured than that of the hydrate $CO_3^- \cdot H_2O$. Since the hydrate electronic transition should basically be the same one, centered on CO_3^-, the CO_3^- absorption cross section is substantially larger than the photodissociation cross section. For the purposes of this discussion we will assume that the total CO_3^- absorption cross section equals the observed $CO_3^- \cdot H_2O$ photodissociation cross section of 7×10^{-18} cm^2 at 6550 Å (see section VII). The electronic state of CO_3^- excited by the laser decays by the competitive process of fluorescence and predissociation. At 0.1 torr and 6550 Å, the photodissociation cross section of 3.6×10^{-18} cm^2 is therefore roughly one-half the photoabsorption cross section of CO_3^-. The radiative decay rate k_R thus approximately equals the CO_3^- photodissociation rate, since the processes compete equally for CO_3^{-*} at 6550 Å.

The radiative lifetime, which is the reciprocal of this rate, can be estimated from the formula of Strickler and Berg,[22]

$$\tau_R^{-1} = 2.88 \times 10^{-9} < \nu_f^{-3} >^{-1} \int \epsilon d(\ln \nu_a) \quad , \qquad (6)$$

where ν_f is the fluorescence frequency in cm^{-1}, ν_a is the absorption frequency, the brackets indicate an average over the emission spectrum, and ϵ is the decadic molar extinction coefficient in mole/l-cm ($\epsilon = 2.6 \times 10^{20} \sigma$). To approximate the unknown $< \nu_f^{-3} >$ term, we assume that

the fluorescence spectrum is a reflection of the absorption spectrum through the origin of the transition at 7000 Å, as is typically the case.[23] Then equation (6) predicts τ_R = 500 nsec, i.e., a radiative decay rate of 2×10^6 sec^{-1} at 6550 Å. The predissociation rate thus is approximately equal to this value.

As shown in Fig. 4, the CO_3^- photodissociation cross section at 6550 Å declines to half its value upon the addition of each 0.20 torr of gas. This can be attributed to collisional quenching of the predissociating electronically excited state. Since the origin of the electronic state lies at a lower energy than the thermodynamic limit for CO_3^- dissociation, only vibrational quenching within the excited state is necessary to prevent dissociation. At 6550 Å, only 0.10 eV need be removed. At 0.20 torr, the quenching rate equals the dissociation rate of 2×10^6 sec^{-1}, giving a quenching rate constant of 3×10^{-10} cm^3/sec. Efficient removal of such small amounts of vibrational energy, at rates approaching gas kinetic, is certainly reasonable.

This model is also consistent with previous observations[24] of no significant pressure dependence from 0.04 to 0.10 torr in the CO_3^- cross section at 5990 Å. At this wavelength 0.27 eV of excess energy must be removed to prevent dissociation, so more collisions--higher pressures--are required.

Figure 5 shows the variation of the CO_3^- cross section with the drift field E/N at 6550 Å, in 0.20 torr N_2 with 1% CO_2. The effect of increasing E/N to 40 Td is to raise the ion translational, rotational, and probably vibrational temperatures to 600 K. As Fig. 3b illustrates, hot nascent CO_3^- has an enhanced photodissociation cross section. Large effects on cross sections near the thresholds have been seen previously,[25] and attributed to vibrational excitation. For CO_3^-, however, we are observing the predissociation of a particular vibronic transition. Since rotation is known to enhance some predissociation rates,[26] this suggests one possible explanation of the E/N dependence. As the drift field and rotational temperature increase, the faster predissociation competes more effectively with collisional quenching and the observed cross section rises.

In conclusion, both the E/N and pressure effects may be attributed to subtle mechanistic details of the predissociation process. Future experiments should provide additional information. The lack of a position or gas mixture dependence of the CO_3^- photodissociation cross section clearly indicates that the pressure dependence of the cross section cannot be explained by the relaxation of excited CO_3^-.

VII. $CO_3^- \cdot H_2O$

Photodestruction cross sections for $CO_3^- \cdot H_2O$ are shown in Fig. 6. The new measurements agree, within statistical uncertainty, with the previous results.[2,4,5] A declining, generally featureless cross section is indicated below 5300 Å. The cross section for the hydrate continues to exceed that of the parent CO_3^- ion at all wavelengths, but to a lesser degree at wavelengths shorter than 4500 Å. The hydrate cross section has the appearance of a single band, while CO_3^- photodissociation has a second peak near 4500 Å.

Previous work has suggested[8] that the electronic states of the hydrate are those of the parent CO_3^-, only slightly perturbed. This type of behavior is more clearly illustrated by the ozonide ion O_3^- and its hydrates.[21] The CO_3^- photodissociation cross section is lower than that of $CO_3^- \cdot H_2O$ because of competition from fluorescence. Dissociation of the hydrate to $CO_3^- + H_2O$ requires less energy and is faster. When CO_3^- photodissociation is closer to its thermodynamic threshold, the predissociation is slower. At the 4500 Å peak, however, the CO_3^- cross section is nearly equal to that of the $CO_3^- \cdot H_2O$. This indicates that the fluorescence yield has probably decreased at higher excitation energies. The lack of CO_3^- structure at these wavelengths also offers evidence for a faster dissociation rate.

VIII. CO_4^- AND $CO_4^- \cdot H_2O$

Table III presents the Kr laser wavelength results for these ions. The upper limits shown for most cross sections are based on one standard deviation statistical counting error. With one exception, all such measurements are consistent with zero cross sections, and limits $\leq 1 \times 10^{-19}$ cm^2 can generally be set. Note that CO_4^- has begun to photodetach or photodissociate in the ultraviolet. The onset of photodestruction appears well above the thermodynamic threshold for either process. We were unable to detect photoproducts due to the large amounts of O^-, O_2^-, and CO_3^- ions also present in the drift tube. The hydrate $CO_4^- \cdot H_2O$ has a cross section less than half the parent's value, and possibly zero, at 3500 Å. Similar behavior[7] has been observed for $NO_2^- \cdot H_2O$. A very small non-zero CO_4^- photodestruction cross section of $(3.7 \pm 2.0) \times 10^{-20}$ cm^2 was previously measured[4] at 5145 Å. The cross section at this wavelength, if it is in fact non-zero, fails to rise significantly at shorter wavelengths.

Vestal and Mauclaire[12] have reported positive cross sections for CO_4^- photodissociation at wavelengths shorter than 5300 Å. Their results show a flat cross section of $(1.0 \pm 0.7) \times 10^{-18}$ cm^2, rather than a sharp rise, between 4000 and 3500 Å. Photoproduction of both O_2^- and a small amount of CO_3^- was observed at 3650 Å. Excited ions from the source of the beam experiments of Ref. 12 are the probable explanation for these results.

IX. HCO_3^- AND $HCO_3^- \cdot H_2O$

No photodestruction was observed for these ions at all wavelengths above 3500 Å, as shown by the limits given in Table III. Previous studies have established similar results[4,8] for wavelengths longer than 5145 Å. Initial reports[2] of a small positive cross section have since been attributed to operation at excessively high total ion densities.[4]

ACKNOWLEDGMENTS

The authors wish to acknowledge useful discussions with Dr. P. C. Cosby and to thank Dr. R. Hodges for his participation in some of the measurements during the conclusion of this research. This work was supported by the U.S. Air Force Office of Scientific Research, the U.S. Air Force Geophysics Laboratory, and by the Atmospheric Sciences Laboratory, U.S. Army Electronics Command, White Sands, N.M., and the use of a laboratory computer system through an equipment grant (PHY76-14436) from the National Science Foundation is acknowledged.

REFERENCES

1. L. Thomas, Radio Sci. 9, 121 (1974); J. R. Peterson, J. Geophys. Res. 81, 1433 (1976).
2. J. T. Moseley, P. C. Cosby, R. A. Bennett, and J. R. Peterson, J. Chem. Phys. 62, 4826 (1975).
3. P. C. Cosby, R. A. Bennett, J. R. Peterson, and J. T. Moseley, J. Chem. Phys. 63, 1612 (1975).
4. P. C. Cosby, J. H. Ling, J. R. Peterson, and J. T. Moseley, J. Chem. Phys. 65, 5267 (1976).
5. G. P. Smith, L. C. Lee, P. C. Cosby, J. R. Peterson, and J. T. Moseley, J. Chem. Phys. 68, 3818 (1978).
6. L. C. Lee and G. P. Smith, J. Chem. Phys. 70, 1727 (1979).
7. G. P. Smith, L. C. Lee, and P. C. Cosby, to be submitted to J. Chem. Phys.
8. J. T. Moseley, P. C. Cosby, and J. R. Peterson, J. Chem. Phys. 65, 2512 (1976).
9. S. P. Hong, S. B. Woo, and E. M. Helmy, Phys. Rev. A 15, 1563 (1977).
10. H. W. Ellis, R. Y. Pai, E. W. McDaniel, E. A. Mason, and L. A. Viehland, At. Data Nucl. Data Tables 17, 177 (1976).
11. R. A. Beyer and J. A. Vanderhoff, J. Chem. Phys. 65, 2313 (1976).
12. M. L. Vestal and G. H. Mauclaire, J. Chem. Phys. 67, 3758 (1977).

13. R.L.C. Wu and T. O. Tiernan, 31st Gaseous Electronics Conference, Abstract HA-7, Buffalo, N.Y., 1978.

14. F. C. Fehsenfeld and E. E. Ferguson, J. Chem. Phys. 61, 318 (1974).

15. I. Dotan, J. A. Davidson, G. E. Streit, D. L. Albritton, and F. C. Fehsenfeld, J. Chem. Phys. 67, 2874 (1977).

16. S. E. Novick, P. C. Engelking, P. L. Jones, J. H. Futrell and W. C. Lineberger, J. Chem. Phys. 70, 2652 (1979).

17. H. Hotop and W. C. Lineberger, J. Phys. Chem. Ref. Data 4, 539 (1975).

18. JANAF Thermochemical Tables, NBS RDS-NBS37, Government Printing Office, Washington, 1970.

19. D. A. Parkes, J. Chem. Soc. Farad I 68, 627 (1972).

20. J. L. Pack and A. V. Phelps, Bull. Am. Phys. Soc. 16, 214 (1971).

21. P. C. Cosby, J. T. Moseley, G. P. Smith, J. Chem. Phys. 69, 2779 (1978).

22. S. J. Strickler and R. A. Berg, J. Chem. Phys. 37, 814 (1962).

23. N. J. Turro, Modern Molecular Photochemistry, Benjamin/Cummings, Menlo Park, California, 1978.

24. P. C. Cosby and J. T. Moseley, Phys. Rev. Lett. 34, 1603 (1975).

25. L. C. Lee and G. P. Smith, Phys. Rev. A 10, 000 (1979).

26. G. Herzberg, Spectra of Diatomic Molecules, Van Nostrand, New York, 1950, p. 418.

lengths. Detailed investigation of this structure is in progress.

ACKNOWLEDGMENTS

We are indebted to Dr. J. T. Moseley, Dr. P. C. Cosby, and Dr. J. R. Peterson for initiating this work and for their advice and assistance during the course of this work. The use of a laboratory system obtained under an equipment grant from the National Science Foundation is acknowledged. This work was supported primarily by the Atmospheric Sciences Laboratory, U.S. Army Electronics Command, White Sands Missile Range, New Mexico, and in part by the U.S. Air Force Office of Scientific Research, and the U.S. Air Force Geophysics Laboratory.

[1]J. T. Moseley, P. C. Cosby, R. A. Bennett, and J. R. Peterson, J. Chem. Phys. **62**, 4826 (1975).
[2]P. C. Cosby, R. A. Bennett, J. R. Peterson, and J. T. Moseley, J. Chem. Phys. 63, 1612 (1975).
[3]P. C. Cosby, J. H. Ling, J. R. Peterson, and J. T. Moseley, J. Chem. Phys. **65**, 5267 (1977).
[4]P. C. Cosby, G. P. Smith, and J. T. Moseley, J. Chem. Phys. **69**, 2779 (1978).
[5]G. P. Smith, L. C. Lee, P. C. Cosby, J. R. Peterson, and J. T. Moseley, J. Chem. Phys. **68**, 3818 (1978).
[6]G. P. Smith, P. C. Cosby, and J. T. Moseley, J. Chem. Phys. **67**, 3818 (1977).
[7]G. P. Smith and L. C. Lee, J. Chem. Phys. **69**, 5393 (1978).
[8]R. P. Turco and C. F. Sechrist, Jr., Radio Sci. **7**, 725 (1972); L. Thomas, P. M. Gondhalekar, and M. R. Bowman, J. Atmos. Terr. Phys. **35**, 397 (1973); L. Thomas, Radio Sci. **9**, 121 (1974); R. P. Turco. Radio Sci. **9**. 655 (1974).
[9]J. R. Peterson, J. Geophys. Res. **81**, 1433 (1976); also J. R. Peterson, P. C. Cosby, and J. T. Moseley, COSPAR Space Research, Vol. XVII, p. 243 (1977).
[10]P. C. Cosby and J. T. Moseley, Phys. Rev. Lett. **34**, 1603 (1975); J. T. Moseley, P. C. Cosby, and J. R. Peterson, J. Chem. Phys. **65**, 2512 (1976).
[11]P. C. Cosby, J. T. Moseley, J. R. Peterson, and J. H. Ling, J. Chem. Phys. **69**, 2771 (1978).
[12]S. E. Novick, P. C. Engelking, P. L. Jones, J. H. Futrell, and W. C. Lineberger, "Laser Photoelectron, Photodetachment, and Photodestruction Spectra of O_3^-," (to be published).
[13]D. S. Burch, S. J. Smith, and L. M. Branscomb, Phys. Rev. **112**, 171 (1958).
[14]L. M. Branscomb, S. J. Smith, and G. Tisone, J. Chem. Phys. **43**, 2906 (1965).
[15]H. Hotop, T. A. Patterson, and W. C. Lineberger, J. Chem. Phys. **60**, 1806 (1974).
[16]L. C. Lee, G. P. Smith, T. M. Miller, and P. C. Cosby, Phys. Rev. A **17**, 2005 (1978).
[17]L. M. Branscomb, D. S. Burch, S. J. Smith, and S. Geltman, Phys. Rev. **111**, 504 (1958).
[18]L. M. Branscomb, Phys. Rev. **148**, 11 (1966).
[19]P. Warneck, "Laboratory Measurements of Photodetachment Cross Sections of Selected Negative Ions," GCA Tech. Report 69-13-N, GCA Corp., Bedford, Massachusetts (1969).
[20]R. A. Beyer and J. A. Vanderhoff, J. Chem. Phys. **65**, 2313 (1976).
[21]J. A. Vanderhoff, Ballistic Research Laboratory, Tech. Report ARBRL-TR-02070 (1978).
[22]Rhodamine 640 perchlorate was obtained from the Exciton Chemical Co.; oxazine 1 perchlorate was from the Eastman Kodak Co. and New England Nuclear; DEOTC was from the Exciton Chemical Co., the Eastman Kodak Co., and the Nippon Kankoh-Shikiso Kenkyusho.
[23]H. W. Ellis, R. Y. Pai, E. W. McDaniel, E. A. Mason, and L. A. Viehland, At. Data Nucl. Data Tables **17**, 177 (1976); E. W. McDaniel and E. A. Mason, "The Mobility and Diffusion of Ions in Gases," (Wiley, New York, 1973).
[24]S. Geltman, Astrophys. J. **136**, 935 (1962).
[25]K. L. Bell and A. E. Kingston, Proc. Phys. Soc. London **90**, 895 (1967).
[26]M. P. Ajmera and K. T. Chung, Phys. Rev. **12**, 475 (1975).
[27]T. N. Rescigno, C. W. McCurdy, Jr., and V. McKoy, J. Chem. Phys. **64**, 477 (1976).
[28]J. T. Broad and W. P. Reinhart, Phys. Rev. A **14**, 2159 (1976).
[29]S. J. Smith and D. S. Burch, Phys. Rev. **116**, 1125 (1959).
[30]H. P. Popp and S. Kruse, J. Quant. Spectrosc. Radiat. Transfer, **16**, 683 (1976).
[31]E. Graham IV, D. R. James, W. C. Keever, I. R. Gatland, and E. W. McDaniel, Tech. Report, Georgia Institute of Technology, 1974.
[32]H. Hotop and W. C. Lineberger, J. Phys. Chem. Ref. Data **4**, 539 (1975).
[33]J. A. Burt, Can. J. Phys. **50**, 2410 (1972).
[34]R. J. Celotta, R. A. Bennett, J. L. Hall, M. W. Siegel, and J. Levine, Phys. Rev. A **6**, 631 (1972).
[35]D. L. Albritton, J. T. Moseley, P. C. Cosby, and M. Tadjeddine, J. Mol. Spectrosc. **70**, 326 (1978).
[36]L. C. Lee and G. P. Smith, "Photodissociation Cross Sections of Ne_2^+, Ar_2^+, Kr_2^+ and Xe_2^+ from 3500 to 5400 Å," Phys. Rev. (in press).
[37]G. Das, A. C. Wahl, W. T. Zemke, and W. C. Stwalley, J. Chem. Phys. **68**, 4252 (1978).
[38]H. Shimamori and Y. Hatano, Chem. Phys. **21**, 187 (1977).
[39]P. H. Krupenie, J. Phys. Chem. Ref. Data **1**, 423 (1972).
[40]J. A. Vanderhoff, DNA Project, Annual Report FY76 and FY77.
[41]J. L. Pack and A. V. Phelps, Bull. Am. Phys. Soc. **16**, 214 (1971).
[42]F. C. Fehsenfeld and E. E. Ferguson, J. Chem. Phys. **61**, 3181 (1974).
[43]G. H. F. Diercksen and W. P. Kraemer, Chem. Phys. Lett. **5**, 570 (1970); H. Lischka, T. Plesser, and P. Schuster, Chem. Phys. Lett. **6**, 263 (1970); K. G. Breitschwerdt and H. Kistenmacher, Chem. Phys. Lett. **14**, 288 (1972); H. Kistenmacher, H. Popkie, and E. Clementi, J. Chem. Phys. **58**, 5627 (1973).
[44]W. P. Kraemer, *Quantum Chemistry*, Proceedings of SRC Atlas Symposium, Vol. 4 (Oxford, 1964), p. 217.
[45]M. Arshadi and P. Kebarle, J. Phys. Chem. **74**, 1483 (1970).
[46]S. F. Wong, T. V. Vorburger, and S. B. Woo, Phys. Rev. A **5**, 2598 (1972).
[47]M. L. Vestal and G. H. Mauclaire, J. Chem. Phys. **67**, 3767 (1977).
[48]R. M. Snuggs, D. J. Volz, J. H. Schummers, D. W. Martin, and E. W. McDaniel, Phys. Rev. A **3**, 477 (1971).
[49]D. C. Conway and L. E. Nesbitt, J. Chem. Phys. **48**, 509 (1968).
[50]J. A. Burt, J. Geophys. Res. **77**, 6280 (1972).
[51]W. Lindinger, D. L. Albritton, F. C. Fehsenfeld, and E. E. Ferguson, J. Chem. Phys. **63**, 3238 (1975).
[52]M. McFarland, D. L. Albritton, F. C. Fehsenfeld, E. E. Ferguson, and A. L. Schmeltekopf, J. Chem. Phys. **59**, 6629 (1973).
[53]G. Herzberg, *Spectra of Diatomic Molecules* (Van Nostrand, New Jersey, 1967).

Appendix C

PHOTODISSOCIATION AND PHOTODETACHMENT OF MOLECULAR NEGATIVE IONS. VIII. NITROGEN OXIDES AND HYDRATES, 3500-8250 Å

PHOTODISSOCIATION AND PHOTODETACHMENT OF MOLECULAR NEGATIVE IONS. VIII. NITROGEN OXIDES AND HYDRATES, 3500-8250 Å *

G. P. Smith, L. C. Lee, and P. C. Cosby
Molecular Physics Laboratory
SRI International, Menlo Park, CA 94025

ABSTRACT

Total photodestruction cross sections for the ions NO_2^-, $NO_2^- \cdot H_2O$, NO_3^-, $NO_3^- \cdot H_2O$, and the peroxy isomers $O_2^- \cdot NO$ and $O_2^- \cdot NO \cdot H_2O$ have been measured at wavelengths between 3500 and 8250 Å, using Ar , Kr , and dye lasers and a drift tube mass spectrometer. A threshold of $\sim$ 2.5 eV was observed for the photodetachment of thermalized NO_2^-. Upper limits were set for the photodestruction cross sections of $NO_2^- \cdot H_2O$, NO_3^-, and $NO_3^- \cdot H_2O$ over this wavelength range. The NO_3^- isomer $O_2^- \cdot NO$ and its hydrate, formed in N_2O, have large photodissociation cross sections at wavelengths shorter than 5500 Å. Observations of collisional dissociation of cluster ions such as $NO_2^- \cdot H_2O$ by laser-excited NO_2 in the drift tube are also discussed.

* Submitted to the Journal of Chemical Physics (in press).

I INTRODUCTION

The ion NO_3^- is a key constituent of the D-region of the earth's ionosphere,[1] due to its stability. With a bond energy[2] of nearly 4 eV, NO_3^- will react with neutrals only to form cluster ions such as $NO_3^- \cdot H_2O$. Once formed, these ions are only slowly removed by neutralization with positive ions or by photodetachment. Efforts to model the D-region require knowledge of the photodestruction processes for the important NO_3^- ion and its hydrates, and for the precursor NO_2^- ion.

During the course of reaction rate measurements relevant to D-region ion chemistry, a second isomer of NO_3^- was discovered.[3,4] Since this second form is produced via switching reactions such as $O_4^- + NO \rightarrow O_2^- \cdot NO + O_2$, the isomeric state is believed to have a peroxide (OONO) rather than nitrate (NO_3) structure. Investigations[3-5] into the reactions producing and destroying $O_2^- \cdot NO$ have fixed this ion's place in the D-region reaction scheme which converts O_x^- and CO_x^- ions to NO_x^- ions, but photodestruction measurements are also needed. In addition, comparison of the photophysics of the two forms of NO_2^-, and their hydrates, can provide important structural information on the isomers. Finally, different photophysical behavior of the two forms allows their differentiation and should be useful in clarifying the chemistry of the production and subsequent reactions of the ions.

In this paper we report total photodestruction cross sections at wavelengths from 3500-8250 Å for the ions NO_2^-, NO_3^-, $O_2^- \cdot NO$, and their

first hydrates. Photochemical destruction of weakly bound cluster ions such as $NO_2^- \cdot H_2O$ by laser-excited NO_2 was also observed in the drift tube, and was briefly investigated.

II EXPERIMENTAL DETAILS

The apparatus is a drift tube-mass spectrometer coupled with an ion or dye laser, and has been described in detail previously.[6] Negative ions formed by gas phase electron attachment and subsequent ion-molecule reactions drift slowly through the ~ 0.50 torr gas mixture under the influence of a weak applied electric field (E/N = 10 Td) toward an exit aperture. Before passing through the aperture into the high vacuum quadrupole mass spectrometer region at the end of the drift tube, the ions intersect an intracavity laser beam, which is chopped at 100 Hz. By counting mass-specific ion intensities, laser on and off, laser photodestruction rates for various ions can be measured. The relative cross sections thus determined are placed on an absolute scale by normalization to the known[7] O_2^- photodetachment cross section, measured in O_2. The ratio of the relative laser powers is measured for this determination. The ratio of ion drift velocities through the laser beam is also needed, and is calculated from the ion mobilities. Mobilities used[8] in this work were 1.3 $cm^2V^{-1}s^{-1}$ for $O_2^- \cdot NO$, 1.25 for $O_2^- \cdot NO \cdot H_2O$ in N_2O, and 1.3 for $NO_2^- \cdot H_2O$ in CO_2, all scaled from the measured mobilities of positive and negative ions in CO_2; and 2.5 $cm^2V^{-1}s^{-1}$ for NO_2^- in O_2 scaled from the measured mobility of O_3^- in O_2.

A variety of laser sources was used. Prism tuned Ar^+ laser lines at 5145, 5017, 4965, 4880, 4765, 4658, and 4579 Å, and Kr^+ laser lines at 5309, 5208, 4825, 4762, 4680, 4131, and 4067 were used, with the drift tube interaction region within the laser cavity. The unseparated Kr^+ laser ultraviolet output, consisting of 25% 3564 Å and 75% 3507 Å, was also used. Intracavity dye laser measurements were made from 4200 to 4650 Å using stilbene 3 dye, pumped by the 4 W UV Ar^+ laser output; from 7150 to 7700 Å using oxazine dye; and at 8350 Å using DEOTC dye pumped by the Kr^+ laser red lines.

III NO_2^- AND $NO_2^- \cdot H_2O$

Photodestruction cross section measurements for NO_2^- are shown in Figure 1. Photodetachment is responsible for the photodestruction, since the photodissociation threshold is above 4.0 eV.[9] The measurements were made in 0.40 torr O_2 with ~ 1% NO and a trace of NO_2 present, at E/N = 10 Td and a drift distance of 20 cm from the ion source to the laser. The ions are formed in the source region by the rapid charge transfer reactions[4,10]

$$O^- + NO_2 \rightarrow NO_2^- + O \qquad (1a)$$

$$O_2^- + NO_2 \rightarrow NO_2^- + O_2 \qquad (1b)$$

and by the three-body association reaction

$$O^- + NO + O_2 \rightarrow NO_2^- + O_2 \quad , \qquad (2)$$

where $k_1 \sim 1.2 \times 10^{-10}$ cm^3/s. Extrapolation of the NO_2^- cross section measurements to wavelengths longer than 4800 Å indicates an approximate threshold of 2.5 eV, in accord with the photodetachment value[11] of 2.36 ± 0.10 eV for the NO_2 electron affinity.

Other studies[12,13] have reported larger cross sections between 4000 and 5000 Å than the current measurements. As Huber et al.[9] have demonstrated, these can be attributed to vibrationally excited NO_2^-. Since vibrationally excited NO_2^- is formed[9] in reaction (1), drift tube conditions were chosen to permit relaxation of the nascent NO_2^- to 300 K prior to their arrival at the laser. Huber et al.[9] have measured an effective relaxation rate of 8.5×10^{-13} cm^3/s in O_2, for excited NO_2^- which can be photodissociated at 5400 Å. Then for the drift tube conditions stated above, only 3% of the nascent NO_2^- ions will remain excited after drifting 2 cm from their point of formation. Measurements of ion composition as a function of drift distance show that less than 7% of the NO_2^- ions arriving at the laser are formed within 2 cm of the laser. Given the photodetachment cross section for nascent, unrelaxed NO_2^- of 0.75×10^{-18} cm^2 at 5400 Å,[9] the contribution of excited NO_2^- to the cross section measurements presented in Figure 1 is thus estimated to be less than 1×10^{-20} cm^2.

At 4680 Å, a constant cross section was observed for drift distances between 10 and 20 cm, indicating complete relaxation of any initially excited NO_2^- ions to a 300 K internal energy distribution. Larger cross sections were measured at shorter drift distances. An analysis similar to that of Ref. 9 gives an effective relaxation rate constant of 3×10^{-13} cm^3/s. This is slower than the relaxation rates observed previously[9] at 5400 and 6300 Å, because photodetachment at the longer wavelengths samples only the more highly excited vibrational levels, which are more quickly depopulated as the ions approach thermal equilibrium via collisions.

A small positive cross section of $2.3 \pm 0.9 \times 10^{-20}$ cm^2 is observed at 5208 Å (2.38 eV). This cross section is larger than that calculated for the contribution from excited NO_2^- ions. Given the current value[11] of 2.36 ± 0.10 eV for the electron affinity of NO_2, this observation is consistent with threshold photodetachment of relaxed NO_2^-.

Warneck[13] has observed a similar threshold for NO_2^- photodetachment, but his cross section measurement at 3500 Å is only 30% of our value. The reason for this discrepancy is unclear, particularly since his experiments utilized a discharge source-beam apparatus and should reflect a larger fraction of vibrationally excited ions.

Measurements on $NO_2^- \cdot H_2O$ were made in a mixture of 0.1-2.0% NO in 0.4 torr CO_2, with traces of impurity NO_2 and added H_2O. Under these conditions no O_4^- contaminates mass 64. Nevertheless, D_2O was also used to produce $NO_2^- \cdot D_2O$ for some experiments, to verify the absence of O_4^-. The amount of NO_2 present is sufficiently low to prevent significant collisional dissociation by excited NO_2 (see Section VI). The $NO_2^- \cdot H_2O$ ions are created from NO_2^- by the fast three-body reaction[4]

$$NO_2^- + H_2O + CO_2 \rightarrow NO_2^- \cdot H_2O + CO_2, \quad k_3 \sim 1.6 \times 10^{-28} \text{ cm}^6/\text{s} \quad . \quad (3)$$

The measured $NO_2^- \cdot H_2O$ photodestruction cross sections are given in Table 1 and Figure 1. A threshold near 4131 Å is evident, and the cross section is nearly one-half that of the parent NO_2^- at 3500 Å. The products of the $NO_2^- \cdot H_2O$ photodestruction could not be experimentally established because of the presence of a large excess of NO_2^- ions in the drift tube. It is likely, however, that dissociative photodetachment is the observed process. This would be consistent with the observed blue-shift in the hydrate threshold with respect to that of NO_2^-. One might expect the same electronic transition to be responsible for the photon absorption in each species, but the hydrate requires additional energy to break the NO_2^--H_2O bond. Given the electron affinity[11] of NO_2 of 2.36 eV and the $NO_2^- \cdot H_2O$ bond energy[14] of 0.62 eV, the thermodynamic threshold for dissociative photodetachment of the hydrate is 2.98 eV, a value essentially identical to the observed photodestruction threshold.

IV NO_3^- AND $NO_3^- \cdot H_2O$

The ground state (nitrate) isomer of NO_3^- was created in a mixture of 2% NO_2 in CO_2 at 0.40 torr by the reaction[4]

$$CO_3^- + NO_2 \rightarrow NO_3^- + CO_2, \quad k_4 = 2.0 \times 10^{-10} \text{ cm}^3/\text{s} \quad , \qquad (4)$$

and, to a minor degree,

$$NO_2^- + NO_2 \rightarrow NO_3^- + NO, \quad k_5 = 4.0 \times 10^{-12} \text{ cm}^3/\text{s} \quad . \qquad (5)$$

Reaction (4) is exothermic by 2.8 ± 0.3 eV, as calculated from the dissociation energies of CO_3^- (1.8 eV)[15] and NO_3^- (see next paragraph), and the NO_2 and O electron affinities.[7,11] Only the ground state NO_3^- isomer should be formed. Since the excited isomer is known to react quickly with CO_2 via reaction (4), its production via (4) must be endothermic and slow.

Table 1 gives upper limits on the NO_3^- photodestruction cross sections from 4131 to 5309 Å. These values represent one standard deviation of statistical uncertainty, and all measurements were consistent with zero cross sections in this region. However, a small positive cross section was measured at the Kr^+ laser UV lines (3.5 eV). This energy is at or near the thermodynamic threshold for either photodetachment or photodissociation. The NO_3^- photodetachment threshold, from the electron affinity[2] of NO_3, is 3.9 ± 0.2 eV. Given an NO_3 dissociation energy[16] of 2.15 ± 0.2 eV and an NO_2 electron affinity[11] of 2.36 eV, the photodissociation

threshold for $NO_3^- \rightarrow NO_2^- + O$ is 3.7 ± 0.4 eV. Although the thermodynamic threshold for the photodissociation channel $NO_3^- \rightarrow O_2^- + NO$ is only 3.6 eV, an energy barrier may be expected for the rearrangement from the NO_3^- nitrate structure. An alternate explanation to NO_3^- photodissociation at 3500 Å is also possible. The isomer $O_2^- \cdot NO$ has a large cross section at 3500 Å of 7×10^{-18} cm^2 (see Section V). The presence of only 1.5% peroxy form at mass 62, produced by reactions other than (4), could account for the observed cross section. A similar effect should have been observed at 4131 Å, but the error limit set there is quite high, and the fraction of excited isomer may easily vary for different drift tube experiments. Future experiments at shorter wavelengths using excimer lasers should resolve this question.

The hydrate of ground state NO_3^- was formed in the same mixture with added traces of H_2O via the three-body reaction[14]

$$NO_3^- + H_2O + CO_2 \rightarrow NO_3^- \cdot H_2O + CO_2, \quad k_6 \sim 7.5 \times 10^{-29} \text{ cm}^6/\text{s} \quad . \quad (6)$$

For a 2% NO_2 fraction, collisional dissociation of $NO_3^- \cdot H_2O$ by laser excited NO_2^* should not affect the measurements (see Section VI). The observations given in Table 1 are consistent with a cross section below 1.0×10^{-19} cm^2 and probably zero, at wavelengths longer than 4100 Å. A positive cross section larger than that of the parent NO_3^- was measured at ~ 3500 Å. The observed photodestruction cannot be attributed to the presence of the hydrate of the peroxy form, $O_2^- \cdot NO \cdot H_2O$. A sizeable

excited isomer fraction of 12% would be required for this explanation, and would produce a larger cross section than is observed at 4131 Å. This case may be similar to CO_3^- and its hydrate,[15] in that an electronic transition centered on the parent ion can result in photodissociation of the hydrate at energies below the thermodynamic threshold for the parent. Photodissociation of $NO_3^- \cdot H_2O$ to NO_3^- and H_2O is the thermodynamically likely process at 3500 Å.

V $O_2^- \cdot NO$, $O_2^- \cdot NO \cdot H_2O$ AND $O_2^- \cdot N_2O$

A second form of NO_3^- can be produced by reaction of NO with O_4^-, CO_4^-, or $O_2^- \cdot H_2O$ via the exchange reactions[3,4]

$$O_2^- \cdot X + NO \rightarrow O_2^- \cdot NO + X , \quad X = O_2, CO_2, H_2O \tag{7}$$

with $k_7 = 0.5\text{-}3.0 \times 10^{-10}$ cm^3/s. This isomeric form is distinguishable from NO_3^- in that it reacts[3,4] with NO and CO_2 by donating an O^- to form NO_2^- and CO_3^-. These reactions are endothermic by 0.5 and 2.7 eV, respectively, for ground state NO_3^-. The formation reactions (7), and the lack of conversion by collisions to form ground state NO_3^-, suggest an oxygen-oxygen bond for the excited isomer, with the negative charge residing on the more electronegative O_2 portion of the molecule.

Since the reverse of reaction (4) occurs[5] for $O_2^- \cdot NO$, it is at least 2.7 eV more energetic than NO_3^-, and has these thermodynamic thresholds for various photoprocesses:

$$
\begin{aligned}
O_2^-\cdot NO + h\nu &\rightarrow NO_2^- + O && \Delta H \leq 1.0 \text{ eV} \\
&\rightarrow O^- + NO_2 && 1.9 \text{ eV} \\
&\rightarrow O_2^- + NO && 0.9 \text{ eV} \\
&\rightarrow OONO + e^- && 1.0 \text{ eV} \\
&\rightarrow O_2 + NO + e^- && 1.3 \text{ eV} \quad .
\end{aligned} \tag{8}
$$

These values are based on a dissociation energy of 3.7 eV for normal NO_3^-, the known electron affinities[7,11] of O, O_2, and NO_2, and an estimate[17] of 0.3 eV for the OO-NO bond energy. Given these low energy photodestruction channels, photodissociation or photodetachment of $O_2^-\cdot NO$ should be observed at visible wavelengths. We attempted to produce $O_2^-\cdot NO$ in the drift tube from other O_2^- cluster ions. Unfortunately, these cluster ions could not be made in large quantities, and the amount of NO required for efficient switching reactions to form $O_2^-\cdot NO$ also produced large amounts of NO_2^- and normal NO_3^-.

In our search for NO_2-free sources of nitrogen oxide ions, we examined negative ions in $\sim$ 0.5 torr N_2O with a trace of O_2 in the drift tube, although previous work[18] indicated no NO_3^- would be formed. However, the major ions we observed were O_2^-, $O_2^-\cdot N_2O$, NO_3^-, and NO_2^-. The $O_2^-\cdot N_2O$ is formed by the reaction[9]

$$
O_2^- + 2N_2O \rightarrow O_2^-\cdot N_2O + N_2O, \qquad k_9 = 5 \times 10^{-29} \text{ cm}^6/\text{s} \quad , \tag{9}
$$

and has a slowly increasing photodestruction cross section of

0.8-1.0 x 10^{-18} cm^2 from 6400 to 5300 Å. The NO_3^- produced in N_2O is observed to photodissociate into O_2^- and NO at wavelengths shorter than 6000 Å, and therefore is probably the peroxy form $O_2^-\cdot NO$.

The amount of $O_2^-\cdot NO$ in the drift tube appears to build up with time and then stabilize after ~ 15 minutes, indicating it may be formed by reactions of the other ions with impurities. A reaction $O_2^-\cdot N_2O + NO \rightarrow O_2^-\cdot NO + N_2O$ is one possibility, but in the excess of N_2O equilibria should favor $O_2^-\cdot N_2O$, which is contrary to observations.

The photodestruction cross section measurements for $O_2^-\cdot NO$ are shown in Figure 2. The data were taken at 10 Td in 0.4 torr N_2O and a drift distance of 20 cm, and show a gradually increasing cross section with little detailed structure. Sizeable O_2^- photofragment signals were observed at 5300 and 4400 Å, indicating photodissociation to O_2^- and NO is the major process throughout this wavelength range, and suggesting that a single electronic transition may be responsible. This is further strong evidence for the peroxy structure of this isomer. The large cross section also suggests using photodissociation as a detection method in differentiating the chemistry of $O_2^-\cdot NO$ and NO_3^-.

There is some discrepancy between ion and dye laser measurements near 5200 Å and between Ar^+ and Kr^+ laser measurements near 4750 Å. Given the uncertainty concerning the production mechanism, we believe these differences are attributable to different fractions of $O_2^-\cdot NO$

and NO_3^- at mass 62 in the drift tube. Since we cannot be certain that all the NO_3^- is the peroxy form, the measured cross sections should be considered lower limits to the true values. Nevertheless, the measurements are generally repeatable, and we believe the cross section magnitudes are accurate. The probable absence of large amounts of normal NO_3^- is supported by the high cross section values observed near 4100 and 3500 Å and by the lack of a position (5-30 cm) or pressure (0.40-1.00 torr) dependence at 5300-5400 Å. In addition, measurements in mixtures up to 50% O_2 gave identical results. In mixtures free of NO, NO_2, and CO_2, and to a degree in the ionosphere, $O_2^-\cdot NO$ appears to be a stable ion. The relevant destruction and interconversion reactions are

$$O_2^-\cdot NO + NO \rightarrow NO_2^- + NO_2 \quad , \tag{10}$$

$$NO_2^- + NO_2 \rightarrow NO_3^- + NO \quad , \tag{11}$$

and

$$O_2^-\cdot NO + CO_2 \rightarrow CO_3^- + NO_2 \tag{12}$$

with rate constants[3,5] of $k_{10} = 1.5 \times 10^{-11}$ and $k_{11} = 4.0 \times 10^{-12}$ cm^3/s.

By adding trace amounts of water, the hydrate ion $O_2^-\cdot NO\cdot H_2O$ can be produced by the reaction

$$O_2^-\cdot NO + H_2O + N_2O \rightarrow O_2^-\cdot NO\cdot H_2O + N_2O \quad . \tag{13}$$

The photodestruction cross section of this ion, shown in Figure 3, is different from that of $NO_3^-\cdot H_2O$ and indicates that the peroxy structure is preserved upon hydration. The cross section has a shape similar to that of the parent $O_2^-\cdot NO$, but is smaller in magnitude. Thus, the electrostatic bonding of H_2O to the parent anion does not significantly alter its peroxy identity. Similar behavior

has been observed for the O_3^- ion and its first two hydrates.[19] Large amounts of $O_2^- \cdot NO$ were detected as a principal product of $O_2^- \cdot NO \cdot H_2O$ photodestruction.

An attempt was made to produce $O_2^- \cdot NO$ by direct three-body association in a mixture of 5% NO in O_2 at 0.50 torr. The NO_3^- cross section measured at 5300 Å was less than 3×10^{-20} cm^2, indicating that only ground state NO_3^- was present. However, upon adding D_2O, $NO_3^- \cdot D_2O$ ions were produced which were photodestroyed at the same rate as $O_2^- \cdot NO \cdot H_2O$ ions formed in N_2O. This suggests that the peroxy isomer of $O_2^- \cdot NO$ is initially formed, and that hydration competes effectively with conversion to normal NO_3^- by reactions (10) and (11). The $O_2^- \cdot NO$ isomer apparently is more easily hydrated than NO_3^-, and $O_2^- \cdot NO \cdot H_2O$ is apparently not readily converted to $NO_3^- \cdot H_2O$ or otherwise consumed by reactions with nitrogen oxides. This is in agreement with the observation of Reference 4 that hydration of O_3^- inhibits the conversion, in CO_2, of O_3^- into CO_3^- ions. These observations suggest the importance of considering the chemistry and photochemistry of the peroxy ion and hydrate in modeling the ionosphere, particularly since the peroxy ion appears easily hydrated with retention of its structural identity.

In 1.0 torr N_2O, ions of mass 60 were also observed. The ion $N_2O_2^-$ has been reported in earlier studies[18] of negative ions in N_2O, but photodestruction cross section measurements made between 5300 and 5650 Å reproduced the structure previously observed[15] for CO_3^-. The magnitude of the mass 60 cross section was 30% of the CO_3^- value. This suggests that the observed photodestruction is due to CO_3^- formed from CO_2 impurity, and that some $N_2O_2^-$ is present, but has only a small photodestruction cross section ($\leq 10^{-19}$ cm^2) in this wavelength region.

VI COLLISIONAL DISSOCIATION BY EXCITED NO_2

During the course of these experiments, a highly structured apparent photodestruction cross section was observed for $NO_2^- \cdot D_2O$ between 5800 and 6300 Å, which varied with NO_2 partial pressure. Measurements for 5% NO_2 in 0.5 torr Ar are shown in Figure 4. As the solid line indicates, the structure closely resembles that of the NO_2 absorption spectrum,[20] and suggests that the observed $NO_2^- \cdot D_2O$ photodestruction is caused by collisions with electronically or vibrationally excited NO_2. Thus the measurements reported in Table 1 were made using NO/CO_2 mixtures, and resulted in zero cross sections.

Similar, but much smaller, effects were observed at 5800 Å for the ions $NO_2^- \cdot NO_2$, $NO_3^- \cdot D_2O$, and $NO_3^- \cdot NO_2$. The cross sections relative to that of $NO_2^- \cdot D_2O$ were 0.014, 0.067, and 0.025, respectively. We believe the much higher rate for collisional dissociation of $NO_2^- \cdot D_2O$ is not caused by any great disparity in the bond energies of these cluster ions, but is due to enhancement by resonant charge transfer. Since the charge is shared equally between NO_2 molecules in $NO_2^- \cdot NO_2$, only $NO_2^- \cdot D_2O$ has an extra electron centered on NO_2. An approaching NO_2 molecule will share this charge. The D_2O will be attracted to both NO_2 molecules, and should the system have sufficient ($\sim$ 0.5 eV) vibrational energy, the D_2O will not remain bound to it.

The observed $NO_2^- \cdot D_2O$ photodestruction is too large to be attributed to electronically excited NO_2^*. Given an NO_2 absorption cross section[21,22] (Q) of $\sim 3 \times 10^{-20}$ cm^2 at 5800 Å and an intracavity laser power of 60 W ($p = 2 \times 10^{20}$ photons/s) over the 0.04 cm^2 cross sectional area of the

laser beam, the excitation rate (Qp/A) is 150/sec·molecule. The quenching rate constant[21,22] of $\sim 10^{-10}$ cm^3/s gives a quenching rate in 0.025 torr NO_2 partial pressure (to vibrationally hot ground state $NO_2^{\ddagger}$) of $9 \times 10^4/s$. [Fluorescence[22] ($\sim 2 \times 10^4/s$) and diffusion[23] ($\sim 10^3/s$) are slower loss processes, and the Ar buffer gas is a much less efficient quencher than NO_2.] At most only $\frac{150}{90000} = 0.002$ of the NO_2 or 1.5×10^{12} cm^{-3} will be electronically excited. For the observed 18% destruction ($\frac{I-I_o}{I_o}$) and a laser beam width $\ell = 0.2$ cm, the expression

$$\ell n(I_o/I) = [NO_2^*]\, \ell\sigma \qquad (14)$$

gives a cross section of 6600 $Å^2$ for collisional dissociation of $NO_2^-\cdot D_2O$ by NO_2^*. This represents interaction at 45 Å, and is unrealistically large.

It thus seems more likely that vibrationally excited $NO_2^{\ddagger}$ is responsible for the observed dissociation. We can modify the above treatment for vibrationally excited $NO_2^{\ddagger}$, but the quenching rate can only be roughly estimated. Several collisions will be required to deactivate the hot $NO_2^{\ddagger}$ (2.3 eV) to energies below the dissociation energy of $NO_2^-\cdot H_2O$ ($\sim$ 0.5 eV). Unfortunately, this energy range lies between the values for which experimental rate data are available. We will thus approach the problem by estimating the effective vibrational quenching rate from two limits.

Some quenching rate constants have been measured for low-lying levels. A typical V → T quenching rate constant[24] for $O_3^{\ddagger}$ in Ar is

$\sim 10^{-14}$ cm^3/s . In these experiments, 0.09 eV of energy was removed, but $NO_2^{\ddagger}$ deactivation requires the removal of $\sim$ 1.6 eV. Thus 17 relaxing collisions will be required, and the effective quenching rate constant is 6×10^{-16} cm^3/s . Of course, at higher vibrational energies, the density of states is high enough to permit more efficient collisions, which remove smaller amounts of energy. Thus the above rate is a lower limit.

Low pressure recombination (three-body association) rate constants can provide some information on energy transfer at high energies (near molecular dissociation limits). Typical results[25] for small molecules in Ar show $\sim$ 0.035 eV vibrational energy is removed in each hard sphere collision. Thus 46 collisions at the rate of $\sim 10^{-10}$ cm^3/s are required to deactivate $NO_2^{\ddagger}$, or $k \sim 2 \times 10^{-12}$ cm^3/s . This is an upper limit since our $NO_2^{\ddagger}$ is less excited. A wide range of rate constants is obviously possible, but for this calculation a value of 5×10^{-14} cm^3/s was chosen, with an order of magnitude uncertainty likely.

Following the method of the electronic quenching calculation, at 0.5 torr Ar this rate constant gives a deactivation rate of 875/s. For a 150/s excitation rate, $\frac{150}{875}$ or 1.5×10^{14} cm^{-3} $NO_2^{\ddagger}$ is excited at steady state. Then Equation (14) gives a collisional dissociation cross section of 66 $\mathring{A}^2$. This is a reasonable value for a process which is enhanced by the resonant exchange of an electron between the two NO_2 groups, but is only accurate to an order of magnitude. Given the uncertainty in the

vibrational deactivation rate, the vibrational mechanism for collisional dissociation, while more likely, is not certain.

Finally, we note a previous example of visible laser induced NO_2 reactions,[26] where the slow reaction $NO_2^* + CO \rightarrow NO + CO_2$ was attributed to electronically excited NO_2^*.

ACKNOWLEDGMENTS

We thank Drs. J. T. Moseley and J. R. Peterson for many useful discussions. This work was supported primarily by the U.S. Army Research Office, and the Atmospheric Sciences Laboratory, U.S. Army Electronics Command, White Sands, New Mexico, and in part by the U.S. Air Force Office of Scientific Research and the U.S. Air Force Geophysics Laboratory. The use of a laboratory computer system obtained under an equipment grant from the National Science Foundation is acknowledged.

REFERENCES

1. F. C. Fehsenfeld and E. E. Ferguson, Planet. Space Sci. 20, 295 (1972).
2. E. E. Ferguson, D. B. Dunkin, and F. C. Fehsenfeld, J. Chem. Phys. 57, 1459 (1972).
3. N. G. Adams, D. K. Bohme, D. B. Dunkin, F. C. Fehsenfeld, and E. E. Ferguson, J. Chem. Phys. 52, 3133 (1970).
4. F. C. Fehsenfeld and E. E. Ferguson, J. Chem. Phys. 61, 3181 (1974).
5. F. C. Fehsenfeld, E. E. Ferguson, and D. K. Bohme, Planet. Space Sci. 17, 1759 (1969).
6. P. C. Cosby, R. A. Bennett, J. R. Peterson, and J. T. Moseley, J. Chem. Phys. 63, 1612 (1975).
7. L. C. Lee and G. P. Smith, J. Chem. Phys. 70, 1727 (1979); D. S. Burch, S. J. Smith, and L. M. Branscomb, Phys. Rev. 112, 171 (1958).
8. H. W. Ellis, R. Y. Pai, E. W. McDaniel, E. A. Mason, and L. A. Viehland, At. Data Nucl. Data Tables 17, 177 (1976); E. W. McDaniel and E. H. Mason, The Mobility and Diffusion of Ions in Gases (Wiley, New York, 1973).
9. B. A. Huber, P. C. Cosby, J. R. Peterson, and J. T. Moseley, J. Chem. Phys. 66, 4520 (1976).
10. E. E. Ferguson, F. C. Fehsenfeld, and A. L. Schmeltekopf, Adv. in Chem. 80, 83 (1969).
11. E. Herbst, T. A. Patterson, and W. C. Lineberger, J. Chem. Phys. 61, 1300 (1974).

12. J. H. Richardson, L. M. Stephenson, and J. I. Brauman, Chem. Phys. Lett. 25, 318 (1974).

13. P. Warneck, Chem. Phys. Lett. 3, 532 (1969).

14. J. D. Payzant, R. Yamdagni, and P. Kebarle, Can. J. Chem. 49, 3308 (1971).

15. J. T. Moseley, P. C. Cosby, and J. R. Peterson, J. Chem. Phys. 65, 2521 (1976).

16. JANAF Thermochemical Tables, NBS RDS-NBS 37, Government Printing Office, Washington, D.C., 1970.

17. S. W. Benson, Thermochemical Kinetics (Wiley, New York, 1976).

18. D. A. Parkes, J. Chem. Soc. 68, 2103 (1972); J. L. Moruzzi and J. T. Dakin, J. Chem. Phys. 49, 5000 (1968).

19. P. C. Cosby, G. P. Smith, and J. T. Moseley, J. Chem. Phys. 69, 2779 (1978).

20. C. G. Stevens and R. N. Zare, J. Mol. Spectrosc. 56, 167 (1975).

21. S. E. Schwartz and H. S. Johnston, J. Chem. Phys. 51, 1286 (1969).

22. V. M. Donnelly and F. Kaufman, J. Chem. Phys. 66, 4100 (1977).

23. R. C. Reid and T. K. Sherwood, The Properties of Gases and Liquids (McGraw-Hill, New York, 1968).

24. D. I. Rosen and T. A. Cool, J. Chem. Phys. 62,466 (1975).

25. H. Vandenbergh, N. Benoit-Guyot, and J. Troe, Int. J. Chem. Kin. 9, 223 (1977).

26. P. Herman, R.P. Mariella, Jr., and A. Javan, J. Chem. Phys. 65, 3792 (1976).

Table 1

PHOTODESTRUCTION CROSS SECTION UPPER LIMITS (10^{-18} cm^2)

E(eV)	λ(Å)	NO_2^-	$NO_2^- \cdot H_2O$	NO_3^-	$NO_3^- \cdot H_2O$	$O_2^- \cdot NO$	$O_2^- \cdot NO \cdot H_2O$
1.503	8250					<0.087	<0.072
1.653	7500		<0.041				<0.036
1.746	7100					<0.054	
2.335	5309	<0.029	<0.014	<0.011	<0.10		
2.381	5208	0.023 ± 0.009	<0.026	<0.054	<0.10		
2.569	4825		<0.046	<0.075	<0.22		
2.603	4762		<0.095	<0.092	<0.12		
2.649	4680		<0.071	<0.106	<0.16		
2.708	4579		<0.045				
3.001	4131		0.16 ± 0.03	<0.074	<0.10		
3.479 3.535	3564 5507		1.23 ± 0.16	0.10 ± 0.03	0.41 ± 0.08		

FIGURE CAPTIONS

Figure 1 Photodetachment cross section of thermal NO_2^- (circles) and $NO_2^- \cdot H_2O$ (triangles), as a function of laser wavelength.

Figure 2 Photodestruction cross section for $O_2^- \cdot NO$ versus wavelength. Solid circles are dye laser measurements and the triangles are ion laser measurements.

Figure 3 Photodestruction cross section for $O_2^- \cdot NO \cdot H_2O$ versus wavelength. Solid circles are dye laser measurements and the triangles are ion laser measurements.

Figure 4 Relative apparent photodestruction cross section for $NO_2^- \cdot D_2O$ measured at 10Td in 5% NO_2 in Ar at 0.50 torr. A relative apparent cross section of 1.0 corresponds to the same destruction rate as would be observed for a true photodestruction cross section of 10^{-18} cm^2. The solid line is the relative NO_2 absorption spectrum from Reference 20.

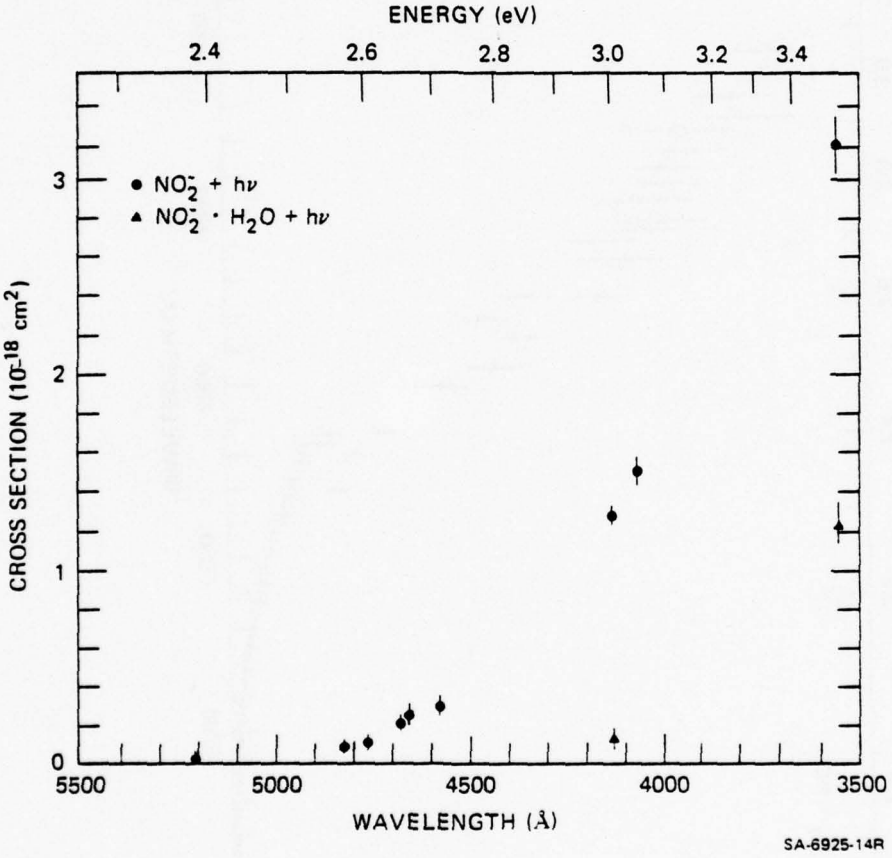
ENERGY (eV)
2.4
2.6
2.8
3.0
3.2
3.4
NO_2^- + hν
NO_2^- · H_2O + hν
CROSS SECTION (10^{-18} cm^2)
0
1
2
3
5500
5000
4500
4000
3500
WAVELENGTH (Å)
SA-6925-14R

Figure 1

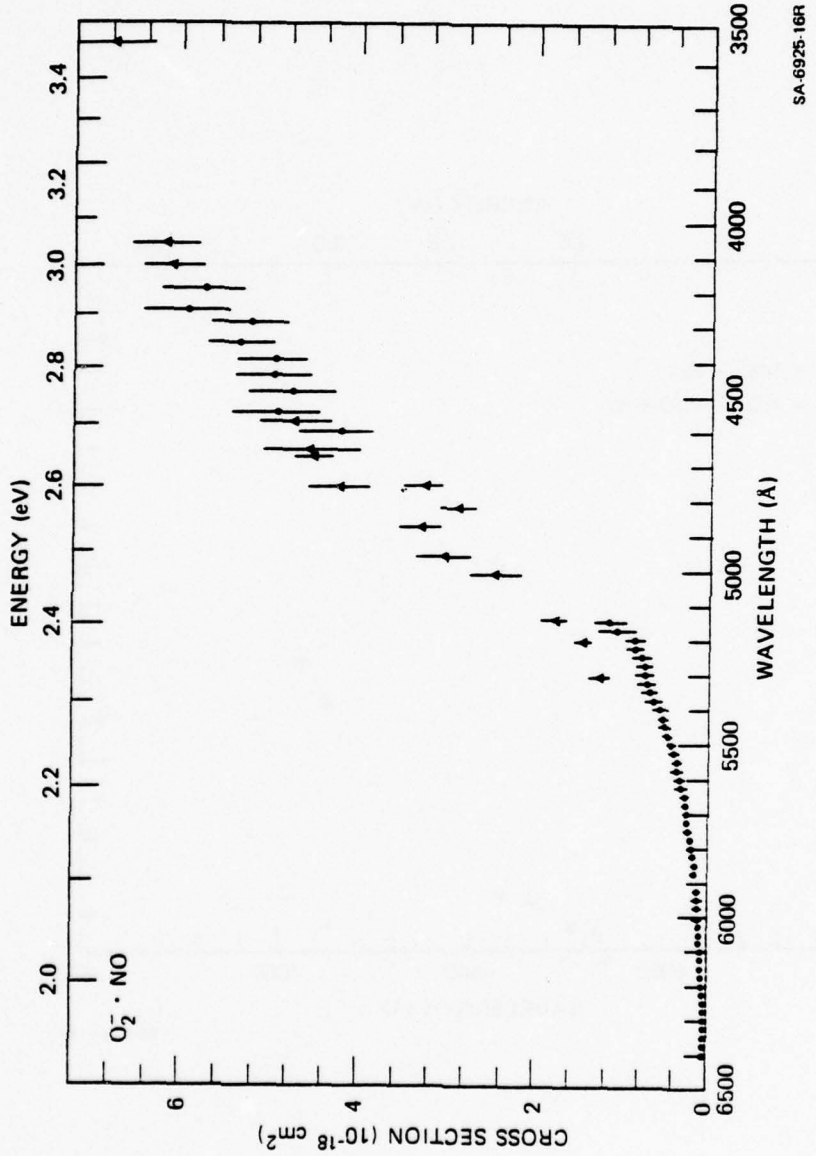
ENERGY (eV)
2.0
2.2
2.4
2.6
2.8
3.0
3.2
3.4
WAVELENGTH (Å)
6500
6000
5500
5000
4500
4000
3500
CROSS SECTION (10^{-18} cm^2)
0
2
4
6
$O_2^- \cdot NO$
SA-6926-16R

Figure 2

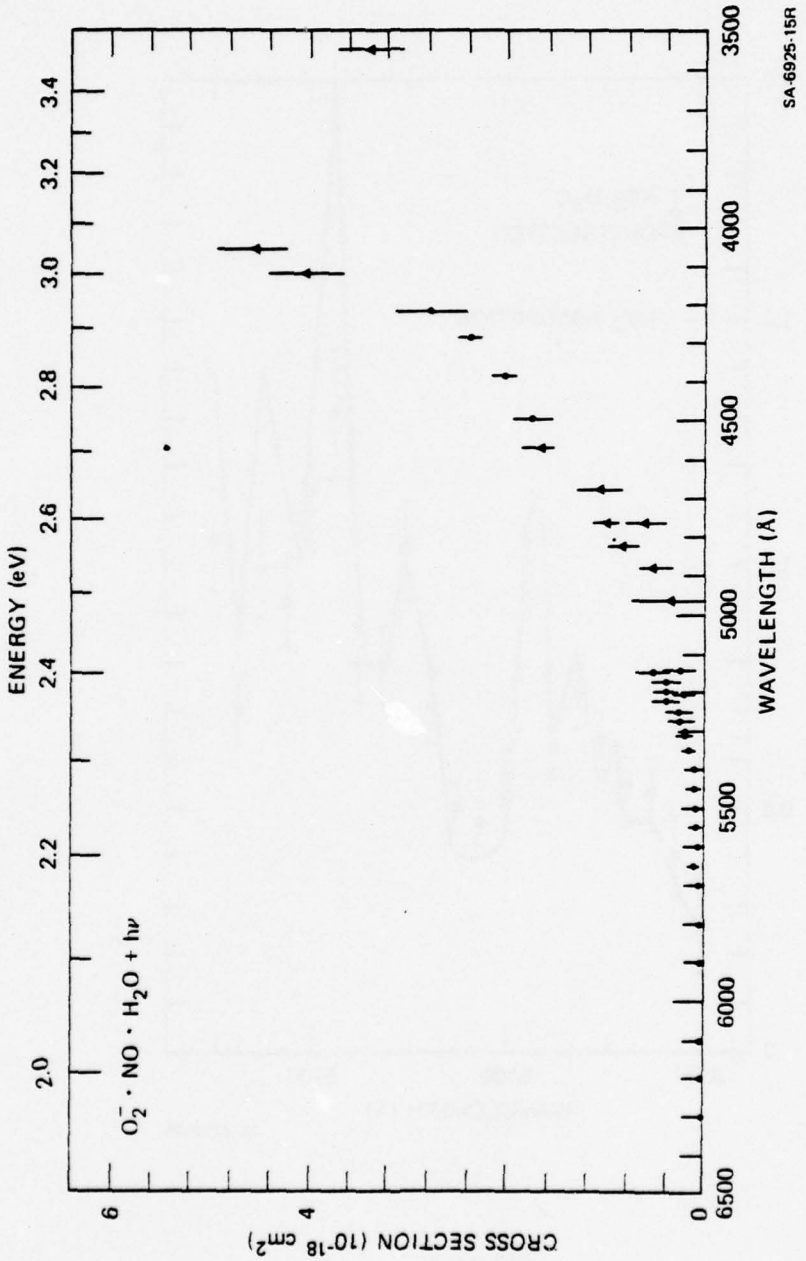
ENERGY (eV)
2.0
2.2
2.4
2.6
2.8
3.0
3.2
3.4
WAVELENGTH (Å)
6500
6000
5500
5000
4500
4000
3500
CROSS SECTION (10^{-18} cm^2)
0
4
6
$O_2^- \cdot NO \cdot H_2O + h\nu$
SA-6925-15R

Figure 3

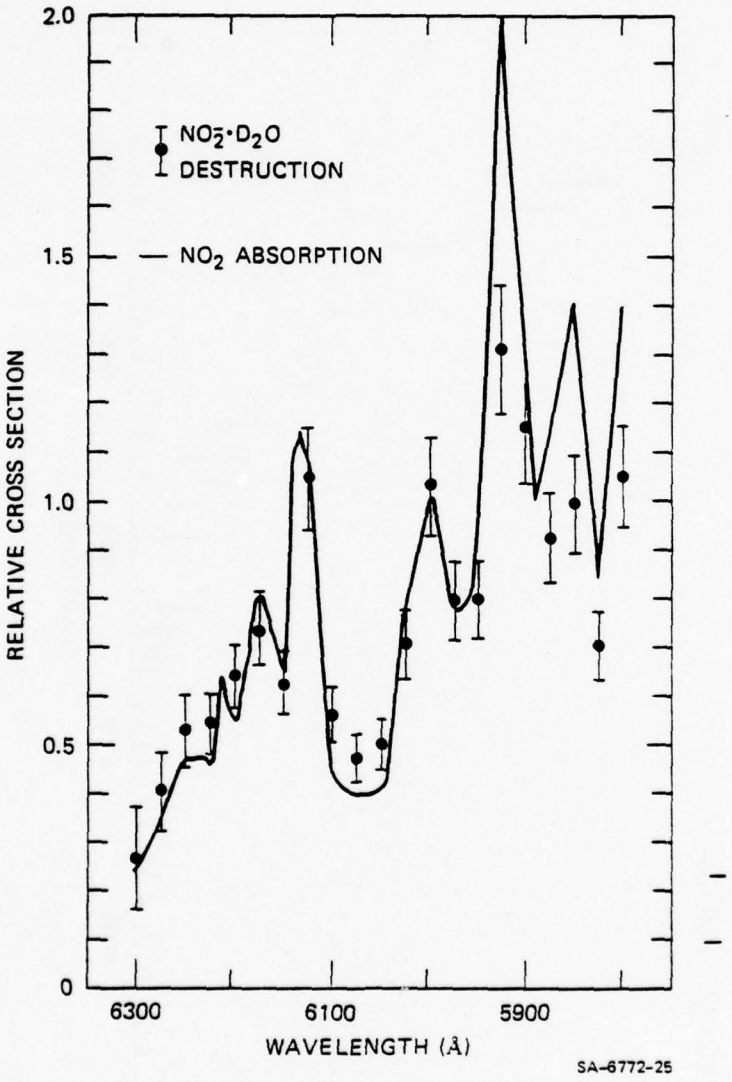
2.0
1.5
1.0
0.5
0
RELATIVE CROSS SECTION
$NO_2^- \cdot D_2O$
DESTRUCTION
NO_2 ABSORPTION
6300
6100
5900
WAVELENGTH (Å)
SA-6772-25

Figure 4

Table I

FRACTION OF O^- PHOTOFRAGMENT OBSERVED FROM THE PHOTODESTRUCTION OF CO_3^-

Wavelength (Å)	Relative O^- Observed*	Maximum Photodetachment $\sigma(10^{-18}\ cm^2)$
4300	.90 ± .34	.24
4400	.79 ± .27	.35
4500	.86 ± .19	.30
4550	.99 ± .19	.25
4579	.87 ± .09	.25
4600	.70 ± .23	.58
4765	.68 ± .04	.26
4880	.59 ± .04	.29

*This is the amount of O^- photofragment observed divided by the observed photodestruction of CO_3^-.

Table II

CO_3^- PHOTODISSOCIATION CROSS SECTION, 6550 Å, 10 Td, 0.4 torr, 30.5 cm

Mixture % CO_2 in O_2	% Reaction (2) Production	$\sigma(10^{-18}$ cm$^2)$
0.0014	98	3.76 ± 0.60
0.003	96	4.08 ± 0.80
0.006	90	4.16 ± 0.48
0.1	62	4.28 ± 0.40
1	15	3.20 ± 0.32
2	8	4.36 ± 0.52
100*	0	4.0 ± 0.30

*See Ref. 8, 0.05 Torr

Table III

PHOTODESTRUCTION CROSS SECTIONS

(10^{-18} cm^2)

λ(Å)	5309	5208	4825	4762	4680	4131	3507 + 3564
E(eV)	2.34	2.38	2.57	2.60	2.65	3.00	3.5
CO_4^-	<0.06	<0.12	<0.32	<0.16	<0.36	<0.06	0.45 ± 0.06
$CO_4^- \cdot H_2O$	<0.07	<0.12	<0.13	<0.17	<0.13	<0.12	<0.17
HCO_3^-	<0.017	<0.085	<0.035	<0.031	<0.051	<0.082	<0.077
$HCO_3^- \cdot H_2O$	<0.013	<0.040	<0.038	<0.029	<0.034	<0.063	<0.066

FIGURE CAPTIONS

1. CO_3^- photodestruction cross section. New data given by Δ. Old data from Ref. 8. The value at 3.5 eV (3500 Å), not shown, is $0.07 \pm 0.02 \times 10^{-18}$ cm^2.

2. Ion currents vs drift distance, with predictions of the kinetic model discussed in the text, for (a) 0.003%, (b) 0.1%, and (c) 1.0% CO_2 in O_2 at 0.4 torr.

3. Position dependence of the relative CO_3^- photodestruction cross section at (a) 6580 Å in 0.2 torr CO_2 and (b) 6550 Å in 0.4 torr O_2 with 1% CO_2. Solid lines give the maximum relaxation rates if excited CO_3^- only is responsible for the dissociation. Dashed line in (b) represents relaxation of nascent CO_3^- (see text).

4. Pressure dependence of the CO_3^- photodestruction cross section at 6550 Å, measured at a drift distance of 10 cm, in N_2 and O_2. Dashed line represents the quenching mechanism described in the text.

5. Dependence of the CO_3^- photodestruction cross section at 6550 Å on E/N.

6. $CO_3^- \cdot H_2O$ photodestruction cross section. New data given by solid squares. Old data from Ref. 4. The value of $0.12 \pm 0.05 \times 10^{-18}$ cm^2 at 3.5 eV is not shown.

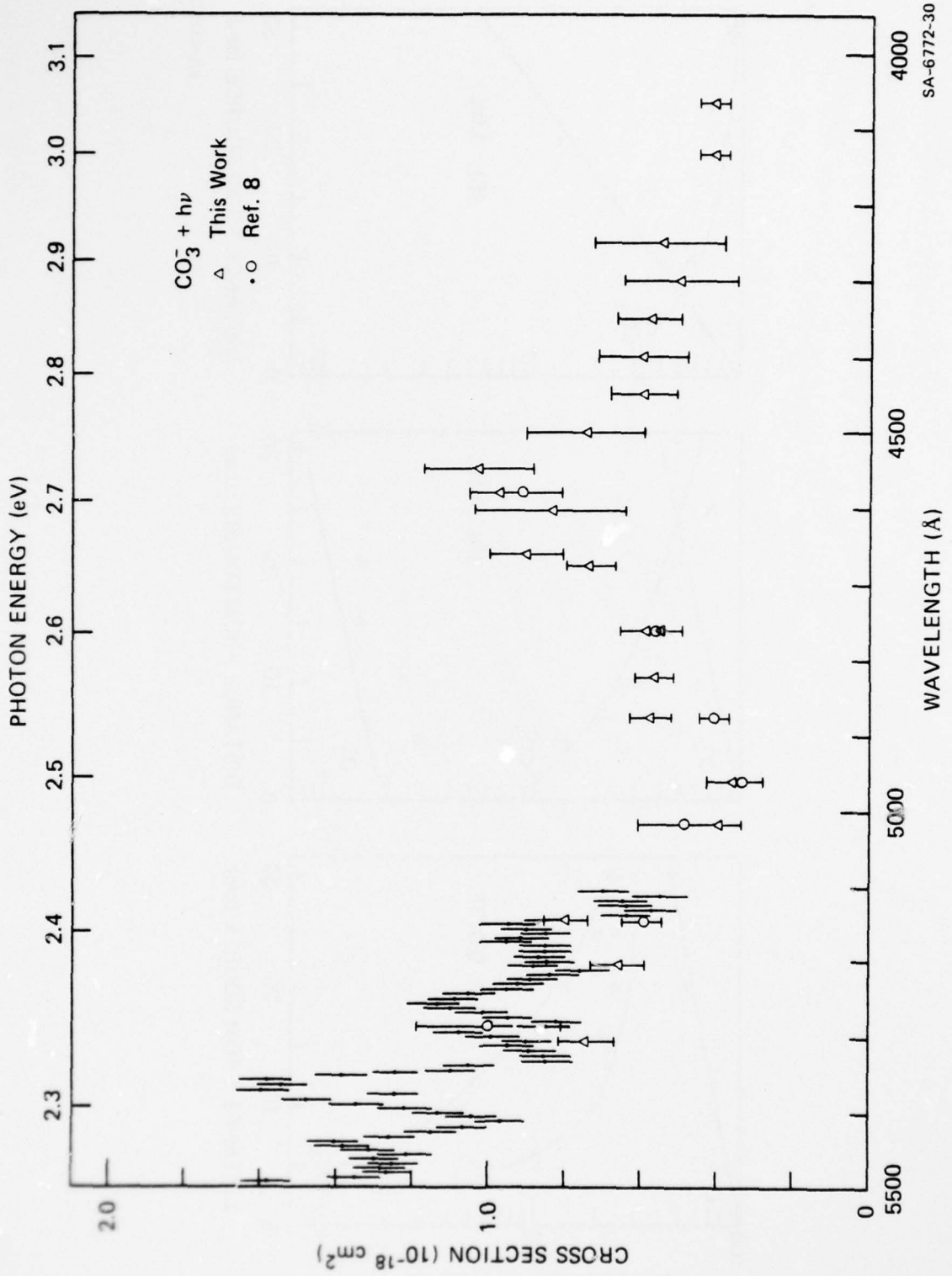
$CO_3^- + h\nu$
△ This Work
• ○ Ref. 8
PHOTON ENERGY (eV)
2.3
2.4
2.5
2.6
2.7
2.8
2.9
3.0
3.1
WAVELENGTH (Å)
5500
5000
4500
4000
CROSS SECTION (10^{-18} cm^2)
0
1.0
2.0
SA-6772-30

Figure 1

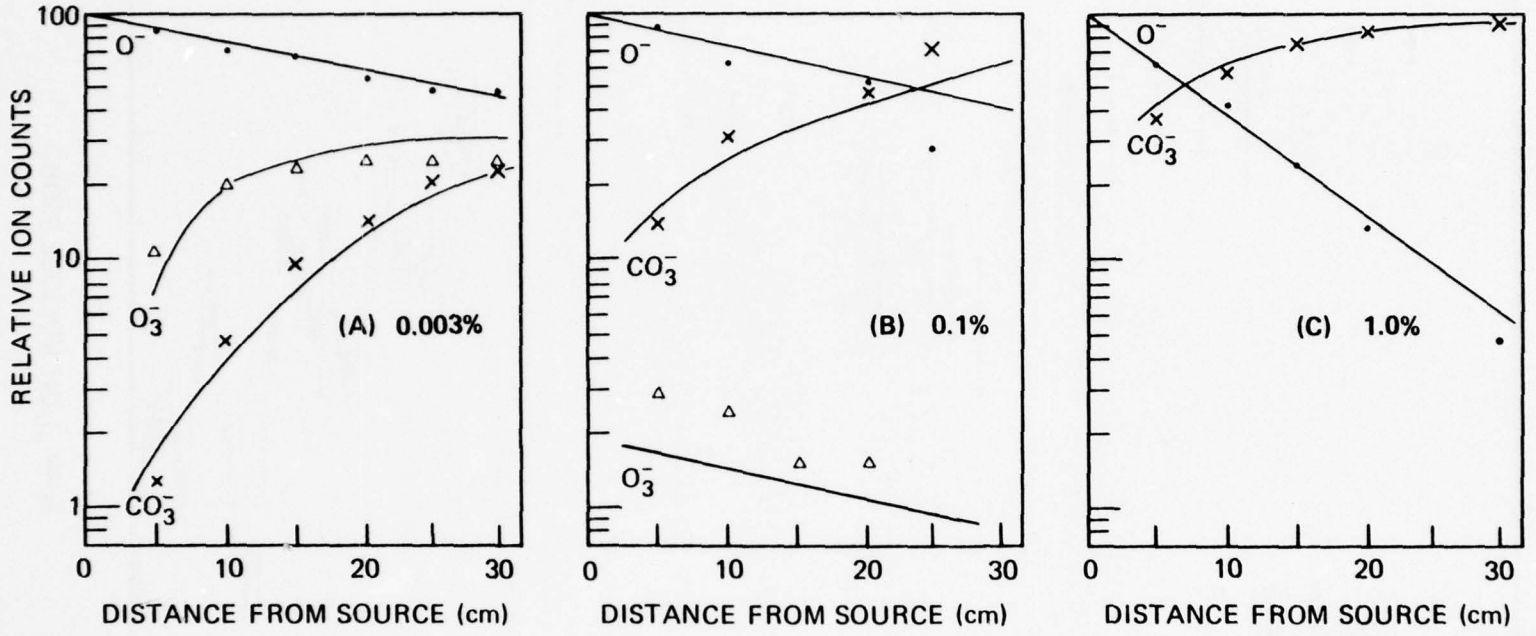
100
10
1
RELATIVE ION COUNTS
O⁻
O₃⁻
CO₃⁻
(A) 0.003%
(B) 0.1%
(C) 1.0%
0
10
20
30
DISTANCE FROM SOURCE (cm)
SA-6772-26

Figure 2

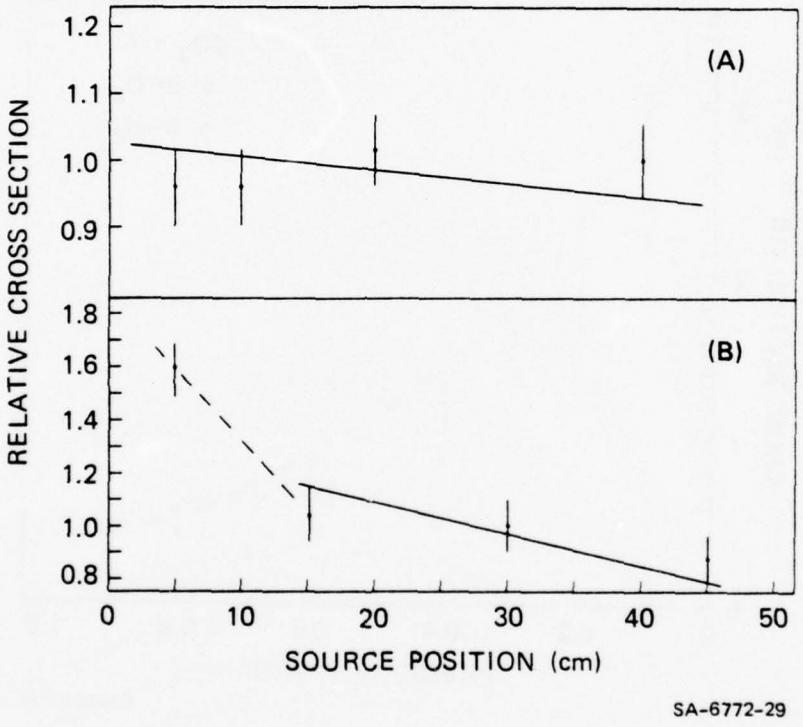
RELATIVE CROSS SECTION
1.2
1.1
1.0
0.9
(A)
1.8
1.6
1.4
1.2
1.0
0.8
(B)
0
10
20
30
40
50
SOURCE POSITION (cm)
SA-6772-29

Figure 3

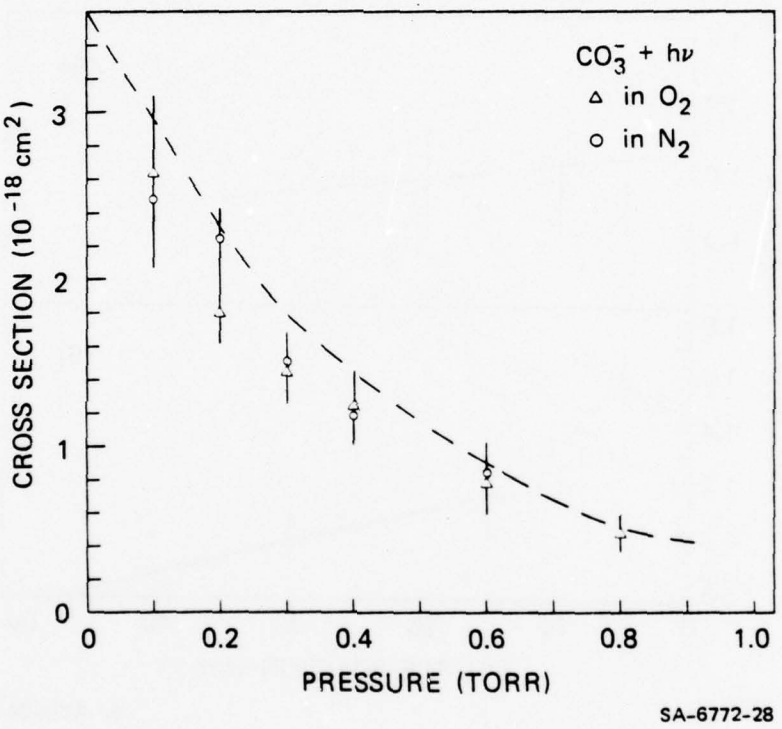
$CO_3^- + h\nu$
△ in O_2
○ in N_2
CROSS SECTION (10^{-18} cm^2)
0
1
2
3
0
0.2
0.4
0.6
0.8
1.0
PRESSURE (TORR)
SA-6772-28

Figure 4

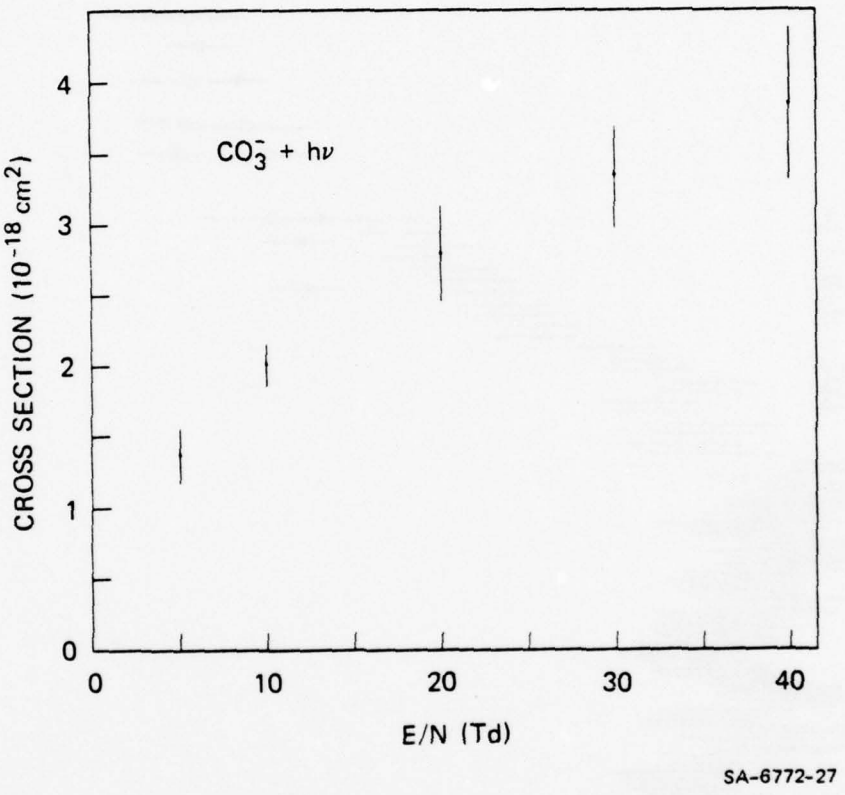
$CO_3^- + h\nu$
CROSS SECTION (10^{-18} cm^2)
0
1
2
3
4
0
10
20
30
40
E/N (Td)
SA-6772-27

Figure 5

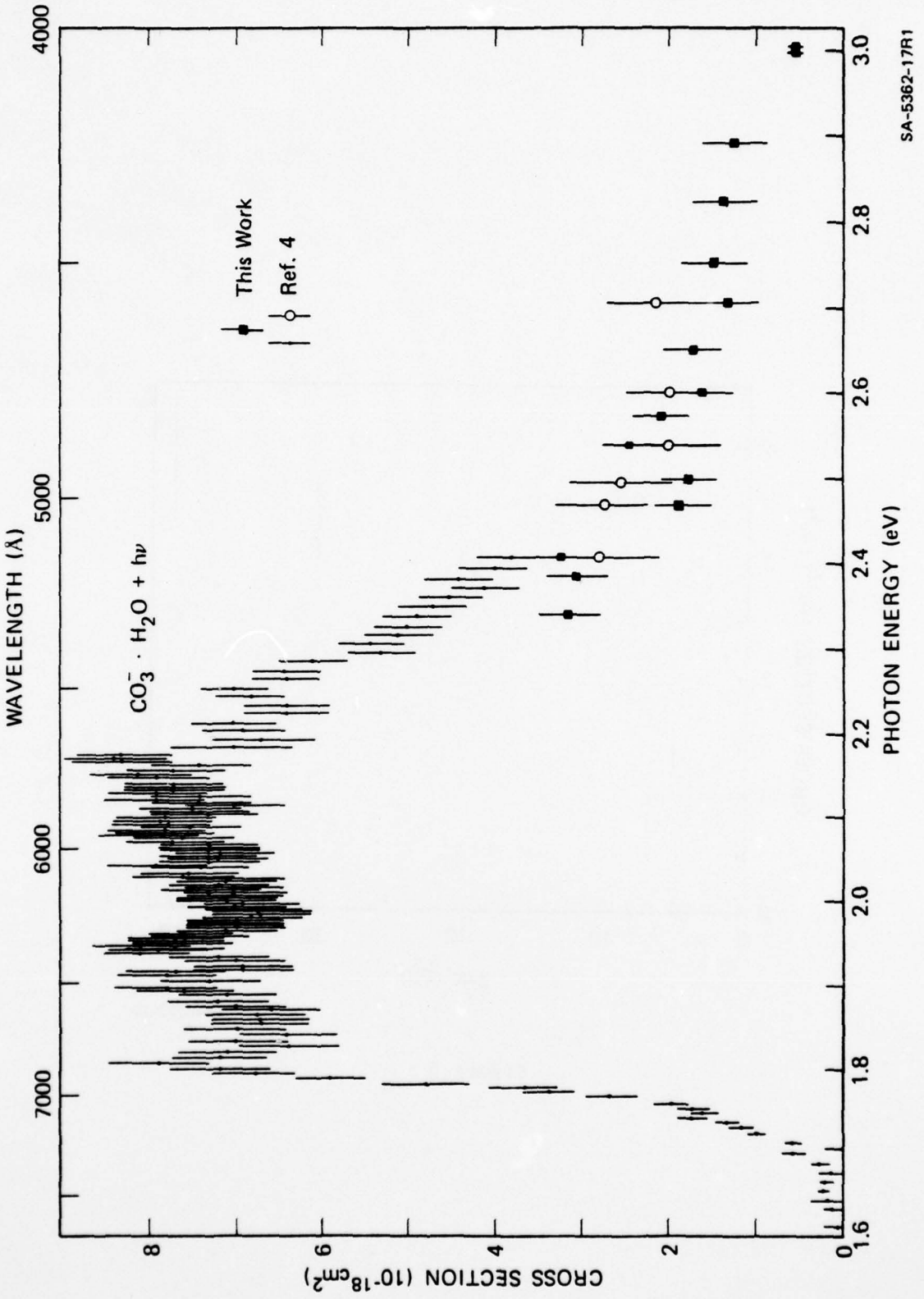
WAVELENGTH (Å)
4000
5000
6000
7000
PHOTON ENERGY (eV)
3.0
2.8
2.6
2.4
2.2
2.0
1.8
1.6
CROSS SECTION (10^{-18} cm^2)
8
6
4
2
0
$CO_3^- \cdot H_2O + h\nu$
This Work
Ref. 4
SA-5362-17R1

Figure 6

Appendix D

PHOTODISSOCIATION AND PHOTODETACHMENT OF Cl_2^-, ClO^-, Cl_3^-, AND $BrCl_2^-$

Photodissociation and photodetachment of Cl_2^-, ClO^-, Cl_3^- and $BrCl_2^-$

L. C. Lee, G. P. Smith, J. T. Moseley, P. C. Cosby, and J. A. Guest

Molecular Physics Laboratory, SRI International, Menlo Park, California 94025
(Received 8 December 1978)

Absolute cross sections for the photodestruction of Cl_2^-, ClO^-, Cl_3^-, and $BrCl_2^-$ were measured over the wavelength range of 3500–7600 Å using a drift tube mass spectrometer–laser apparatus. The photodissociation cross section for Cl_2^- has two bands, as has been observed for the isoelectronic Ar_2^+ ion. The wavelength dependence of these bands is used to adjust the calculated potential curves of the ion in the Franck–Condon region. The photodestruction cross section for ClO^- has a narrow band peaked at 4300 Å with a width of 400 Å, superimposed on a continuum that slowly increases with photon energy. The narrow band is attributed to photodissociation and the continuum to photodetachment. Cl_3^- and $BrCl_2^-$ have no significiant photodestruction cross sections for wavelengths longer than 4700 Å. At shorter wavelengths, the cross sections increase with increasing photon energy. The photodestruction of these ions is attributed to photodissociation. The present gas phase measurements are compared with optical spectra for the ions obtained in different environments.

I. INTRODUCTION

Chlorine-containing negative ions are believed to be important constituents in rare gas–chlorine laser media[1] and in the *D*-region of the ionosphere.[2] Experimental determinations of the photoabsorption or photodestruction spectra of such species are important because they are useful for characterizing laser operation and for modeling ionospheric photochemistry. Furthermore, the photodestruction spectra can also be used to characterize the electronic states of the ions,[3,4] the oscillator strengths for transitions between these states,[3] and the electron affinities of the corresponding neutral molecules.[5–7]

Photoabsorption spectra of chlorine-containing negative ions have been measured in crystals,[8–11] aqueous solutions,[12–15] and argon matrices.[16] However, quantitative measurements for ions in these dense environments are rarely made, because it is difficult to determine the negative ion concentrations accurately. It is also frequently difficult to assess the degree to which the spectrum of the ions has been influenced by the environment.

Gas-phase spectral measurements avoid such problems and, at least in principle, permit quantitative cross section measurements. However, depending on the method used to produce the ions, the observed spectra can be influenced by the presence of ions in excited states. To date, gas-phase spectra have been measured only for the Cl_2^- ions, using both ion beam[17] and ion cyclotron resonance techniques.[18,19] In neither case were absolute cross sections for the ground state ion reported.

We report here absolute cross sections for the photodissociation of Cl_2^-, ClO^-, Cl_3^-, and $BrCl_2^-$ ions in the gas phase at 300 K over the wavelength region at 3500–7600 Å.

II. EXPERIMENTAL

The experimental apparatus used for the measurements reported here has been described in some detail in several previous publications.[20] Briefly, a drift tube mass spectrometer apparatus was used as the ion source, drift region, mass analyzer, and ion detector. The source and drift region were filled with the appropriate gas mixtures (Table I) at a pressure of 0.2 or 0.4 torr. The negative ions were formed in the various gas mixtures by electron attachment processes and subsequent ion–molecule reactions. Under the influence of a weak uniform electric field, the negative ions drift toward a 1 mm diameter exit aperture and intersect a laser beam just in front of this aperture. For photodestruction cross section measurements, the ratio of the applied electric field to the neutral gas density E/N was limited to 10 or 20 Td (1 Td = 10^{-17} V cm^2). At such E/N, the ion drift velocity was only about one tenth the mean thermal speed of the ions and neutral molecules at room temperature. The drift distance between the ion source and the laser beam was set at 5 or 10 cm. While drifting this distance, the ions experience many thermalizing collisions after their production and are essentially in thermal equilibrium[3] with the neutral molecules near 300 K. This conclusion is supported by the fact that the measured photodestruction cross sections do not depend on the drift distance.

The various lines of Ar^+ and Kr^+ lasers were used as photon sources. The visible lines were isolated by an intracavity prism, but the Kr^+ laser UV lines, consisting of 25% 3569 Å and 75% 3507 Å, were not separated. A tunable dye laser using stilbene-3,[21] pumped by the UV lines of the Ar^+ laser, was used in the 4200 to 4650 Å

TABLE I. Experimental conditions.

Ion		Pressure (torr)	Normalized to	K_0 (cm^2/V s)
Cl_2^-	1% Cl_2 in Ar	0.2	O^- in O_2	2.45
	3% Cl_2 in O_2	0.2	O^- and O_2^- in O_2	2.43
ClO^-	Trace Cl_2, 10% N_2O in Ar	0.4	O_2^- in O_2	2.52
	Trace Cl_2 in O_2	0.2	O^- and O_2^- in O_2	2.58
Cl_3^-	4% Cl_2 in Ar	0.2	O^- in O_2	2.34
$BrCl_2^-$	4% Cl_2 in Ar	0.2	O^- in O_2	2.25

 0021-9606/79/073237-10$01.00

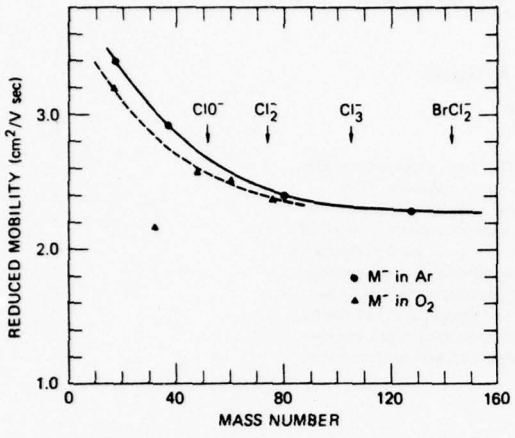

FIG. 1. The reduced mobilities for various negative ions in O_2 (Ref. 25) and Ar (Ref. 26). The mass numbers for the Cl_2^-, ClO^-, Cl_3^-, and $BrCl_2^-$ ions are indicated.

region. The ions intersect the laser photons inside the laser cavity, except for the UV measurements, which were made extracavity. The photon intensity, which varies from 1 to 100 W for the various wavelengths, was adjusted so that (1) the laser was intense enough for the data to be acquired rapidly and (2) the percentage of ions photodestroyed was less than 15%, so that the measured cross section was not affected by ion diffusion from the noninteraction region into the photon interaction region.[22]

The photodestruction cross sections for the negative ions were measured relative to O^- and O_2^- photodetachment (Table I), for which the cross sections are known,[7] i.e., $\sigma(A^-) = \sigma(O^-)\,[\ln(I_0/I)K/\varphi]_A / [\ln(I_0/I)K/\varphi]_{O^-}$, where K is the ion mobility, φ is the photon flux, and I and I_0 are the ion intensities when the laser is on and off, respectively. The mobilities of the chlorine-containing negative ions in O_2 or Ar, which were used to place the cross sections on absolute scale, have not been explicitly measured. However, these mobilities can be obtained to good accuracy by mass scaling[23,24] from other negative ions, for which the mobilities are known. The mobilities of various negative ions in O_2[25] or Ar[26] are shown in Fig. 1, where the data are joined together by the dashed and solid lines, respectively. The mobilities have a smooth dependence on the mass number of various ions, except for the case of O_2^- in O_2, where the mobility is lowered by resonant charge exchange. The reduced mobilities K_0 used for the present measurements are listed in Table I.

At each wavelength, ion counts were accumulated until the statistical uncertainty in the photodestruction signal was less than 10%. The statistical uncertainties are indicated by error bars and error limits given along with the cross section data in the figures and tables. The laser power was measured to an accuracy within 5%. The ion mobilities obtained from the mass scaling should be accurate to within 5%. The experimental uncertainty in the absolute photodissociation cross section is estimated to be ± 20%, including the uncertainty due to the normalization procedure.

The Cl_2 gas of purity 99.99% was obtained from Union Carbide Corporation. Ultra-high purity O_2, Ar, and N_2O were obtained from Matheson Company. The gas mixtures of a few percent Cl_2 in O_2, Ar, or N_2O (Table I) were premixed in a bulb before use.

III. RESULTS AND DISCUSSION

A. Cl_2^- ions

The Cl_2^- ions were produced in a gas mixture of a few percent Cl_2 in Ar or O_2. The negative ion mass spectrum for a Cl_2 partial pressure of 15 mtorr in 85 mtorr Ar is shown in Fig. 2, where the drift distance is 5 cm and $E/N = 10$ Td. The Cl_2^- ion density at the drift tube exit aperture increases slowly as the Cl_2 partial pressure is increased up to a few millitorr and then decreases with increasing pressure. The ion density also decreases with increasing drift distance more rapidly than can be accounted for by diffusion alone. These facts indicate that the Cl_2^- ions are formed primarily in the ion source region, but are converted to other ion species in the drift region. The process that forms the Cl_2^- ions is probably three-body electron attachment to Cl_2:

$$e^- + Cl_2 + M \rightarrow Cl_2^- + M, \quad \Delta H = -2.5 \text{ eV} . \tag{1}$$

The Cl_2^- ions are probably removed by the reaction

$$Cl_2^- + Cl_2 \rightarrow Cl_3^- + Cl, \quad \Delta H = -0.4 \text{ eV} . \tag{2}$$

The ΔH values shown in Reactions (1) and (2) are obtained from the electron affinity of Cl_2[27] and the dissociation energies of Cl_2^-[28,29] and Cl_3^-.[30]

The photodestruction cross section for Cl_2^- over the wavelength region 3500 to 7600 Å is listed in Table II and shown in Fig. 3. The relative measurements of Delbecq *et al.*,[8,9] Andrews,[16] and Sullivan *et al.*[19] are also shown in Fig. 3 for comparison. These relative measurements are normalized to the present measurements at (3507 + 3567) Å for the ultraviolet band and at 7525 Å for the visible band. The Cl_2^- ions in the mea-

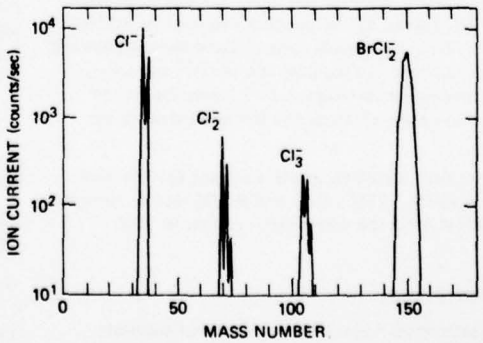

FIG. 2. Negative ion mass spectrum for the Cl_2 partial pressure of 15 mtorr in Ar. The total pressure is 100 mtorr. The ion drift distance is 5 cm and E/N is 10 Td.

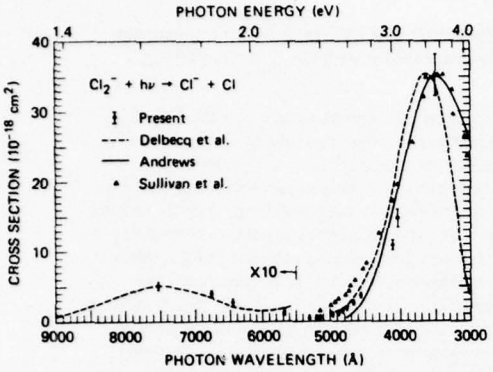

FIG. 3. Photodissociation cross section for Cl_2^-. Shown for comparison are the measurements of Delbecq *et al.* (Refs. 8 and 9) in KCl crystal, Andrews (Ref. 16) in $K^+Cl_2^-$ in an Ar matrix, and Sullivan *et al.* (Ref. 19) using ion cyclotron resonance. The ordinate is magnified tenfold at wavelengths above 5500 Å.

surements of Delbecq *et al.*[8,9] were obtained by x-ray irradiation of pure KCl and KCl–M (M = Ag, Tl, and Pb) crystals at liquid nitrogen temperature. The Cl_2^- ions were formed[31] by the bonding of a Cl^- ion with a neighboring Cl atom produced by x-ray irradiation. As shown in Fig. 3, the absorption peaks for the ultraviolet band in KCl crystals[8] are shifted to slightly longer wavelengths than those of the present gas-phase measurements. The KCl measurements[9] show a strong photon polarization dependence in the visible band. For comparison with the present gas-phase measurements, which are orientation independent, the optical spectra in KCl are averaged over all orientations. As shown in Fig. 3, the present measurements agree well with the KCl crystal measurements. The Cl_2^- optical spectra of Andrews[16] were obtained from $M^+Cl_2^-$ (M = Li, Na, K, and Cs), matrix isolated in argon at 17 K. As shown in Fig. 3, the results for matrix-isolation measurements are also very close to the gas-phase measurements.

The measurements of Sullivan *et al.*[19] are in the gas phase. However, since these Cl_2^- ions were produced by electron impact and undergo relatively few collisions while trapped by ion cyclotron resonance, their effective vibrational temperature was not well established. The band measured by Sullivan *et al.*[19] is slightly broader than the present measurements, indicating that the ions of Sulliven *et al.*[19] are vibrationally hotter than a 300 K Boltzmann distribution. Not included in Fig. 3 are the measurements of Rackwitz *et al.*[17] and Asubiojo *et al.*,[18] using ion beam and ion cyclotron resonance techniques, respectively. The vibrational temperature of the ions in these measurements, while not known, was apparently quite high, so their optical bands are much broader than the present measurements.

The potential curves for Cl_2^- have been investigated theoretically.[26,29,31,32] Self-consistent field potential curves have been calculated by Gilbert and Wahl,[28] and semiempirical potential curves have been determined by Tasker *et al.*[29,33] Given a set of potential curves, it is straightforward to calculate the photodissociation cross section. Thus, to obtain potential curve information from the observed data, we can adjust the best available calculated or inferred potential curves so that they reproduce the shape of the experimental photodissociation cross section, as described for a previous study on Ar_2^+.[34]

The ground $^2\Sigma_u^+$ potential curve of Cl_2^- was constructed as a Morse function with parameters[28] of $R_e = 5.0$ a.u., $D_e = 1.26$ eV, and $\omega_e = 260$ cm^{-1}. The repulsive $^2\Sigma_g^+$ and $^2\Pi_g$ potential curves were adopted from Gilbert and Wahl.[28,35] There are no calculated transition dipole moments for this system. For the $^2\Sigma_g^+ - {}^2\Sigma_u^+$ transition, the transition moment was approximated[36,37] by $R/2$, the value that it approaches asymptotically, as shown for the isoelectronic Ar_2^+ case.[37] Although spin–orbit coupling has not been considered explicitly, the $^2\Sigma_g^+$ curve was taken to correlate asymptotically to the correct fine structure limit $Cl^-(^1S) + Cl(^2P_{1/2})$, which is 0.109 eV above the $Cl^-(^1S) + Cl(^2P_{3/2})$ limit. Best agreement with the measured photodissociation cross section was found by lowering the calculated $^2\Sigma_g^+$ curve by 0.346 eV in the Franck–Condon region of the ground state, resulting in the potential curve shown in Fig. 4 and the cross section shown in Fig. 5. The first four vibrational levels of the ground state were assumed to be populated in a Boltzmann distribution at 300 K. The resulting calculated cross sections are divided by 1.65 to match the absolute magnitude of the experimental maximum, implying that the estimate of $R/2$ for the transition moment is too large. The potential curve of Cl_2 and the electron affinity of Cl (3.615 eV) were adopted from Refs. 28 and 38, respectively.

For the $^2\Pi_g - {}^2\Sigma_u^+$ transition in the red region of the spectrum, the analogy with the Ar_2^+ system was again invoked. The perturbative treatment of spin–orbit coupling used for Ar_2^+[34] indicated that the main contri-

TABLE II. Photodestruction cross sections (10^{-18} cm^2) for Cl_2^-, ClO^-, Cl_3^-, and $BrCl_2^-$.

λ (Å)	Cl_2^-	ClO^-	Cl_3^-	$BrCl_2^-$
3507, 3569	35.1 ± 3.0	3.06 ± 0.32	6.72 ± 0.65	3.29 ± 0.28
4067	14.9 ± 1.1	3.49 ± 0.82		
4131	10.8 ± 0.4	3.64 ± 0.30	0.79 ± 0.07	0.94 ± 0.20
4579	3.55 ± 0.42			
4680	2.41 ± 0.28	2.77 ± 0.32	< 0.3	0.30 ± 0.12
4762	1.64 ± 0.19	1.75 ± 0.25		< 0.24
4765	1.85 ± 0.20			
4825	1.46 ± 0.18	1.44 ± 0.24		
4880	1.19 ± 0.13	1.82 ± 0.27		
4965	0.99 ± 0.1[illegible]			
5145	0.43 ± 0.06	0.82 ± 0.32		
5208	0.39 ± 0.05	0.60 ± 0.11		< 0.14
5309	0.28 ± 0.03	0.44 ± 0.06	< 0.15	< 0.08
5682	0.11 ± 0.05	< 0.23		
6471	0.25 ± 0.03	0.11 ± 0.05	< 0.02	< 0.03
6764	0.37 ± 0.04			
7525	0.51 ± 0.06	< 0.01		

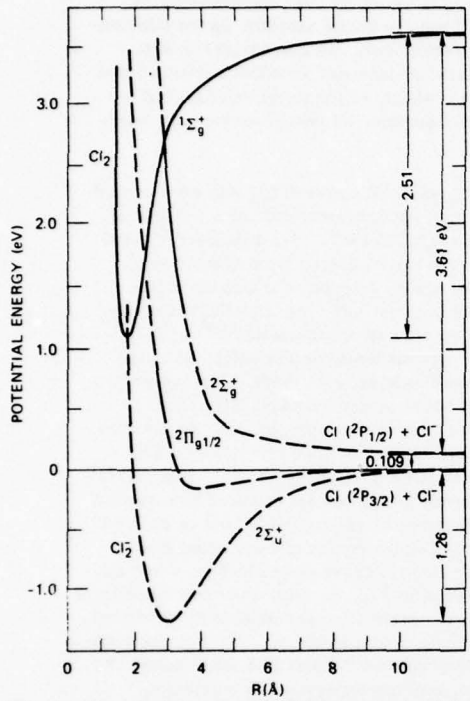

FIG. 4. The potential curves for Cl_2^- determined in this work and the ground state of Cl_2. The solid portions of the Cl_2^- curves were studied here; the dashed portions came from Gilbert and Wahl's calculations (Refs. 28 and 35) adjusted as discussed in the text. The ground $^2\Sigma_u^+$ state for Cl_2^- is the Morse function described in the text.

bution to this transition came from the parallel transition $^2\Pi_{g1/2} - {}^2\Sigma_{u1/2}^+$ (in a mixed notation), which "borrows" intensity from the strong $^2\Sigma_g^+ - {}^2\Sigma_u^+$ transition as well as from the strong $^2\Pi_g - {}^2\Pi_u$ transition. The mixing coefficient can be estimated by perturbation theory from the atomic spin–orbit parameter by the method used previously for Ar_2^+.[34,37]

Using this approximation and the previously used $R/2$ transition moment for the $^2\Sigma_g^+ - {}^2\Sigma_u^+$ transition, we calculated the $^2\Pi_g - {}^2\Sigma_u^+$ photodissociation cross section, as plotted in Fig. 5. The $^2\Pi_g$ potential curve of Gilbert and Wahl[28] was translated down by 0.207 eV in the Franck–Condon region and correlated with the correct asymptote $Cl^-(^1S) + Cl(^2P_{3/2})$. Beyond the Franck–Condon region, the translation factor was multiplied by a decreasing exponential. The cross section was multiplied by 5.35 to agree in magnitude with the experimental point at 7525 Å, implying that the transition moment obtained using this approximate procedure is much too small.

In Fig. 4, the Π potential is labeled $^2\Pi_{g1/2}$ since this final state accounts for most of the ir absorption cross section. The $^2\Pi_{g3/2}$ curve is not included in this figure since it cannot borrow intensity from the $^2\Sigma_{g1/2}^+$ state. It is approximately 0.073 eV lower in energy than the $^2\Pi_{g1/2}$ and also correlates with the $Cl^-(^1S) + Cl(^2P_{3/2})$ asymptote.

Table III contains numerical values for the $^2\Sigma_u^+$, $^2\Pi_g$, and $^2\Sigma_g^+$ potential curves that provide an adequate fit to the experimental photodissociation cross sections determined in this work. A reasonable estimate for the $^2\Pi_u$ potential curve may be obtained from the $^2\Pi_g$ results presented here and the difference potential of Gilbert and Wahl.[28] It should be pointed out that the Cl_2^- potential curves determined here are less accurate than those previously determined for Ar_2^+[34] and Kr_2^+.[39] Those potential curves were based also on extensive data on the kinetic energies of the photofragments. However, the present $^2\Sigma_g^+$ curve is clearly more accurate than the best available calculated curves, since our calculated $^2\Sigma_g^+ - {}^2\Sigma_u^+$ cross section matches experimental measurements. The $^2\Pi_{g1/2}$ is less conclusive, because very few data are available for $^2\Pi_{g1/2} - {}^2\Sigma_u^+$ transition. Nevertheless, the new $^2\Pi_{g1/2}$ potential curve shown in Fig. 4 also fits the experimental data much better than the previously calculated curves.

The photodissociation processes discussed above dominate the photodestruction cross section at the photon wavelengths of this study. The electron affinity[27] of Cl_2 is 2.51 ± 0.1 eV, so photodetachment of Cl_2^- may contribute to the photodestruction cross section for the ultraviolet band. However, as shown in Fig. 4, the vertical threshold for photodetachment is about 4.0 eV. This is higher than the highest photon energy used here, so the photodetachment cross section is expected to be negligible compared with the photodissociation cross section. This was previously discussed by Sullivan *et al.*[19]

The potential curves for Cl_2^- in the alkali halide crystals[31] resemble those in the gas phase.[28,29] Especially in the Franck–Condon region of the ground state, the shapes of the potential curves are nearly identical for both cases.[28,31] This similarity suggests that the oscil-

TABLE III. Cl_2^- potential curves used in this work.

R (bohr)	$^2\Sigma_u^+$ (eV)	$^2\Pi_g$ (eV)	$^2\Sigma_g^+$ (eV) ($^2P_{1/2}$ asymptote)
4.00	0.0613	3.6025	7.7073
4.250	−0.6439	2.2383	5.7167
4.500	−1.0306	1.3626	4.2542
4.750	−1.2105	0.7468	3.1734
5.000	−1.2596	0.3726	2.3713
5.250	−1.2290	0.0425	1.7712
5.500	−1.1526	−0.0997	1.3198
5.750	−1.0528	−0.1610	0.9778
6.000	−0.9439	−0.1630	0.7170
6.250	−0.8347	−0.1513	0.5040
6.500	−0.7305	−0.1344	0.4262
6.750	−0.6343	−0.1193	0.3859
7.000	−0.5473	−0.1067	0.3507
7.250	−0.4699	−0.0970	0.3200
7.500	−0.4018	−0.0865	0.2932
7.750	−0.3425	−0.0776	0.2699
8.000	−0.2912	−0.0692	0.2494

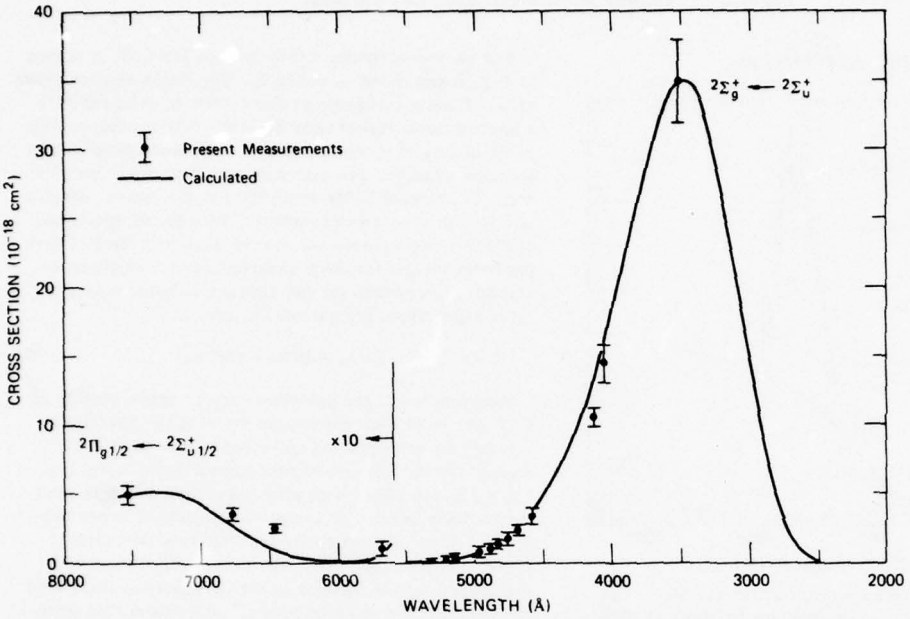

FIG. 5. Photodissociation cross section for Cl_2^- calculated from the potential curves determined in this work. To fit the experimental data, we multiply the calculated $^2\Sigma_g^+ \leftarrow {}^2\Sigma_u^+$ and $^2\Pi_{g1/2} \leftarrow {}^2\Sigma_{u1/2}$ cross sections by 0.61 and 5.35, respectively. The dots are the absolute cross section measurements of this work.

lator strength for the ultraviolet band may be nearly the same for photodissociation of Cl_2^- both in the gas phase and in a solid environment. In fact, the transition moment for the ultraviolet band is so large that its oscillator strength is probably relatively unaffected by the surrounding environment. Therefore, the present gas-phase measurements can provide useful estimates of the photoabsorption cross section for Cl_2^- in a solid environment, or, perhaps more importantly, can provide a method for determining Cl_2^- densities in solid environments.

To investigate the effect of vibrational excitation on the photodissociation cross section, we measured the dependence of the Cl_2^- photodissociation cross section on E/N. When an ion drifts under the influence of an electric field, it acquires kinetic energy in addition to its thermal energy. This additional kinetic energy may result in excitation of the ions into higher rotational or vibrational states. Since each state has its own transition probability, the apparent photodissociation cross sections of the ions can depend strongly on their vibrational populations.[37,40] The cross sections can thus be affected by the acquired kinetic energy. A detailed discussion of such an E/N dependence has been given in a previous paper.[4] Table IV lists results for the Cl_2^- photodissociation cross section at 4880 Å for various values of E/N. The ion kinetic energy and the effective translational temperature are also listed. The ion kinetic energy E_K is calculated from the ion drift velocity v_d as given by[23,41]

$$E_K = \tfrac{1}{2} m v_d^2 + \tfrac{1}{2} M v_d^2 + \tfrac{3}{2} k T ,$$

where m and M are the masses of ion and neutral gas molecule, respectively, and T is the gas temperature. The effective kinetic "temperature" is defined as

$$T^* = \tfrac{2}{3} E_K / k$$

where k is the Boltzmann constant. The ion drift velocity is calculated from the product of the reduced ion mobility, E/N, and the gas density at STP (2.69×10^{19} molecules/cm^3). The "effective kinetic temperature" is not a true temperature. The translational, rotational, and vibrational populations at an effective kinetic temperature are not expected to have Boltzmann distributions. However, the effective kinetic temperature can provide a qualitative measure of the degree to which the ions are vibrationally excited.[4]

TABLE IV. Apparent photodissociation cross section for Cl_2^-, i.e., $\sigma(10^{-18}\ \text{cm}^2)$, average ion kinetic energy E_K (meV), and effective kinetic temperature T^* (K) at various E/N (10^{-17} V cm^2). Cl_2^- was produced by 0.1% Cl_2 in Ar and photodissociated at 4880 Å.

E/N (Td)	E_K (meV)	T^* (K)	$\sigma(10^{-18}\ \text{cm}^2)$
0	38.8	300	
5	39.4	305	1.01 ± 0.12
10	41.3	319	1.05 ± 0.11
20	48.9	378	1.10 ± 0.11
40	79.1	611	1.99 ± 0.20

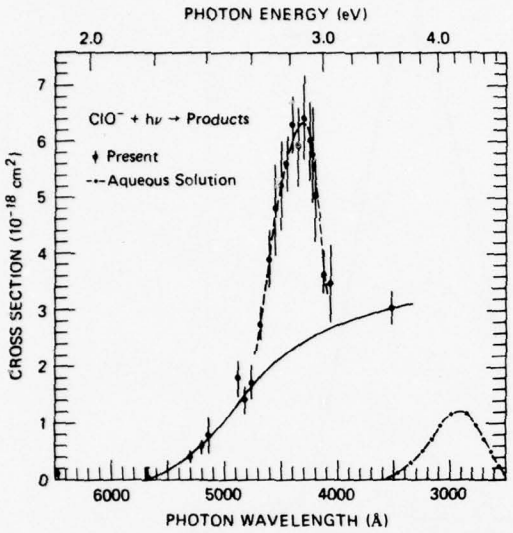

FIG. 6. The photodestruction cross section for ClO^-. The cross section is divided into two components shown as solid and dashed lines, which are attributed to photodetachment and photodissociation, respectively. The measurements for ClO^- in an aqueous solution (Ref. 12) are shown for comparison.

As shown in Table IV, the apparent photodissociation cross section increases with increasing E/N. This indicates that at 4880 Å the photodissociation cross section increases as the ions are vibrationally excited. This further suggests that the ions in the measurements of Sullivan *et al.*[19] were vibrationally excited.

B. ClO^- ions

The ClO^- ions were formed in the drift tube with a gas mixture of a trace of Cl_2 in O_2 or N_2O. The processes that create ClO^- are not known, but may include the reaction

$$O^- + Cl_2 \rightarrow ClO^- + Cl, \quad \Delta H = -0.9 \text{ eV}, \tag{3}$$

where ΔH is derived from dissociation energies of Cl_2[42] and ClO^- (see later discussion). It is also possible that ClO^- is created directly on the filament surface. The ClO^- ion density decreases very rapidly with increasing Cl_2 partial pressure and increasing drift distance. These facts suggest that ClO^- is destroyed quickly by Cl_2 by processes such as

$$ClO^- + Cl_2 \rightarrow Cl_3^- + O, \quad \Delta H = -0.4 \text{ eV}, \tag{4}$$

where ΔH is derived from the dissociation energies of Cl_3^-[30] and ClO^-.

While searching for an effective way to produce ClO^-, we found that $Cl^- \cdot CO_2$ and $Cl^- \cdot N_2O$ ions could be produced in quantities similar to $BrCl_2^-$ (see Fig. 2) when the drift tube was filled with a gas mixture of a few percent Cl_2 in CO_2 or N_2O, respectively. These ions have no significant photodissociation cross sections ($< 5 \times 10^{-19}$ cm^2) in the 4579–5145 Å region.

The photodestruction cross section for ClO^- is shown in Fig. 6 and listed in Table II. The cross section rises slowly from a threshold at about 5700 Å, then exhibits a narrow band peaked near 4300 Å. The measurements of Friedman,[12] in which the ClO^- ions were prepared in aqueous solution, are also shown in Fig. 6 for comparison. In contrast to the similarity of the optical spectra of Cl_2^- in different environments, the optical spectrum of ClO^- in the aqueous solution is obviously very different from the gas-phase measurements. The photodestruction processes for the aqueous solution may possibly differ from the gas phase, e.g.,

$$ClO^- \cdot HOH(aq) + h\nu \rightarrow HOCl + OH^-(aq). \tag{5}$$

Examination of the photodestruction cross section of ClO^- shown in Fig. 6 suggests dividing the spectrum into two components, as indicated by the solid and dashed lines. The broad band shown by the solid line has a slow increase with photon energy, which is similar to many molecular ion photodetachment cross sections.[7] Thus, it most likely results from photodetachment. On the other hand, the narrow band shown by the dashed line is similar to the photodissociation band for Cl_2^- and other diatomic ions.[4] This band thus probably results from a photodissociation. This is supported by the fact that Cl^- was observed as a photofragment at 4400 Å, where counts of the Cl^- ions resulting from photodestruction of ClO^- were observed in an amount of $40\% \pm 15\%$ of the counts of the ClO^- ions photodestroyed. Such a photodissociation is further corroborated by the other facts discussed below.

In contrast to the extensive theoretical investigation of Cl_2^-, the potential curves for ClO^- are not known. However, since ClO^- is isoelectronic with ArO, the ClO^- potential curves relevant to the present measurements can be sketched from those of ArO, which has been well studied.[43,44] The ArO potential curves calculated by Dunning and Hay[44] using *ab initio* configuration interaction methods are adopted for illustration of the ClO^- potential curves, as shown in Fig. 7. The energy limits for dissociating ClO and ClO^- into various atomic products are determined from the $O(^1D)$ excitation energy[45] and the electron affinities of $O(^3P)$[7,38] and $Cl(^2P)$.[38] The triplet states $^3\Pi$ and $^3\Sigma^-$, which correlate with the $Cl^-(^1S) + O(^3P)$, and the singlet states $^1\Sigma^+$, $^1\Pi$, and $^1\Delta$, which correlate with the $Cl^-(^1S) + O(^1D)$ limit, are all assumed to be repulsive by analogy to ArO. For clarity, the $^1\Pi$ and $^1\Delta$ curves are not shown in Fig. 7.

Among the states that dissociate adiabatically into $Cl(^2P) + O^-(^2P)$, the $^1\Sigma^+$ state is expected to be strongly bound, similar to Ar^+O^-.[44] As a result of the noncrossing rule for states of the same symmetry, an avoided crossing occurs at large internuclear distances between this state and the repulsive $^1\Sigma^+$ curve arising from the lower $Cl^-(^1S) + O(^1D)$ limit. Thus, the $ClO^-(^1\Sigma^+)$ ground state dissociates adiabatically to $Cl^-(^1S) + O(^1D)$, as shown in Fig. 7. The $Cl(^2P) + O^-(^2P)$ limit also gives rise to $^3\Sigma^-$, $^3\Pi$, $^3\Delta$, $^1\Pi$, and $^1\Delta$ states. One or more of these states may be slightly bound, in which case additional consideration must be given to other avoided crossings.

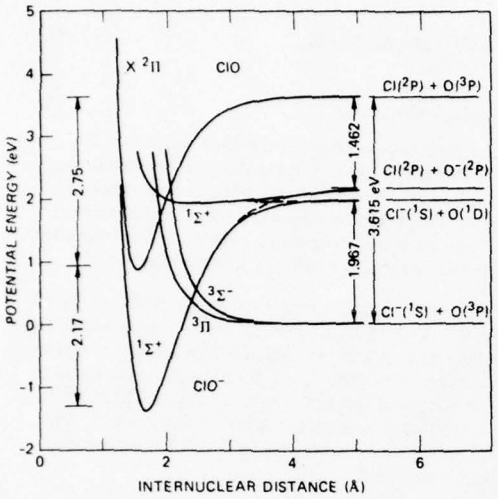

FIG. 7. The tentative potential curves for ClO^- and ClO. The Morse potential curve for ClO is plotted using the parameters $D_e = 2.80$ eV ($D_0 = 2.75$ eV), $\omega_e = 853.8$ cm^{-1}, and $r_e = 1.56965$ Å (Ref. 46). The ground state for ClO^- is plotted using the parameters $D_e = 3.50$ eV, $\omega_e = 713$ cm^{-1}, and $r_e = 1.71$ Å (see text). The other curves are derived from ArO (Ref. 44) and are modified by the noncrossing rule.

The potential curve for the $ClO^-(^1\Sigma^+)$ ground state can be estimated from the dissociation energy and electron affinity of ClO and the equilibrium bond length and vibrational frequency of ClO^- in the ground state as described below. Using the dissociation energy of 2.7505 eV, the vibrational frequency of 853.8 cm^{-1}, and the equilibrium bond length of 1.56965 Å given by Coxon *et al.*,[46] we first calculate the Morse potential curve for $ClO(X^2\Pi)$, as shown in Fig. 7. From Fig. 6, the threshold for the photodestruction cross section is near 2.17 eV (5700 Å), and is clearly less than 2.3 eV (5400 Å). This threshold value is reasonable when compared with the ClO electron affinity values of 2.2 ± 0.4 eV determined from thermochemical data by O'Hare and Wahl,[47] of $\geq 1.6 \pm 0.2$ eV measured in endoergic ion–molecule collisions of Cl^- on O_2 by Vogt *et al.*,[48] and of 1.95 ± 0.25 eV determined from ion–molecule reactions by Dotan *et al.*[49] Taking the ClO dissociation energy of 2.75 eV and the ClO electron affinity of 2.17 eV, the energy for dissociating $ClO^-(^1\Sigma^+)$ into $Cl(^2P) + O^-(^2P)$ is $D_0 = 3.46$ eV ($D_e = 3.50$ eV). Combining this dissociation energy with the ClO^- equilibrium bond length[50] of 1.71 Å and the vibrational frequency[50,51] of 713 cm^{-1}, we calculate the Morse potential curve for $ClO^-(^1\Sigma^+)$ as shown in Fig. 7.

The observed photodissociation band is apparently an optically allowed transition, so it must be a $^1\Sigma^+ \leftarrow {}^1\Sigma^+$ or a $^1\Pi \leftarrow {}^1\Sigma^+$ transition. The $^1\Sigma^+ \leftarrow {}^1\Sigma^+$ transition, as estimated from the potential curves in Fig. 7, has the peak position of 3.4 eV and a bandwidth of 0.2 eV, in contrast to the observed band at peak 2.9 eV and width 0.3 eV. Nevertheless, the sketched potential curves can easily be adjusted to fit the experimental observation as described below. First, the ClO electron affinity of 2.17 eV used to construct the $ClO^-(^1\Sigma^+)$ ground state is obtained from the photodestruction spectrum shown in Fig. 6. This measured value is reflected by the vertical transition and is higher than the adiabatic value. The adiabatic electron affinity of ClO is almost certainly lower than 2.17 eV, so the potential energy of the $ClO^-(^1\Sigma^+)$ ground state is very likely shifted to higher energy than the curve shown in Fig. 6. Second, the optically allowed upper states $^1\Sigma^+$ and $^1\Pi$, which dissociate into $Cl^-(^1S) + O(^1D)$, may be repelled by the states of same symmetries that dissociate into $Cl(^2P) + O^-(^2P)$, so the upper states will be shifted to lower energy. Considering these adjustments, the sketched potential curves are reasonably consistent with the experimental observations.

At 4400 Å, Cl^- photofragments have been detected, but not O^-. Thus, ClO^- may photodissociate to $Cl^-(^1S) + O(^1D)$ or $Cl^-(^1S) + O(^3P)$. If the energy in the upper state is higher than the $Cl^-(^1S) + O(^1D)$ limit, the ClO^- ions can dissociate either to $Cl^-(^1S) + O(^1D)$ by crossing the potential curves or to $Cl^-(^1S) + O(^3P)$ by a spin-forbidden predissociation through the $^3\Sigma^-$ or $^3\Pi$ state. On the other hand, if the upper state has an energy lower than the $Cl^-(^1S) + O(^1D)$ limit, only dissociation to $Cl^-(^1S) + O(^3P)$ is energetically possible. This alternative requires sufficiently strong spin–orbit coupling to make predissociation competitive with electron detachment and fluorescence. The photodissociation process could be determined by measuring the kinetic energy of the Cl^- photofragment. If the kinetic energy is low, the Cl^- ions result from photodissociation to $Cl^-(^1S) + O(^1D)$, but if the kinetic energy is high, the dissociation is to $Cl^-(^1S) + O(^3P)$. The symmetry of the potential curve of the upper state can also be determined by measuring the dependence of the photofragment intensity on laser polarization.[34] Such an experiment is not possible in the drift tube because the photofragments undergo a number of collisions with the neutral gas after their formation. We plan to investigate the photofragment kinetic energies and the polarization dependence in a beam apparatus in the future.

The potential curves shown in Fig. 7 are consistent with the assertion that the photodetachment cross section for ClO^- slowly increases with increasing photon energy. The bond length for ClO^- is larger than ClO, so the photodetachment cross section for ClO^- will increase as the number of accessible states of ClO^- increases. This results in a photodetachment cross section that increases as the photon energy increases, similar to the photodetachment of other negative molecular ions.[7]

Because Turco[2] has indicated that ClO^- may be a major ionospheric chlorine-containing ion, we calculated[52] the total solar photodestruction rate (to 3500 Å) using the measured cross sections. The rate is 0.2 s^{-1}, which is an order of magnitude below Turco's value for the reaction $ClO^- + O \rightarrow Cl^- + O_2$. However, since this reaction rate constant has not been measured, the dominance of reactive destruction is not at all certain.

AD-A078 091 SRI INTERNATIONAL MENLO PARK CA F/G 7/4
PHOTODISSOCIATION AND PHOTODETACHMENT OF ATMOSPHERIC NEGATIVE I--ETC(U)
AUG 79 J T MOSELEY , L C LEE , R V HODGES F49620-78-C-0119
UNCLASSIFIED SRI-MP-79-66 AFOSR-TR-79-1262 NL

2 OF 2
ADA
078091

END
DATE
FILMED
1 -80
DDC

C. Cl_3^- ions

The Cl_3^- ions were produced in a gas mixture of a few percent Cl_2 in Ar or O_2, for which a typical mass spectrum is shown in Fig. 2. Cl_3^- may be formed by a three-body reaction[53]

$$Cl^- + Cl_2 + M \rightarrow Cl_3^- + M, \quad \Delta H = -1.69 \text{ eV} \tag{6}$$

and by a two-body reaction (2). The ion count rate increases as the Cl_2 concentration in the buffer gas increases. ΔH in Reaction (6) is calculated from the dissociation energy of Cl_3^-.[30]

The photodestruction cross section for Cl_3^- is listed in Table II. For wavelengths longer than 4680 Å, Cl_3^- does not have a significant cross section. The photodestruction cross section appears to rise at 4131 Å and quickly increases to $(6.72 \pm 0.65) * 10^{-18}$ cm^2 at (3507 and 3569) Å. An ultraviolet absorption band, which resembles the present measurements, has been observed for Cl_3^- in aqueous chlorine solution.[13]

The only energetically accessible photodestruction process in the wavelength region of interest is photodissociation. Combining the dissociation energies for Cl_3^- (1.69 eV)[30] and Cl_3 (0.17 eV),[54] and the electron affinity for Cl (3.615 eV),[38] we estimate the electron affinity for Cl_3 to be 5.14 eV. Thus, the photodestruction of Cl_3^- observed here at photon energies less than 3.5 eV can only be by photodissociation.

The lowest asymptotic limit $Cl_2(^1\Sigma_g^+) + Cl^-(^1S)$ correlates to only one Cl_3^- state, the ground $^1\Sigma_g^+$ state, which is bound by 1.69 eV.[30] $Cl_2^-(^1\Sigma_g^+)$ must photodissociate through one of the four states $^1\Sigma_u^-$, $^3\Sigma_u^-$, $^1\Pi$, and $^3\Pi$, which correlate to the lowest excited asymptotic limit $Cl_2^-(^2\Sigma_u) + Cl(^2P)$. Combining the dissociation energy of $Cl_3^-(^1\Sigma^+)$ (1.69 eV)[30] and the electron affinities of Cl (3.615 eV)[38] and Cl_2 (2.51 eV),[27] we estimate the energy for the $Cl_2^-(^2\Sigma_u^+) + Cl(^2P)$ limit to be 2.8 eV. As shown in Table II, Cl_3^- photodissociation begins near 4131 Å (3.0 eV), which is nearly equal to the estimated dissociation limit. This is possible only if the upper state is relatively flat or bound near the Franck–Condon region. Tasker[30] has calculated that the first optically allowed excited state $Cl_3^-(^1\Sigma_u^-)$ is bound by 1.57 eV. Therefore, the observed transition may correspond to $Cl_3^-(^1\Sigma_u^+ - {}^1\Sigma_g^+)$. This assignment is different from Tasker's assignment[30] of the $Cl_3^-(^1\Sigma_u^+ - {}^1\Sigma_g^+)$ transition to the peak absorption at 2300 Å observed in aqueous solution.[13] However, if the 3300 and 2300 Å bands observed in aqueous solution[13] are assigned to the $Cl_3^-(^1\Sigma_u^+ - {}^1\Sigma_g^+)$ and $Cl_3^-(^1\Pi_u - {}^1\Sigma_g^+)$ transitions, respectively, their peak separation of 1.6 eV is consistent with Tasker's estimation[30] that this separation is 1.67 eV. Furthermore, the large cross section observed in the current study would not support an alternative assignment of the 3300 Å band to a spin-forbidden transition to the remaining $^3\Sigma$ or $^3\Pi$ state. More experiments will be needed to resolve this question.

D. $BrCl_2^-$ ions

The $BrCl_2^-$ ions were also observed when Cl_2^- and Cl_3^- were produced in the drift tube. $BrCl_2^-$ is probably formed by[53]

$$Br^- + Cl_2 + M \rightarrow BrCl_2^- + M \tag{7}$$

and

$$Br_2^- + Cl_2 \rightarrow BrCl_2^- + Br\ , \tag{8}$$

where Br^- and Br_2^- were produced from the trace Br_2 impurity in the Cl_2 gas. A typical mass spectrum is shown in Fig. 2. The $BrCl_2^-$ ion density increases as the Cl_2 partial pressure increases, in contrast to the Br^- ion density which decreases rapidly. The formation of $BrCl_2^-$ has been described in a previous paper.[53]

The photodestruction cross section for $BrCl_2^-$ is listed in Table II. The cross section is small for wavelengths longer than 4762 Å and increases with decreasing wavelength shorter than 4680 Å. A similar photoabsorption band was observed for $BrCl_2^-$ in $CsBrCl_2$ and Et_4NBrCl_2 and was attributed to spin forbidden transitions.[11] The large cross section we observe at 3500 Å does not support this assignment.

The dissociation energy of $BrCl_2^-$ and the electron affinity of $BrCl_2$ are not known, so the photodestruction process for $BrCl_2^-$ cannot be determined. However, considering the similarity between the dissociation energies of Cl_3^- and Br_3^-,[30] of Cl_2^- and $BrCl^-$,[29] and the electron affinities of Cl and Br,[38] the dissociation energy for $BrCl_2^-$ and electron affinity for $BrCl_2$ are probably very similar to those for Cl_3^- and Cl_3, respectively. The photodestruction process for $BrCl_2^-$ may thus be very similar to Cl_3^- and is probably attributable to photodissociation. Further investigations into the production of various possible photofragments (Br^-, Cl^-, $BrCl^-$, Cl_2^-) from photodissociation of $BrCl_2^-$ will be conducted in the near future.

IV. CONCLUDING REMARKS

The photodestruction cross sections for Cl_2^-, ClO^-, Cl_3^-, and $BrCl_2^-$ in the gas phase have been measured in the 3500 to 7600 Å region. Except for ClO^-, the cross sections observed in the present measurements are consistent with the optical absorption spectra of the various ions in crystals,[8–11] aqueous solutions,[12–15] and argon matrices.[17–19] If the potential curves (or surfaces) are similar for the ions in different environments, as was shown for Cl_2^-,[28,29,31] then the photodestruction cross sections for the ions in solid or solution may be the same as in the gas phase. Therefore, these absolute measurements in the gas phase may, in turn, be useful for the quantitative determination of ion concentrations in solids or in solutions.

The photodestruction cross section for Cl_2^- is now well understood, owing to the availability of calculated potential curves and its similarity to Ar_2^+. However, explanation of the photodestruction cross section for ClO^- is based only on the potential curves sketched by analogy with the isoelectronic molecule ArO, for which the potential curves have been calculated.[43,44] For a better understanding of the ClO^- optical spectrum, further investigations of its potential curves are needed. The optical data for Cl_3^- and $BrCl_2^-$ are very limited. The available data[30,38,54] for Cl_3^- and Cl_3 indicate that photodetachment is not energetically possible for Cl_3^- at photon

wavelengths longer than 3500 Å, and only photodissociation occurs. Considering the similarity between the Cl and Br compounds, the observed photodestruction process for $BrCl_2^-$ is probably photodissociation also.

After this paper was submitted for publication, we found that Ellis, Eisele, and McDaniel [J. Chem. Phys. **69**, 4710 (1978)] had recently measured the reduced mobility for Cl_2^- in O_2, obtaining a value of 2.46 cm^2/V s at 300 K. This is in good agreement with the value of 2.43 cm^2/V s listed in Table I, which was obtained from the scaling procedure described in the text. The agreement supports the validity of this scaling procedure.

ACKNOWLEDGMENTS

The authors wish to thank Drs. J. R. Peterson and D. L. Huestis of this laboratory for helpful discussions and comments. We are also indebted to Dr. R. P. Saxon of this laboratory for the advice on the Cl_2^- photodissociation cross section calculation and to Professor K. Sando for the use of his computer program. The use of a laboratory computer system through an equipment grant (PHY76-14436) from the National Science Foundation is acknowledged. This work was supported primarily by the Atmospheric Science Laboratory, U.S. Army Electronics Command, White Sands Missile Range, New Mexico, and in part by the U.S. Air Force Office of Scientific Research and the Air Force Geophysics Laboratory.

[1]J. J. Ewing and C. A. Brau, Appl. Phys. Lett. **27**, 350 (1975); J. R. Murray and H. T. Powell, Appl. Phys. Lett. **29**, 252 (1976); J. I. Levatter, J. H. Morris, and S. C. Lin, Appl. Phys. Lett. **32**, 630 (1978).
[2]R. P. Turco, J. Geophys. Res. **82**, 3585 (1977).
[3]L. C. Lee, G. P. Smith, T. M. Miller, and P. C. Cosby, Phys. Rev. A **17**, 2005 (1978).
[4]L. C. Lee and G. P. Smith, "Photodissociation cross sections of Ne_2^+, Ar_2^+, Kr_2^+, and Xe_2^+ from 3500 to 5400 Å," Phys. Rev. A (in press).
[5]D. S. Burch, S. J. Smith, and L. M. Branscomb, Phys. Rev. **112**, 171 (1958).
[6]H. Hotop, T. A. Patterson, and W. C. Lineberger, J. Chem. Phys. **60**, 1806 (1974).
[7]L. C. Lee and G. P. Smith, J. Chem. Phys. **70**, 1727 (1979).
[8]C. J. Delbecq, B. Smaller, and P. H. Yuster, Phys. Rev. **111**, 1235 (1958).
[9]C. J. Delberq, W. Hayes, and P. H. Yuster, Phys. Rev. **121**, 1043 (1961).
[10]D. L. Griscom, J. Chem. Phys. **51**, 5186 (1969).
[11]W. Gabes and D. J. Stufkens, Spectrochim. Acta Part A **30**, 1835 (1974).
[12]H. L. Friedman, J. Chem. Phys. **21**, 319 (1953).
[13]G. Zimmerman and F. C. Strong, J. Am. Chem. Soc. **79**, 2063 (1957).
[14]L. I. Grossweiner and M. S. Matheson, J. Phys. Chem. **61**, 1089 (1957).
[15]D. M. Brown and F. S. Dainton, Nature (London) **209**, 195 (1966).
[16]L. Andrews, J. Am. Chem. Soc. **98**, 2147 (1976).
[17]R. Rackwitz, D. Feldmann, E. Heinicke, and H. J. Kaiser, Z. Naturforsch. Teil A **29**, 1797 (1974).
[18]O. I. Asubiojo, H. L. McPeters, W. N. Olmstead, and J. I. Brauman, Chem. Phys. Lett. **48**, 127 (1977).
[19]S. A. Sullivan, B. S. Freiser, and J. L. Beauchamp, Chem. Phys. Lett. **48**, 294 (1977).
[20]J. T. Moseley, P. C. Cosby, R. A. Bennett, and J. R. Peterson, J. Chem. Phys. **62**, 4826 (1975); P. C. Cosby, R. A. Bennett, J. R. Peterson, and J. T. Moseley, J. Chem. Phys. **63**, 1612 (1975); P. C. Cosby, J. H. Ling, J. R. Peterson, and J. T. Moseley, J. Chem. Phys. **65**, 5267 (1976).
[21]The stilbene-3 dye was obtained from the Exciton Chemical Campany.
[22]G. P. Smith, P. C. Cosby, and J. T. Moseley, J. Chem. Phys. **67**, 3818 (1977).
[23]E. W. McDaniel and E. A. Mason, *The Mobility and Diffusion of Ions in Gases* (Wiley, New York, 1973).
[24]R. A. Beyer and J. A. Vanderhoff, J. Chem. Phys. **65**, 2313 (1976).
[25]H. W. Ellis, R. Y. Pai, E. W. McDaniel, E. A. Mason, and L. A. Viehland, At. Data Nucl. Data Tables **17**, 177 (1976).
[26]I. Dotan and D. L. Albritton, J. Chem. Phys. **66**, 5238 (1977).
[27]W. A. Chupka, J. Berkowitz, and D. Gutman, J. Chem. Phys. **55**, 2724 (1971).
[28]T. L. Gilbert and A. C. Wahl, J. Chem. Phys. **55**, 5247 (1971).
[29]P. W. Tasker, G. G. Balint-Kurti, and R. N. Dixon, Mol. Phys. **32**, 1651 (1976).
[30]P. W. Tasker, Mol. Phys. **33**, 511 (1977).
[31]A. N. Jette, T. L. Gilbert, and T. P. Das, Phys. Rev. **184**, 884 (1969).
[32]P. W. Tasker and A. M. Stoneham, J. Phys. Chem. Solids **38**, 1185 (1977).
[33]P. W. Tasker (private communication). The excitation energies presented in Ref. 29 were evaluated from the potential curves at $R = 5.25$ bohr to match solid-state data. At R_e, Tasker estimates the $^2\Sigma_g^+ \leftarrow {}^2\Sigma_u^+$ and $^2\Pi_g \leftarrow {}^2\Sigma_u^+$ cross section peaks to be 3.73 and 1.93 eV, respectively.
[34]J. T. Moseley, R. P. Saxon, B. A. Huber, P. C. Cosby, R. Abouaf, and M. Tadjeddine, J. Chem. Phys. **67**, 1659 (1977).
[35]T. L. Gilbert and A. C. Wahl, Argonne National Laboratory (unpublished report, 1971).
[36]At intermediate to large R, we can approximate the transition moment (μ) for the $Cl_2^-(^2\Sigma_g^+ \leftarrow {}^2\Sigma_u^+)$ transition as

$$\mu = \langle \Psi_{^2\Sigma_g^+} | z | \Psi_{^2\Sigma_u^+} \rangle \cong \tfrac{1}{2} \langle [(p_a + p_b) | z | (p_a - p_b)\rangle$$

$$\cong \tfrac{1}{2} [\langle p_a | z | p_a \rangle - \langle p_b | z | p_b \rangle] ,$$

where p_a and p_b are the atomic p orbitals at infinite internuclear separation. The cross terms $\langle p_a | z | p_b \rangle$ and $\langle p_b | z | p_a \rangle$ cancel at intermediate R and go to zero at large R. The transition moment, then, measures charge and $|\mu| \sim R/2$ (Ref. 37).
[37]W. J. Stevens, M. Gardner, A. Karo, and P. Julienne, J. Chem. Phys. **67**, 2860 (1977).
[38]H. Hotop and W. C. Lineberger, J. Phys. Chem. Ref. Data **4**, 539 (1975).
[39]R. Abouaf, B. A. Huber, P. C. Cosby, R. P. Saxon, and J. T. Moseley, J. Chem. Phys. **68**, 2406 (1978).
[40]W. R. Wadt, J. Chem. Phys. **68**, 402 (1978).
[41]M. McFarland, D. L. Albritton, F. C. Fehsenfeld, E. E. Ferguson, and A. L. Schmeltekopf, J. Chem. Phys. **59**, 6620 (1973).
[42]G. Herzberg, *Spectra of Diatomic Molecules* (Van Nostrand, Princeton, 1967).
[43]P. S. Julienne, M. Krauss, and W. Stevens, Chem. Phys. Lett. **38**, 374 (1976).
[44]T. H. Dunning, Jr. and P. J. Hay, J. Chem. Phys. **66**, 3767 (1977).
[45]C. E. Moore, "Atomic Energy Levels," Vol. 1, Natl. Stand. Ref. Data Ser. **35**, 1971).
[46]J. A. Coxon, W. E. Jones, and E. G. Skolnik, Can. J. Phys. **54**, 1043 (1976).

[47]P. A. G. O'Hare and A. C. Wahl, J. Chem. Phys. **54**, 3770 (1971).
[48]D. Vogt, W. Dreves, and J. Mischke, Int. J. Mass Spectrom. Ion Phys. **24**, 285 (1977).
[49]I. Dotan, D. L. Albritton, F. C. Fehsenfeld, G. E. Streit, and E. E. Ferguson, J. Chem. Phys. **68**, 5414 (1978).
[50]E. L. Wagner, J. Chem. Phys. **37**, 751 (1962).
[51]G. Kujumzelis, Phys. Z. **39**, 665 (1938).
[52]J. R. Peterson, J. Geophys. Res. **81**, 1433 (1976).
[53]B. A. Huber and T. M. Miller, J. Appl. Phys. **48**, 1708 (1977).
[54]V. A. Medvedev, *Energiya Razryva Khimicheskikh Svyazei: Potentsialy Ionizatsii i Srodstvo k Eletronu* (Academy of Sciences, USSR, Moscow, 1962).

Appendix E

PHOTODISSOCIATION AND PHOTODETACHMENT OF MOLECULAR NEGATIVE IONS. IX. ATMOSPHERIC IONS AT 2484 AND 3510 Å

Photodissociation and photodetachment of molecular negative ions. IX. Atmospheric ions at 2484 Å and 3511 Å

Ronald V. Hodges, L. C. Lee, and J. T. Moseley[a]
Molecular Physics Laboratory
SRI International
Menlo Park, California 94025

ABSTRACT

A rare-gas–halogen laser has been used with a drift-tube mass spectrometer to extend measurements of the photodestruction cross sections of atmospheric negative ions to 2484 Å. Ions studied include O^-, O_2^-, O_3^-, O_4^-, CO_3^-, CO_4^-, HCO_3^-, NO_2^-, $O_2^- \cdot NO$, and NO_3^-; hydrates of many of these ions were also studied. As expected, the cross sections for most of the ions were substantially larger at 2484 Å than at wavelengths longer than 3500 Å.

---

[a] Present address: Department of Physics, University of Oregon, Eugene, Oregon 97403.

10/16/79
MP 79-79

I. INTRODUCTION

Investigations of the photodestruction of ions have produced spectroscopic and thermodynamic data for a variety of gas-phase ions. Among the quantities that have been determined are photodestruction cross sections as a function of wavelength,[1-5] bond dissociation energies,[2] electron affinities,[3] ion vibrational frequencies,[4] and parameters of excited state potential surfaces.[5] These data for ions that occur in the atmosphere are required for an understanding of the effect of radiation on atmospheric ion chemistry.[6] Photodestruction cross sections for many positive and negative ions of atmospheric interest have been measured over the wavelength range 8400 Å to 3500 Å in our laboratory. The study apparatus consisted of a drift-tube mass spectrometer, cw rare-gas ion lasers, and a tunable dye laser.[7,8]

Measurements at shorter wavelengths are needed for assessment of the effect on the ionosphere of solar radiation below 3500 Å. Although solar radiation decreases rapidly with decreasing wavelength below 3500 Å, the photodestruction cross sections are generally expected to be increasing with decreasing wavelength in this region. Further, atmospheric disturbances, both natural and man-made, can introduce increased radiation into the atmosphere. Unfortunately, no intense cw laser is presently available in this region. We report here the successful application of a pulsed, rare-gas–halogen laser to the measurement of photodestruction cross

sections for several negative ions at 2484 Å and 3511 Å.

II. EXPERIMENTAL APPARATUS AND PROCEDURES

The SRI drift-tube mass spectrometer, described in detail previously,[7,8] was used with a Lambda Physik EMG 500 excimer laser. Laser pulses of several tens of millijoules with durations of ~15 ns and a repetition rate of 20 Hz were used. The light pulse was directed into the drift tube by a 50-cm-radius mirror that focused the beam to an oval (about 0.5 cm x 1 cm) in front of the drift-tube exit aperture. The average power of the beam exiting the drift tube was monitored by a power meter (Scientech, Inc.).

Since the ion swarm is effectively stationary (drift velocity $\sim 10^4$ cm/sec) during the short laser pulse, photodestruction by the laser creates a region of lower ion density, which reflects the beam size and intensity profile. The change in ion density Δn in the volume Adx (see Fig. 1) during a laser pulse is given by

$$\frac{\Delta n}{n_o} = 1 - e^{-\sigma\phi(x)}, \qquad (1)$$

where n_o is the ion density before the laser pulse, σ is the photodestruction cross section, and $\phi(x)$ is the number of photons per square centimeter that pass through the volume Adx. If 30% or fewer of the ions are destroyed, Eq. (1) is approximated to within 10% by

$$\frac{\Delta n}{n_o} = \sigma\phi(x). \qquad (2)$$

Integrating over the hatched cylinder (Fig. 1) yields the total number of ions destroyed, Δn, which would otherwise exit the drift tube,

$$\Delta N = N_o \sigma \Phi ,$$

or

$$\sigma = \frac{\Delta N}{N_o} \frac{1}{\Phi} , \qquad (3)$$

where N_o is the number of ions originally in the cylinder and Φ is the number of photons per square centimeter averaged over the cylinder. A corresponding drop in ion count rate occurs following the laser pulse, during the time of arrival at the detector of the irradiated ions. This decrease is monitored by an ND100 multichannel analyzer with a time-of-flight module, which is triggered by the laser pulse. Representative time of arrival data are shown in Fig. 2. The time span of arrival of the irradiated ions is equal to ℓ/v_d, where ℓ is the width of the laser beam and v_d is the ion drift velocity.

An SSR Digital Synchronous Computer Model 1110 operated in the chop mode is used to measure the ratio $\Delta N/N_o$. The SSR is set to accumulate data counts for a time τ, which contains the entire dip. A background count is obtained during an equal time window several milliseconds after the laser pulse. If τ were set at exactly the peak width, ℓ/v_d, then the ratio of the difference count $\Delta N'$ (background minus data) to the background count N'_o, would equal $\Delta N/N_o$. In practice it is not practical to set τ to exactly match the peak. Instead, τ is set to be somewhat larger and

the measured ratio, $\Delta N'/N'$, is related to $\Delta N/N$ by the factor $v_d\tau/\ell$. The working equation for this experiment is then

$$\sigma = \frac{\Delta N'}{N'_o} \frac{v_d \tau}{\Phi \ell} . \qquad (4)$$

Since absolute measurements of Φ and ℓ are impractical, the absolute cross section is obtained by normalizing to a known cross section, that for O^-.[9] The cross section for the ion of interest, A^-, can be expressed in terms of σ_{O^-} by Eq. (5),

$$\sigma_{A^-} = \sigma_{O^-} \frac{(\Delta N'/N_o)_{A^-}}{(\Delta N'/N'_o)_{O^-}} \frac{K_{A^-} \tau_{A^-} P_{O^-}}{K_{O^-} \tau_{O^-} P_{A^-}} , \qquad (5)$$

where the laser flux ratio Φ_{O^-}/Φ_{A^-} is replaced by the ratio of the power measurements P, and the drift velocities are replaced by ion mobilities K. Normalization to O_2^- is more convenient for most of the ions studied, since O_2^- is usually present in much larger quantities than O^- in the gas mixtures used to form the other ions. Consequently, the cross section for O_2^- was carefully measured relative to O^-, and then used as a normalization standard for all other ions except $O_2^- \cdot NO$, which photodissociates to yield O_2^-.

Since laser peak powers of several megawatts are attainable with the excimer laser, higher order processes might reasonably be expected to interfere with the measurement of single photon photodestruction cross

sections. In fact, we have observed multiphoton ionization at 2484 Å and 1933 Å in O_2 and in several of the other gases employed in these experiments. However, no change in the cross sections measured for O_2^- photodestruction was observed for a power variation of a factor of 3. Although the power dependence of the cross section for the other ions was not examined systematically, in several cases where measurements were made on an ion at substantially different powers, no power dependence was noted. Variations of the ratio of the drift field to the gas number density, E/N, from 10 to 40 Td, and of the pressure from 50 to 400 mTorr, had no effect on the measured O_2^- cross section. Data on all of the ions studied were taken under conditions of drift field, drift distance, and pressure similar to those used in the earlier measurements at larger wavelengths.[1,2,4,10,11]

III. RESULTS

The cross sections measured in this study and representative values at longer wavelengths measured previously with cw lasers,[1,2,4,10,11] are given in Table I. Cross sections measured using the 3511 Å line from the excimer laser agree within experimental uncertainty with measurements made using the 3507 Å and 3564 Å lines of a Kr^+ laser. The cross sections for most of these ions are increasing rapidly with decreasing wavelength. Several ions (CO_4^-, HCO_3^-, $HCO_3^- \cdot H_2O$ and NO_3^-) for which photodestruction is very weak or too small to be observed at wavelengths longer than 3500 Å, have large cross sections at 2484 Å.

In the UV region, both photodetachment and photodissociation channels are accessible for most of these ions. In gas mixtures containing $O_2^-\cdot NO$, observation of an increase in the count rate of O_2^- following the laser pulse establishes that $O_2^-\cdot NO$ photodissociates according to

$$O_2^-\cdot NO + h\nu(3511 \text{ and } 2484 \text{ Å}) \rightarrow O_2^- + NO \,, \qquad (6)$$

consistent with earlier observations using cw lasers.[10] No ion photoproduction was observed for the other ions studied. However, photodissociation cannot be unambiguously ruled out for most of these ions. The possible photoproduct ions were generally already present in the drift tube. Photodestruction of these ions may have masked their photoproduction from parent ions. It is certainly of interest to establish the photodestruction mechanism. To do so will require an experimental arrangement in which possible photofragment ions are not present in large quantities under the conditions of the photodestruction measurements.

Attempts to measure photodestruction cross sections at 1933 Å were unsuccessful. At this wavelength, scattered laser light striking the drift tube walls ejected photoelectrons. Attachment of these electrons to the gas produced an increase in ion current that was larger than the photodestruction signal. Measurements this far into the ultraviolet will require both focusing and collimation of the laser beam.

The uncertainty limits given in Table I represent the uncertainty of the measurement relative to the normalization cross section. Included in these values are the statistical counting uncertainty, the uncertainty ($\pm 5\%$) in the parameters that affect the ion mobilities (pressure, temperature, and drift field), and the uncertainty ($\pm 10\%$) in the measurement of the power ratio. By repeating measurements, the relative uncertainty was further reduced. Absolute uncertainty in these measurements arises from the uncertainty in the mobilities, $\pm 5\%$, and in the cross sections for the normalization ion, which for O^- = $\pm 10\%$ and for O_2^- = $\pm 11\%$. The root mean square of these uncertainties yields a total absolute uncertainty of $\pm 12\%$. Thus, typically, the total uncertainty in the values listed in Table I is in the range $\pm 20 - 30\%$.

IV. ACKNOWLEDGMENTS

We thank Dr. G. P. Smith, Dr. P. C. Cosby, and Dr. J. R. Peterson for many helpful discussions during this work.

This research was supported by the U. S. Air Force Office of Scientific Research and the U. S. Air Force Geophysics Laboratory. The use of a laboratory computer system obtained under an equipment grant from the National Science Foundation is acknowledged.

REFERENCES

1. L. C. Lee and G. P. Smith, J. Chem. Phys. 70, 1727 (1979).

2. G. P. Smith, L. C. Lee, and J. T. Moseley, J. Chem. Phys., Photodissociation and Photodetachment of Molecular Negative Ions. VII. Ions Formed in $CO_2/O_2/H_2O$ Mixtures, 3500-5300 Å. (in press)

3. B. K. Janousek, J. I. Brauman, and J. Simons, J. Chem. Phys. 71, 2057 (1979).

4. P. C. Cosby, J. T. Moseley, J. R. Peterson, and J. H. Ling, J. Chem. Phys. 69, 2771 (1978).

5. T. M. Miller, J. H. Ling, R. P. Saxon, and J. T. Moseley, Phys. Rev. A 13, 2171 (1976).

6. J. R. Peterson, J. Geophys. Res. 81, 1433 (1976).

7. P. C. Cosby, R. A. Bennett, J. R. Peterson, and J. T. Moseley, J. Chem. Phys. 63, 1612 (1975).

8. J. T. Moseley, P. C. Cosby, R. A. Bennett, and J. R. Peterson, J. Chem. Phys. 62, 4826 (1975).

9. P. Warneck, Laboratory Measurements of Photodetachment Cross Sections of Selected Negative Ions, GCA Tech. Report 69-13-N, GCA Coys. Bedford, Massachusetts (1969).

10. G. P. Smith, L. C. Lee, and P. C. Cosby, J. Chem. Phys., Photodissociation and Photodetachment of Molecular Negative Ions. VIII. Nitrogen Oxides and Hydrates, 2500-8250 Å. (in press)

11. P. C. Cosby, J. H. Ling, J. R. Peterson, and J. T. Moseley, J. Chem. Phys. 65, 5267 (1976).

TABLE I Photodestruction cross section measurements at representative wavelengths from 2484 to 6200 Å.[a] Cross sections are in units of 10^{-18} cm^2.

Ion	Wavelength (Å)					
	2484	3511	(3507 +3564)	4067	4131	6200
O^-	11.3	8.2	8.2	6.3	6.3	6.3
O_2^-	9.5 ± .04	3.4 ± 0.5	3.7	2.6	2.6	1.3
$O_2^- \cdot H_2O$	8.5 ± 1.0	-	2.6	1.6	1.5	0.3
O_3^-	10.2 ± 1.0	2.3 ± 0.6	2.1	5.0	3.7	0.09
O_4^-	13.1 ± 1.4	8.4 ± 1.1	8.6	2.9	3.2	1.1
CO_3^-	2.7 ± 0.4	-	0.07	0.4	0.4	1.5
$CO_3^- \cdot H_2O$	1.6 ± 0.4	-	0.1	0.5	0.5	7.0
CO_4^-	10.1 ± 1.1	-	0.45	-	<0.06	<0.02
HCO_3^-	4.0 ± 0.6	-	<0.08	-	<0.08	<0.03
$HCO_3^- \cdot H_2O$	2.9 ± 0.4	-	<0.07	-	<0.06	-
NO_2^-	10.2 ± 0.1	-	3.2	1.5	1.3	<0.01
$NO_2^- \cdot H_2O$	9.8 ± 1.2	-	1.2	-	0.16	<0.02
NO_3^-	10.2 ± 1.0	-	0.1	-	<0.07	-
$O_2^- \cdot NO$	9.8 ± 1.0	9.1 ± 1.3	7.0	-	6.1	0.1

[a] Cross sections were measured relative to the O^- cross section.[1,9] Values at the last four wavelengths are taken from References 1,2,4,10, and 11.

FIGURE CAPTIONS

Fig. 1. Schematic diagram for the laser-beam–ion interaction region.

Fig. 2. Time-of-arrival spectrum of ions; ℓ is the laser width, v_d is the ion drift velocity.

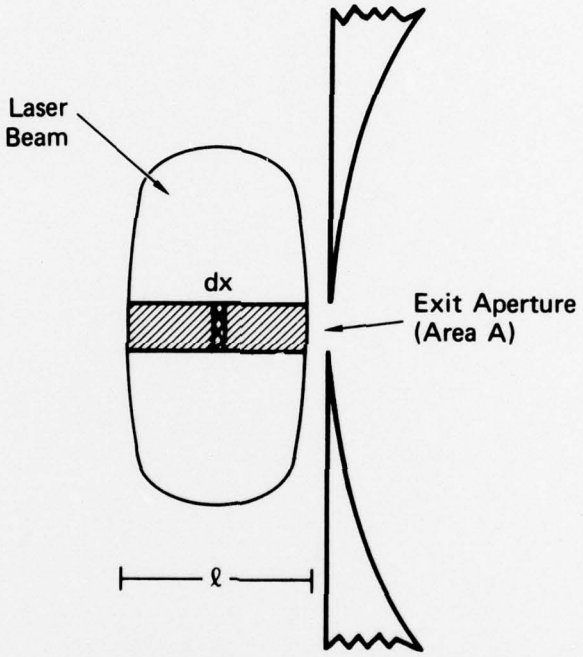
Laser
Beam
dx
Exit Aperture
(Area A)
ℓ
ION DRIFT
REGION
ION DETECTION
REGION
TA-330522-149R

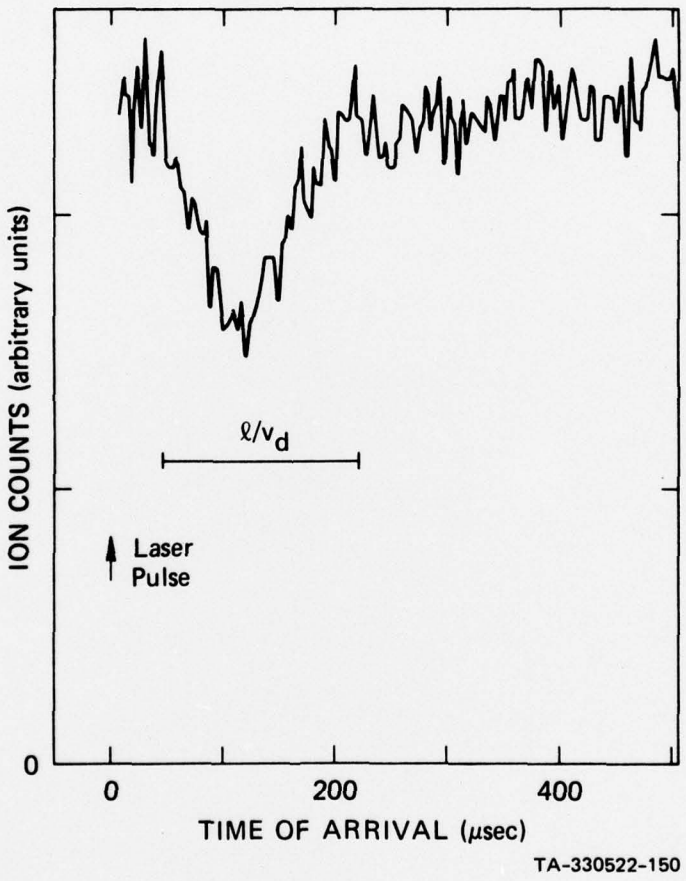
ION COUNTS (arbitrary units)
ℓ/v_d
Laser
Pulse
0
0
200
400
TIME OF ARRIVAL (μsec)
TA-330522-150